Statistical Analysis of the Sources of Flexible Pavement Variability

Final Report

Prepared by

Randal J. Barnes
Igor Jankovic
Arnaud Froment

Department of Civil Engineering
University of Minnesota
500 Pillsbury Drive S.E.
Minneapolis, MN 55455-0220

Statistical Analysis of the Sources of Flexible Pavement Variability

Final Report

Prepared by

Randal J. Barnes
Igor Jankovic
Arnaud Froment

Department of Civil Engineering
University of Minnesota
500 Pillsbury Drive S.E.
Minneapolis, MN 55455-0220

February 1999

Published by
Minnesota Department of Transportation
Office of Research Administration
200 Ford Building, Mail Stop 330
117 University Avenue
Saint Paul, MN 55155

TABLE OF CONTENTS

LIST OF TABLES

LIST OF FIGURES

EXECUTIVE SUMMARY

This research project attempts to identify, quantify, and statistically characterize the components of asphalt pavements that may lead to spatial variability of pavement performance. This assessment is based upon the extensive data sets collected at the Mn/ROAD project. The physical site characterization is carried out using data collected by *falling weight deflectometer*, *ground penetrating radar*, and *physical core specimens*. The applied load information is inferred from the data collected by the state-of-the-art *weigh-in-motion* system in operation at the Mn/ROAD site. The pavement performance is characterized by *international roughness index* data, *crack count* data, and *rutting depth* data.

On the average the as-built thickness is slightly thicker than the design. However, even at this carefully constructed site, there is a significant chance that the as-built pavement thickness can be in error by more than 2.5 cm (1 inch). Spatial statistics indicates that overly thin zones will occur in areas on the order of 10's of square meters, on the average.

Due the geologic and environmental homogeneity of the Mn/ROAD site the impact of spatial variability for such potentially critical parameters as the subgrade strength, and soil moisture can not be discerned from the available data. By design, the applied loading histories on the various mainline sections are equivalent: any vehicle that enters the test sites traverses all of the test sections. As such, the only significant variations in the loading histories are the differences between the inside and outside lanes.

While the more heavily traveled lane shows a consistent increase in the measures of pavement distress (e.g. rutting depths), a quantitative and predictive conclusion is impossible with the data available at the time of this study. At the time of this study the pavement structures have not degraded sufficiently to clearly correlate long term pavement performance with the available measures of pavement stiffness.

CHAPTER 1

INTRODUCTION

PROBLEM STATEMENT

The objective of this research project is to identify, quantify, and statistically characterize the components of asphalt pavements that may lead to spatial variability of pavement performance. This assessment is based upon the extensive data sets collected at the Mn/ROAD project. Specifically, the strengths, dimensions, and magnitudes necessary for this research are inferred from currently available Falling Weight Deflectometer (FWD) data, Ground Penetrating Radar (GPR) data, core analysis, and loading history data on the 22 asphalt test sections.

INTRODUCTION TO MN/ROAD

Mn/ROAD consists of two roads segments lying parallel to Interstate 94 outside Otsego, Minnesota. The site is comprised of a 3.5-mile mainline roadway carrying live interstate traffic, plus a 2.5-mile low-volume loop where controlled truck weight and traffic volume simulate conditions on rural roads (see Figure 1.1).

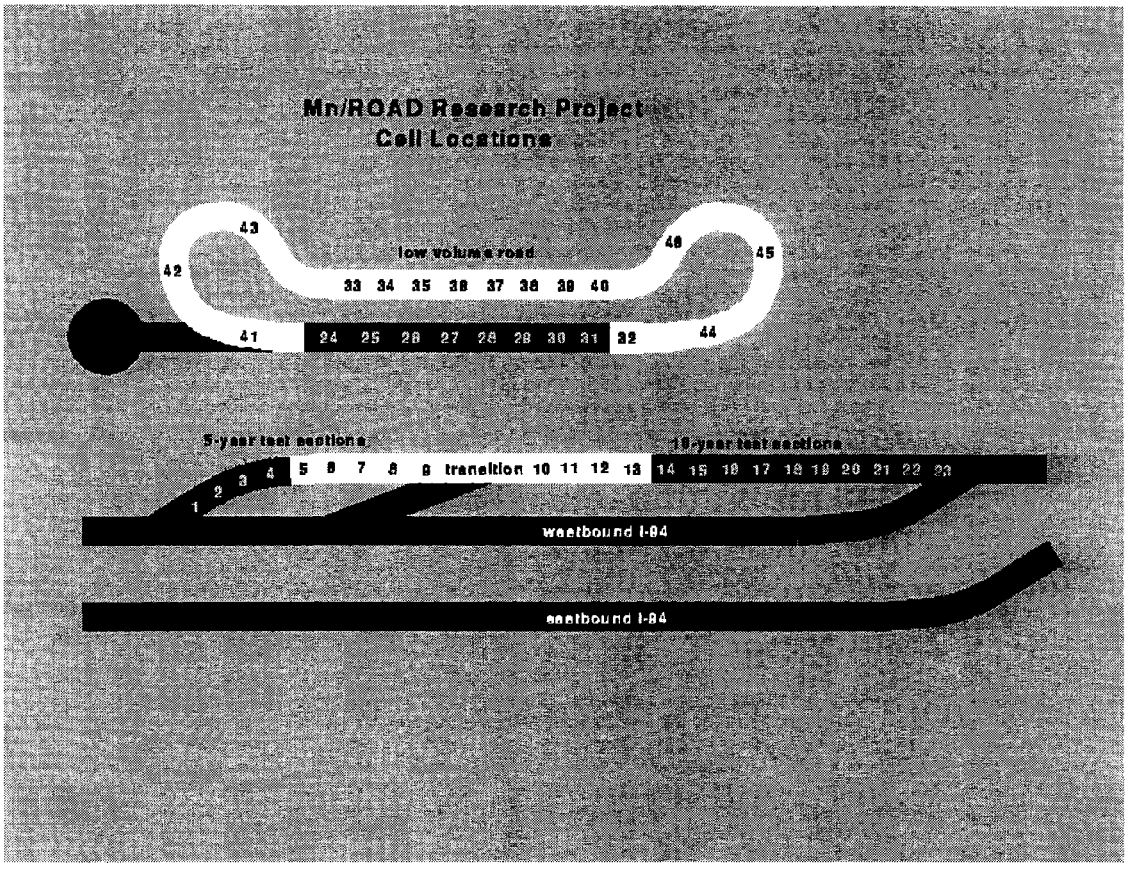

Figure 1.1 Mn/ROAD Cell Layout

Mn/ROAD's 40 test cells, each 500 feet in length, are paved with different thickness of concrete, asphalt , and aggregate. The cells are distributed over the two roadways to represent a wide range of pavement types, with varying combinations of surface, base, subbase, drainage, and compaction.

The 22 asphalt test sections of Mn/ROAD are considered in this research project. These are the low volume road (cells 24 to 31), and the mainline asphalt sections (cells 1 to 4 and 14 to 23).

CHAPTER 2

DATA CONSIDERED

DATA SET TYPES AND EXTENTS

- **Falling weight deflectometer (FWD) data**: This data set is comprised of 211,817 reflection records, resulting in computed subgrade modulus records. These data have passed an extensive error screening process. These data cover June 1994 through June 1997.
- **Ground penetrating radar (GPR) data for asphalt concrete**: This data set is comprised of 2,428 measurements for both the low volume and mainline sections.
- **Ground penetrating radar (GPR) data for granular base and subbase**: This data set is comprised of 3,447 records.
- **Core data**: This data set is comprise of 43 samples. These data were taken at locations close enough to asphalt concrete GPR samples to allow an examination of the correlation between the core data and the GPR data.
- **Load data for the low volume sections**: This data set is comprised of 4,381 equivalent single axle load records for every section. These data cover June 15, 1994 through April 18, 1996.
- **Load data for the mainline sections**: This data set is comprised of 3,444,420 equivalent single axle load records for each mainline section. These data cover July 15, 1994 through October 9, 1997.
- **Air temperature data**: This data set includes 1,253 data records from Buffalo, MN covering June 1, 1992 through October 15, 1995. Also included are 563 records from the CRREL weather station covering October 30, 1994 through April 19, 1996.
- **International roughness index (IRI) data**: This data set is comprised of 14 measurements for every mainline section, and 15 measurements for each low volume section. These data cover July 8, 1994 through February 26, 1997.
- **Groundwater elevation data**: This data set is comprised of 730 records covering June 1994 through April 3, 1996.
- **Pore pressure profiles**: This data set is comprised of 23,999 records covering June 1994 through December 31, 1995.
- **Moisture content profiles**: This data set is comprised of 4,447 records covering June 1994 through December 31, 1995.
- **Crack Count Data**: This data set is comprised of observations covering June 1994 through April 1996.
- **Rutting Depths**: This data set is comprised of 6-foot straight edge data covering June 1994 through May 1997.

DATA PROBLEMS

Most of the data available for this project are of high quality. This is especially true for the FWD measurements where very few records out of more than 200,000 records could not be used due to typographical errors.

The exceptions to this rule are the volumetric moisture content data and pore pressure data. Many volumetric moisture content records show the readings near the value of 1.0, which is physically impossible. The upper limit of the volumetric moisture content is the porosity, which is typically in the 0.25 to 0.35 range.

Similarly, the pore pressure data also seem to suffer from quality problems. The pore pressure should increase with depth (due to gravity) and in many records the pore pressure actually decreases with depth.

The problems with moisture content data and pore pressure data will be demonstrated later in the section that deals with load and environmental factors. Because of these problems, these data are not used in other sections of this report.

CHAPTER 3

INFLUENTIAL PARAMETERS

It is convenient to partition the potential influential parameters into three categories: (1) Measures of Spatial Variability; (2) Load and Environmental Factors; and (3) Measures of Performance. Items in the first category reflect the engineered structure, while the second category includes the externally imposed factors.

MEASURES OF SPATIAL VARIABILITY

- Subgrade Modulus
- Structural Number
- Granular Equivalent
- Deflection Basin Area
- Benkelman Beam Adjusted to 80°F
- Benkelman Beam Adjusted to 80°F and Spring Conditions
- G.P.R. Asphalt Concrete Thickness

These seven parameters are selected for three main reasons. First, this combination of parameters captures the overall behavior of the structure, and offers insight into the individual components of the engineered section. Second, the data is available. There is excellent site coverage over both space and time. Third, these parameters are regularly used for engineering characterization of MnDOT roads across the state.

LOAD AND ENVIRONMENTAL FACTORS

- Groundwater Elevation
- WIM Data
- Temperature (air temperature)

These three parameters are selected based upon the current understanding of pavement degradation. However, the groundwater data was unreliable and the air temperature data was uniform across all sections and, as such, did not allow for a discriminating comparison.

MEASURES OF PERFORMANCE

- International Roughness Index (IRI)
- Rutting
- Crack Counts

These three parameters are selected because it is believed that this combination captures both the degradation in ride and the degradation in structural integrity. Furthermore, the data is available.

CHAPTER 4
LAYER THICKNESS AND GROUND PENETRATING RADAR

GPR DATA

Ground penetrating radar (GPR) uses high frequency radio waves to acquire subsurface information from a small antenna which is moved slowly across the surface of the ground. The radar video record shows soil strata and other features much as they would appear to an observer looking at the wall of a vertical trench. GPR technology is widely perceived as one of the most powerful remote sensing instruments capable of locating buried objects beneath the ground and identifying ground layers.

The GPR data considered in this project are measurements of the asphalt layer thickness on each of the 22 asphalt test sections. On each of these sections, thickness measurements were taken on each lane, every 3.048 meters (10 feet). Thus, for each section, there are about 110 data available. Overall, the data set is comprised of 2,428 data.

RELIABILITY OF GPR DATA

The initial issue considered is the reliability of GPR data. To check the reliability of these measurements, they are compared and correlated with core sample data that were taken as close as possible to the GPR measurement locations.

Each GPR measurement was taken on the outer wheel paths of each particular lane (these locations correspond to the falling weight deflectometer (FWD) offsets 1 and 7 at 2.99 meters (9.8 feet from centerline). In most cases, however, the locations where the core samples were

taken did not exactly coincide with the locations where the GPR measurements were carried out.

A set of 43 core samples is identified for further analysis. These data were collected close enough to GPR measurement locations to allow a detailed comparison. Figure 4.1 compares the GPR and core sample thickness data at neighboring locations:

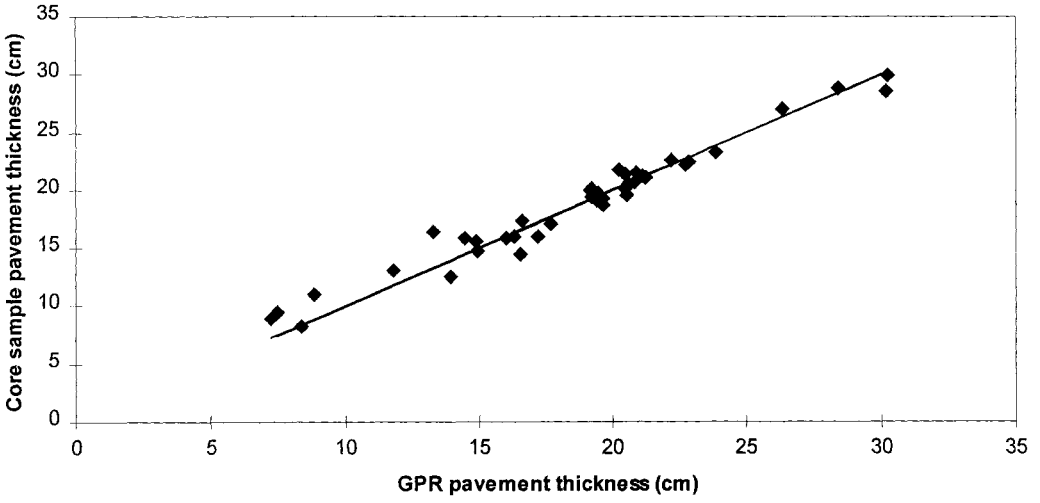

Figure 4.1 Correlation Between Cores and GPR Data

From this plot, it can be seen that a strong correlation exists between the core sample thickness and the GPR thickness (data correlation equals 0.98), which suggests a strong reliability of the GPR measurements.

The format of the GPR data is such that it enables a one dimensional statistical analysis of these data. However, these measurements are taken on the outer wheel paths of the lanes. Are these measurements representative of the average thickness of a transverse section of each lane? To answer this question, the core sample data is considered, since core sample thickness measurements on the same transverse section are available. They show that on a transverse section for each lane, the thickness values are extremely well correlated (the difference is at most 2.54 mm), so that the analysis can be done in one dimension without any problem.

DESIGN VERSUS ACTUAL PAVEMENT THICKNESS

In this section, GPR measurements of asphalt layer thickness are analyzed and compared with the design thickness of each section. This analysis characterizes the uncertainty in the as-built thickness and quantifies the mismatches that occurred between design and construction. Two measures of error are considered: the *error* and the *relative error*. The error is defined by:

$$\text{Error} = \text{Actual thickness} - \text{Design thickness}$$

The unit for *error* is inches. The relative error is defined by

$$\text{Relative Error} = \frac{\text{Actual thickness} - \text{Design thickness}}{\text{Design thickness}} \times 100\%$$

The unit for *relative error* is %. The actual thicknesses are given by the GPR data.

Global Statistics

The global summary statistics for all 2,428 data are given in Table 4.1.

	Error (mm)	Relative Error (%)
Mean	5.08	3.63
Standard Deviation	11.18	8.8
Skew	9.14	1.48
Minimum	-37.08	-25.39
25th percentile	-2.29	-1.37
Median	5.08	3.07
75th percentile	12.19	7.48
Maximum	75.44	66.66

Table 4.1 Global Summary Statistics

As shown in Figure 4.2, the distribution of errors is well-modeled by a common bell-shaped curve (i.e. a Normal distribution). The overlying continuous curve is a theoretical Normal distribution with the same mean and standard deviation as the available data.

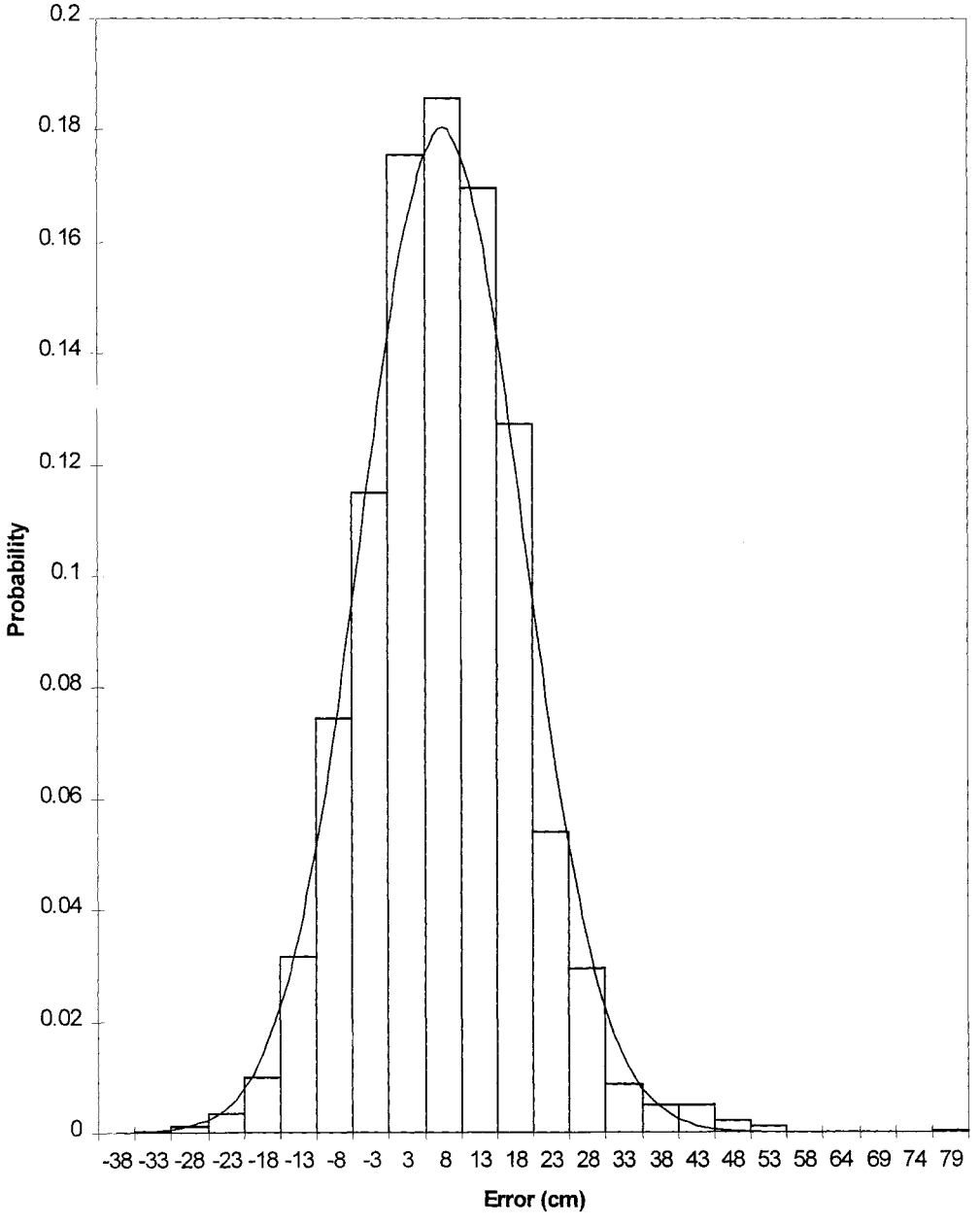

Figure 4.2 Histogram of Errors

The same type of analysis is performed using the relative errors. The resulting histogram is shown in Figure 4.3.

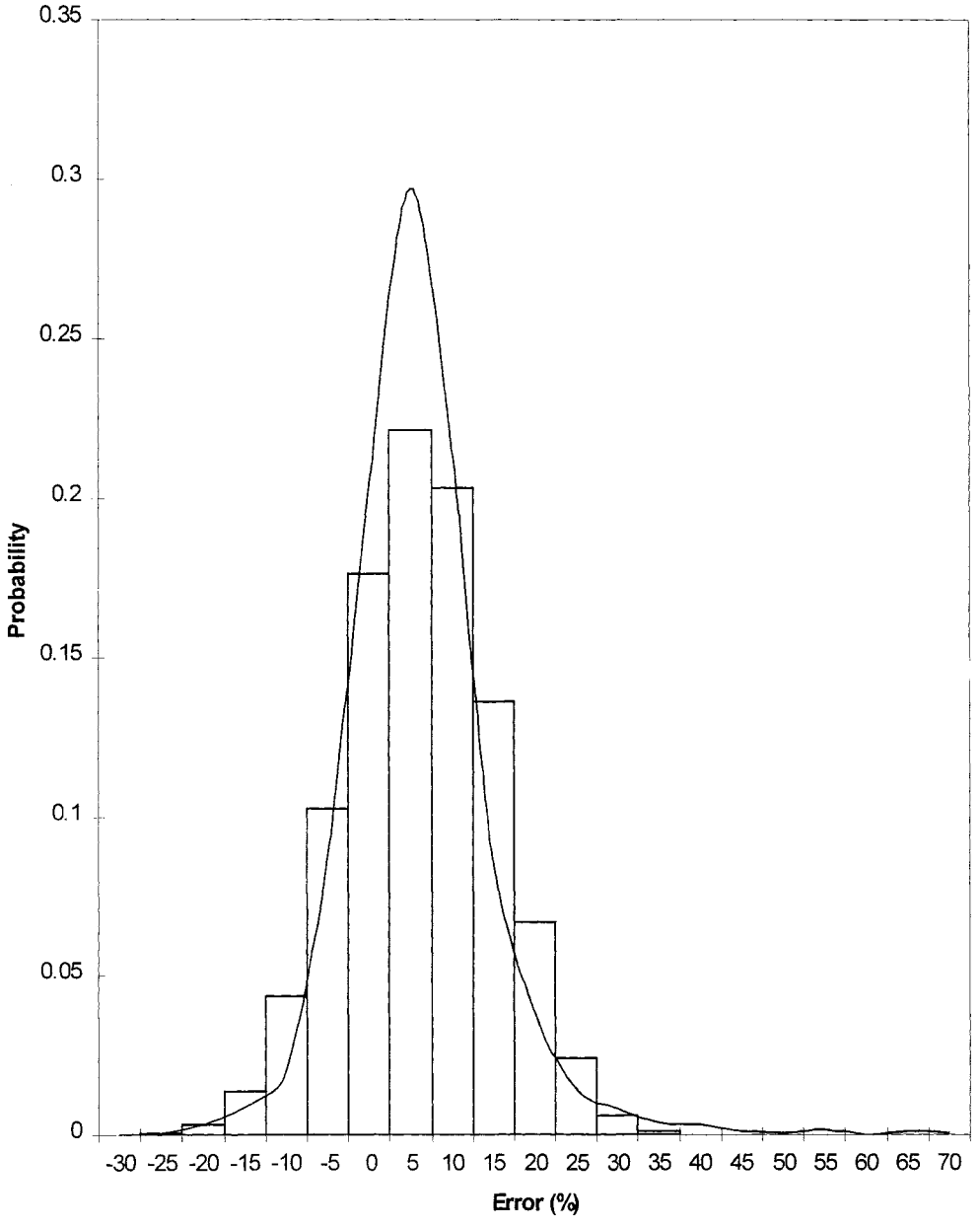

Figure 4.3 Histogram of Relative Errors

Again, the distribution of the relative errors appears to be well-modeled by a Normal distribution (although the fit is not as good as that for absolute errors). It is interesting to see if there are significant statistical differences between the Low Volume Road and the Mainline. A statistical comparison for each of them is given in Table 4.2.

	Errors (in)		Relative Errors (%)	
	Low Volume	Mainline	Low Volume	Mainline
Average	3.81	5.84	4.66	3.04
Standard Deviation	11.18	11.18	12.33	5.82
Minimum	-30.23	-37.08	-24.67	-25.39
25th percentile	-3.30	-1.27	-3.23	-0.65
Median	3.05	6.10	3.33	2.97
75th percentile	10.41	12.7	10.33	6.61
Maximum	50.8	75.44	66.67	38.32
Count	888	1540	888	1540

Table 4.2 Low Volume Versus Mainline Statistics

From these summaries, it appears that the relative error of the Low Volume road is much more variable than that of the Mainline. It is conjectured that this is due to the smaller design thickness of low volume sections.

Correlation Between Lanes.

Figures 4.4 and 4.5 show the means and the standard deviation of the errors, comparing the south lane and the north lane for each section.

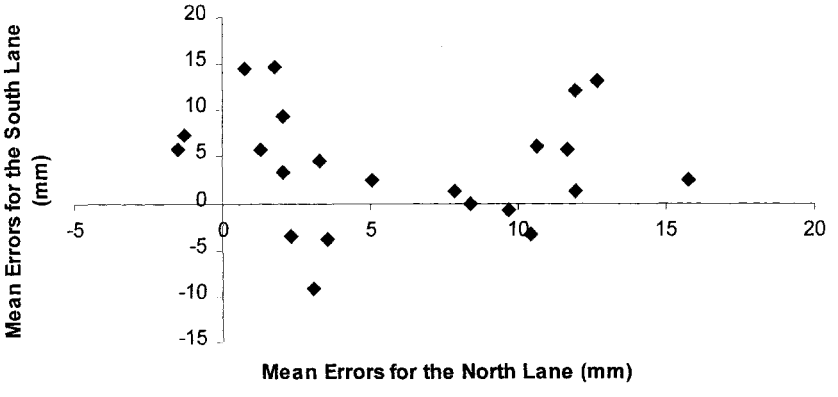

Figure 4.4 Section-By-Section Mean Error Plot Comparing the North Lanes With the South Lanes

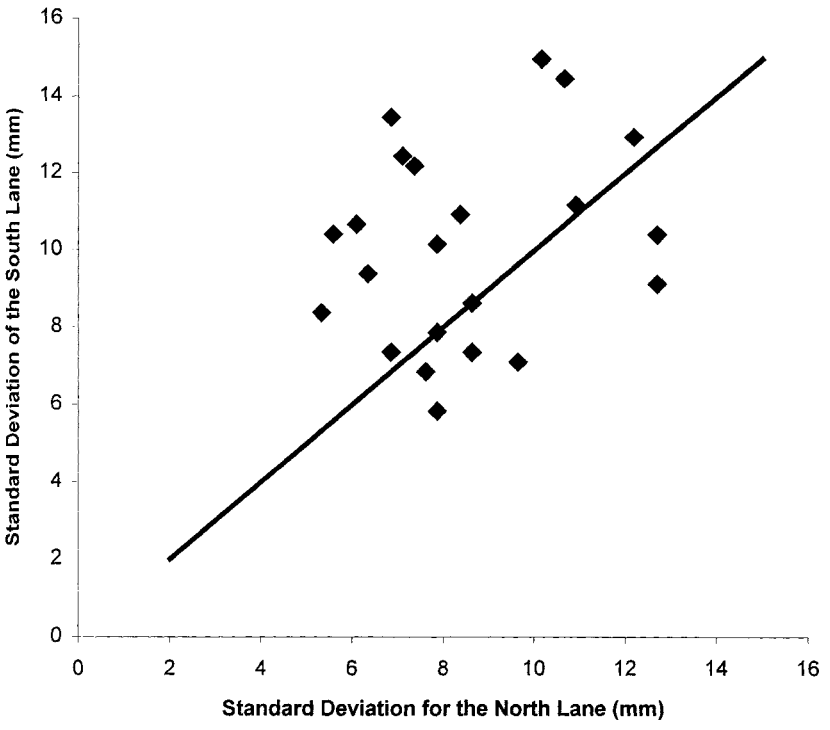

Figure 4.5 Section-by-Section Error Standard Deviation Plot Comparing the North Lanes With the South Lanes

There is no apparent correlation between the north lane and the south lane errors; furthermore, both lanes appear to have about the same level of variability. This observation justifies a lane-by-lane analysis.

Lane-By-Lane Statistics

Tables 4.3 and 4.4 show the statistics for errors on a section-by-section basis.

Section	Mean	Std Dev	Min	25%-tile	Median	75%-tile	Max
24, north	3.3	10.9	-12.2	-4.3	1.5	9.4	41.7
24, south	4.6	11.2	-13.5	-2.5	3.6	12.4	28.4
25, north	2.0	6.9	-11.7	-2.8	1.8	6.9	16.5
25, south	9.4	13.5	-16.8	0.5	9.9	18.5	37.6
26, north	3.0	8.6	-18.5	-2.0	2.8	9.4	20.6
26, south	-9.1	8.6	-30.2	-13.7	-9.7	-3.6	10.7
27, north	0.8	10.7	-18.8	-6.6	0.5	7.9	22.9
27, south	14.5	14.5	-13.2	5.8	12.4	18.0	50.8
28, north	-1.3	5.3	-15.5	-4.3	-0.8	2.0	14.5
28, south	7.4	8.4	-14.0	2.0	7.1	12.2	24.6
29, north	-1.5	7.9	-15.0	-7.9	-1.5	4.6	14.2
29, south	5.8	7.9	-13.2	-0.8	6.4	10.9	19.8
30, north	1.3	6.1	-13.2	-3.0	1.5	5.8	13.0
30, south	5.8	10.7	-19.6	-2.0	7.6	15.7	20.3
31, north	1.8	5.6	-10.7	-2.0	1.8	6.1	14.0
31, south	14.7	10.4	-6.6	7.9	13.0	19.6	48.0

Table 4.3 Errors for the Low Volume Sections (mm)

Section	Mean	Std Dev	Min	25%-tile	Median	75%-tile	Max
1, north	5.1	7.1	-7.9	0.0	4.3	9.4	22.4
1, south	2.5	12.4	-27.2	-6.6	4.3	10.9	29.0
2, north	11.7	7.9	-3.0	4.6	11.9	17.3	28.2
2, south	5.8	10.2	-37.1	-0.3	5.3	13.2	24.1
3, north	12.7	7.9	-3.8	8.6	12.2	16.8	40.9
3, south	13.2	5.8	-5.3	10.4	13.0	17.0	25.9
4, north	10.7	12.7	-15.2	3.3	7.9	16.5	47.0
4, south	6.1	9.1	-20.8	2.0	7.9	12.2	21.8
14, north	7.9	8.6	-11.4	2.3	7.6	14.5	26.7
14, south	1.3	7.4	-19.1	-1.8	1.5	7.1	14.0
15, north	15.7	7.4	-1.5	11.2	15.5	19.6	34.3
15, south	2.5	12.2	-19.8	-6.9	1.0	9.9	40.6
16, north	11.9	7.6	-4.6	7.1	11.4	16.3	30.2
16, south	1.3	6.9	-15.0	-3.0	0.8	5.6	17.5
17, north	9.7	9.7	-29.0	4.8	9.7	15.5	30.2
17, south	-0.8	7.1	-15.7	-5.8	-0.5	4.1	17.0
18, north	10.4	6.4	-4.8	6.9	9.4	14.2	24.6
18, south	-3.3	9.4	-27.4	-9.7	-2.8	4.6	16.3
19, north	8.4	12.7	-30.7	2.5	10.7	17.5	26.7
19, south	0.0	10.4	-17.8	-7.4	0.0	5.3	31.8
20, north	3.6	8.4	-23.9	-0.5	5.3	9.1	22.9
20, south	-3.8	10.9	-26.9	-12.2	-3.8	3.8	18.0
21, north	2.3	6.9	-14.5	-2.3	1.5	7.4	15.5
21, south	-3.6	7.4	-19.6	-8.4	-4.3	1.8	17.3
22, north	2.0	10.2	-15.0	-5.3	0.0	8.1	34.5
22, south	3.3	15.0	-15.0	-8.4	2.5	9.1	75.4
23, north	11.9	12.2	-18.5	4.3	10.2	15.5	42.9
23, south	12.2	13.0	-13.5	7.9	13.0	17.5	49.5

Table 4.4 Errors for the Mainline Sections (mm)

Tables 4.5 and 4.6 show the statistics for the relative errors on a section-by-section basis.

Section	Mean	Std Dev	Min	25%-tile	Median	75%-tile	Max
24, north	4.3	14.4	-16.0	-4.8	3.3	14.8	54.7
24, south	6.2	14.6	-17.7	-3.4	4.5	16.2	37.3
25, north	1.5	5.4	-9.2	-2.2	1.4	5.3	13.0
25, south	7.4	10.6	-13.2	0.5	7.8	14.6	29.6
26, north	2.0	5.7	-12.2	-1.3	1.8	6.1	13.5
26, south	-6.0	5.7	-19.8	-9.0	-6.3	-2.3	7.0
27, north	0.9	14.1	-24.7	-8.5	0.8	10.3	30.0
27, south	19.0	19.0	-17.3	7.6	16.2	23.6	66.7
28, north	-1.6	6.8	-20.3	-5.5	-1.0	2.5	19.0
28, south	9.6	11.1	-17.7	-3.4	4.5	16.0	32.3
29, north	-1.2	6.2	-11.8	-6.1	-1.2	3.6	11.2
29, south	4.6	6.1	-10.4	-0.7	4.9	8.6	15.6
30, north	0.9	4.8	-10.4	-2.3	1.2	4.5	10.2
30, south	4.5	8.3	-15.4	-1.7	5.9	12.4	16.0
31, north	2.5	7.5	-14.0	-2.5	2.3	8.0	18.3
31, south	19.2	13.7	-8.7	10.3	17.0	25.7	63.0

Table 4.5 Relative Errors for the Low Volume Sections (%)

Section	Mean	Std Dev	Min	25%-tile	Median	75%-tile	Max
1, north	3.5	4.9	-5.4	0.1	2.9	6.4	15.3
1, south	1.7	8.5	-18.6	-4.4	3.0	7.5	19.8
2, north	8.0	5.4	-2.1	3.0	8.2	11.7	19.3
2, south	4.0	7.0	-25.4	-0.2	3.6	9.0	16.5
3, north	8.7	5.4	-2.6	5.8	8.4	11.5	28.0
3, south	9.1	4.1	-3.7	7.0	8.9	11.7	17.7
4, north	4.8	5.8	-6.9	1.5	3.5	7.4	21.1
4, south	2.8	4.1	-9.4	0.9	3.5	5.5	9.8
14, north	2.9	3.2	-4.2	0.8	2.8	5.3	9.8
14, south	0.5	2.7	-7.0	-0.7	0.6	2.6	5.1
15, north	5.8	2.7	-0.6	4.1	5.7	7.2	12.6
15, south	0.9	4.5	-7.3	-2.5	0.4	3.6	14.9
16, north	6.1	3.9	-2.3	3.6	5.8	8.2	15.4
16, south	0.7	3.4	-7.6	-1.5	0.5	2.8	7.2
17, north	4.9	4.9	-14.7	2.5	4.9	7.9	15.4
17, south	-0.4	3.6	-8.0	-2.9	-0.3	2.0	8.7
18, north	5.3	3.2	-2.5	3.5	4.8	7.2	12.5
18, south	-1.7	4.8	-13.9	-4.9	-1.4	2.3	8.3
19, north	4.3	6.5	-15.6	1.2	5.4	8.8	13.6
19, south	0.1	5.3	-9.0	-3.8	0.0	2.7	16.1
20, north	1.8	4.2	-12.1	-0.3	2.7	4.7	11.6
20, south	-1.9	5.5	-13.7	-6.1	-1.9	1.9	9.2
21, north	1.2	3.4	-7.4	-1.1	0.8	3.7	7.9
21, south	-1.8	3.8	-9.9	-4.3	-2.2	0.9	8.8
22, north	1.0	5.2	-7.6	-2.7	0.0	4.1	17.6
22, south	1.7	7.6	-7.6	-4.2	1.3	4.7	38.3
23, north	5.3	5.5	-8.3	1.9	4.6	7.0	19.3
23, south	5.5	5.9	-6.1	3.5	5.8	7.9	22.3

Table 4.6 Relative Errors for the Mainline Sections (%)

The absolute errors have a consistent mean and a consistent standard deviation throughout all of the sections, whereas the relative errors are much more variable between the low volume road and the mainline sections.

Construction Errors and Bias

The average error over all sections is about 5.08 mm (0.2 inches). Thus, on average the actual pavement thickness is slightly thicker than the design requires. The standard deviation of the error over all sections is about 11.18 mm, (0.44 inches) which (together with the average error) indicates that a significant fraction of the errors are negative.

Mismatches between the actual thickness and the design thickness can become critical when the actual thickness is significantly less than the design thickness; in this situation, the performance of pavement can be affected by the mismatch. Figures 4.6, 4.7 and 4.8 show box plots of errors for each section. (A box plot shows the 25 percentile and the 75 percentile at the bottom and top of the boxes, along with the minimum and maximum at the bottom and the top of the line emanating from the boxes.) These box plots are meaningful because they give a graphical insight into the distribution of errors.

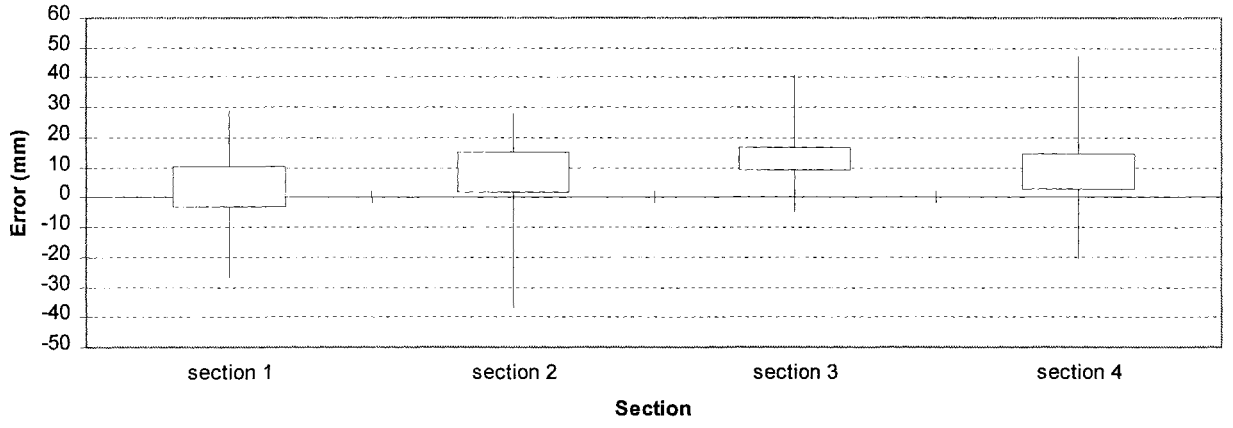

Figure 4.6 Box Plots of the Errors for the Mainline 5-year Asphalt Sections

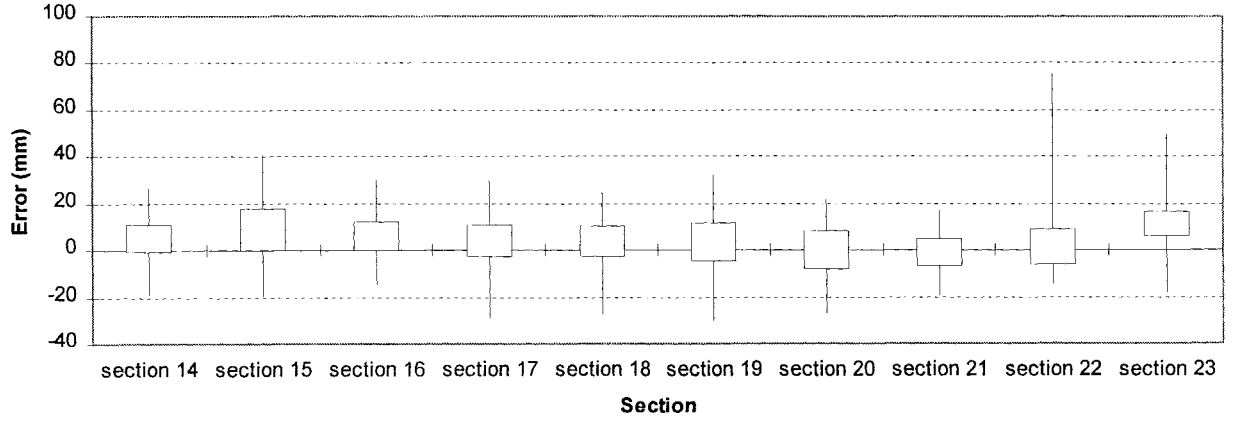

Figure 4.7 Box Plots of the Errors for the Mainline 10-year Asphalt Sections

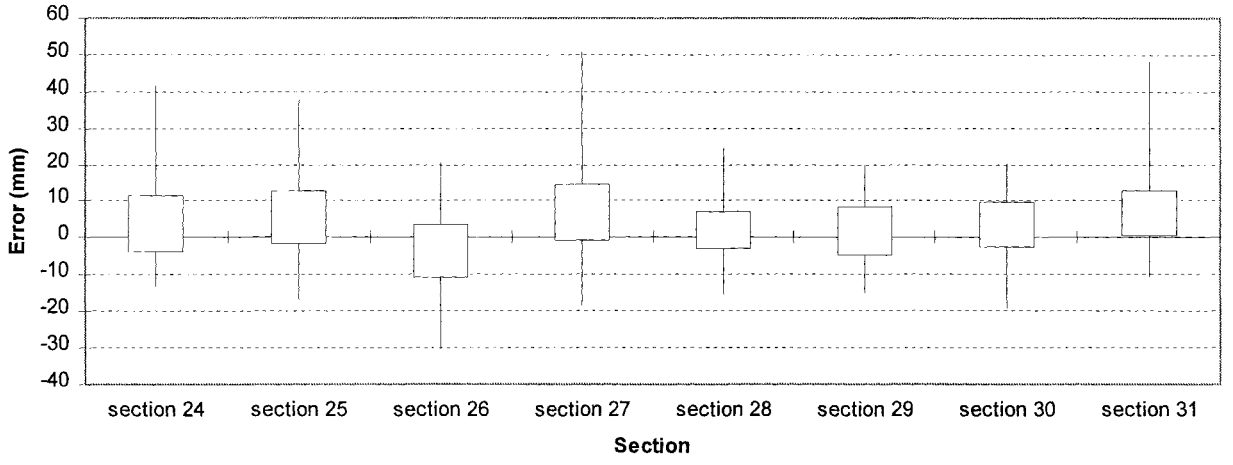

Figure 4.8 Box Plots of the Errors for the Low Volume Sections

Sections which tend to have negative errors have to be dealt with most carefully. In these situations the pavement thickness is less than the design thickness. For example, more than half of the thickness measurements in Section 26 of the low volume road fall below the design thickness. While the magnitude of the errors is relatively small, there is a clear bias and the long-term performance of this section can be expected to suffer. Sections 20, 21, 22, and 29 also have a significant proportion of their thickness measurements falling below their design.

Furthermore, even sections whose measurements exceed the design thickness in a significant majority of the cases may suffer. For example, more than 75 percent of the thickness measurements in Section 2 (see Figure 4.6) are above the design thickness, but at least one measured thickness is 3.5 cm (about one and a half inches) too thin.

Errors in the constructed pavement thickness is a potential source of adverse pavement performance, and should be considered when developing design methodologies and guidelines. A simple "factor of safety" could be incorporated to account for this apparent bias: for example, one could always add 1 cm of thickness beyond the mechanistically required design thickness. However, such an approach does not account for the potential impact of such errors on the pavement performance.

Nonetheless, 21 out of 22 sections have at least one location where the constructed thickness is at least 1 cm less than the design thickness. For 15 out of 22 sections at least 25 percent of the measurements (25 percent of the area) fall below the design thickness. And, for 3 sections out of 22 the median thickness is below the design thickness (i.e. more than half of the area).

Such shortfalls in the constructed thickness are significant and potentially serious. This issue warrants further consideration with a focus on two particular issues. First, can construction practices be modified to minimize the area of occurrence and magnitudes of such overly thin sections? Second, how should a mechanistic design account for such ubiquitous thin sections within a pavement reliability methodology?

SPATIAL ANALYSIS

The spatial statistical analysis consists of analyzing the spatial continuity of the data in order to identify some potential spatial correlation between the data. This analysis is carried out by computing the error variograms for every lane and every section. The variogram plots the average difference squared (ordinate) for spatially separated measurements versus the separation distance (abscissa). Thus, the variogram is a presentation of "dis-similarity" as a function of separation: two neighboring measurements are (on the average) more similar than two relatively distant measurements. (See [1], [2], or [3] for a detailed introduction and disccussion on variograms and spatial data analysis.)

The computation of the individual section variograms resulted in 44 variograms of about 55 data each (so about 1400 pairs). With so few pairs the interpretation of the individual variograms is problematic.

Furthermore, the spatial continuity of all sections is quite similar. As such, a summary variogram for all the sections is computed in order to identify and characterize the "average"

behavior of a lane. This variogram is computed with all the data; thus, each plotting point of the variogram is calculated with at least a 1000 pairs of data.

The resulting experimental variogram and a fitted model are presented in Figure 4.9. This variogram show and unambiguous form and shape allowing clear and specific interpretation. The parameters for the fitted model are:

Nugget Effect:	none
Model Type:	Exponential
Sill:	69.67 mm^2
Correlation Length:	7.62 m

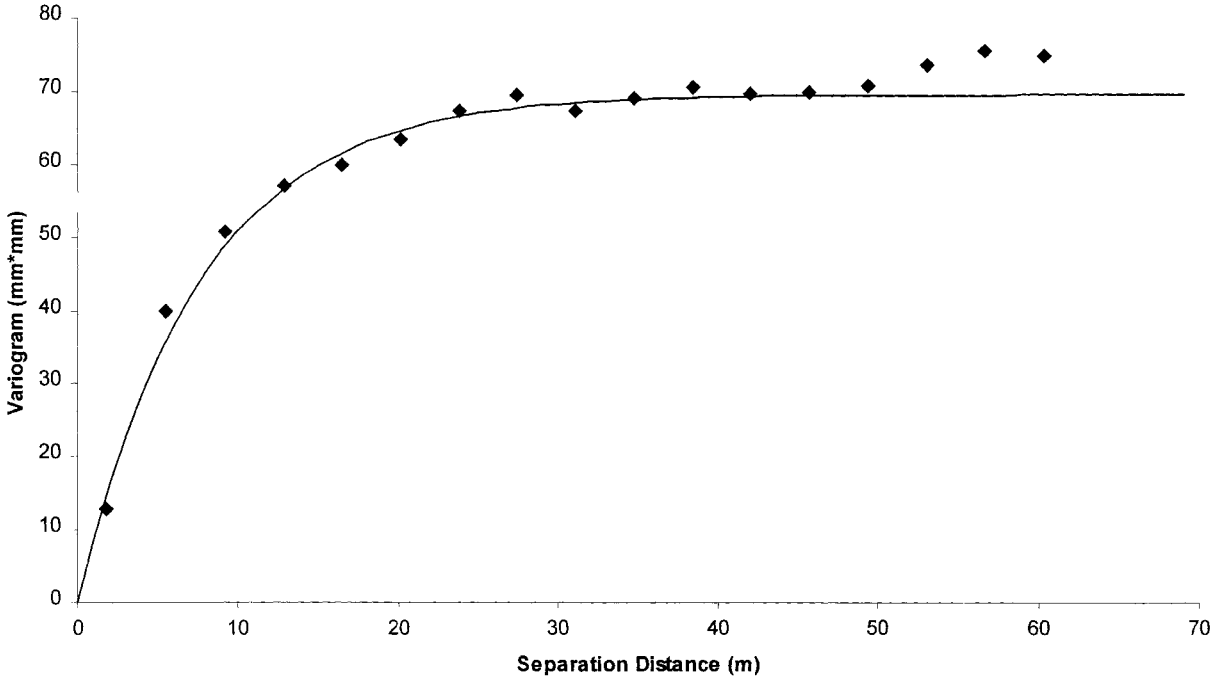

Figure 4.9 Variogram of Errors for All Sections

An immediate application of this correlation length is a maximum sample spacing when characterizing the *as-built* pavement thickness. For example, if measurements are taken at a separation distance greater than twice the correlation length (15 m), then there will be areas in between measurements that are uncorrelated with the available data. Recommended sample spacing would be between 4 and 8 m, depending on the required level of local certainty.

The lack of a *nugget effect* also has some practical significance. No significant short scale variability implies that the GPR provides consistent and reliable measurements. This observation reinforces the assessment of GPR data as *highly reliable*.

CHAPTER 5

ANALYSIS OF FWD DATA

STIFFNESS MEASURES

Six different, but highly correlated measures of pavement stiffness are considered in this analysis.

- Subgrade Modulus [4]
- Structural Number [4]
- Granular Equivalent [6]
- Benkelman Beam at 80° [5]
- Spring Benkelman Beam [5]
- Deflection Basin Area

Each of these measures is computed from falling weight deflectometer measurements. (The deflection basin area was computed using a normalized trapezoidal rule.)

RAW DATA SUMMARY

This section presents the basic statistical measures for each of the six parameters that are computed from FWD measurements. For each measure and each section this table presents the average value, coefficient of variations and data count. The data that are represented in this table are all available data. Note that the data count for the Benkelman Beam with spring correction (referred to as the Spring Benkelman Beam) is less than for other parameters. This is because the spring correction is not available for all records.

In tables 5.2 and 5.2 (and in all subsequent tables) the coefficient of variation, "CV", is defined as the data standard deviation divided by the data mean.

	Modulus (Mpa)			Structural Number			Granular Equivalent		
Section	Average	CV	Count	Average	CV	Count	Average	CV	Count
1	197	0.54	7227	7.1	0.3	7227	50.7	0.3	7227
2	195	0.54	7200	7.2	0.3	7200	51.4	0.3	7200
3	210	0.54	7487	8.19	0.29	7487	58.5	0.29	7487
4	218	1.5	7632	2.74	0.13	7632	19.6	0.13	7632
14	252	1.25	5580	3.51	0.12	5580	25.1	0.12	5580
15	229	1.16	6507	3.71	0.11	6507	26.5	0.11	6507
16	189	0.52	5787	7.86	0.25	5787	56.2	0.25	5787
17	194	0.53	6183	7.69	0.25	6183	54.9	0.25	6183
18	168	0.55	6039	6.44	0.25	6039	46	0.25	6039
19	214	0.52	5868	7.81	0.26	5868	55.8	0.26	5868
20	209	0.56	6363	7.29	0.28	6363	52.1	0.28	6363
21	198	0.53	6804	6.7	0.26	6804	47.8	0.26	6804
22	178	0.79	6822	5.58	0.22	6822	39.9	0.22	6822
23	189	1.1	6255	4.21	0.17	6255	30	0.17	6255
24	146	0.48	10179	1.63	0.14	10179	11.6	0.14	10179
25	138	0.58	10287	1.79	0.14	10287	12.8	0.14	10287
26	149	1.84	10304	1.71	0.17	10304	12.2	0.17	10304
27	103	0.87	10482	2.22	0.16	10482	15.8	0.16	10482
28	113	1.47	10485	2.46	0.22	10485	17.6	0.22	10485
29	118	1.49	10465	2.69	0.22	10465	19.2	0.22	10465
30	138	2.43	10480	3.08	0.2	10480	22	0.2	10480
31	145	1.76	10556	2.94	0.2	10556	21	0.2	10556
ALL	169	1.16	174992	4.32	0.61	174992	30.9	0.61	174992

Table 5.1 Raw Data Summary

	BB at 80° (Mils)			Spring BB (Mils)			Deflection Area (mm)		
Section	Average	CV	Count	Average	CV	Count	Average	CV	Count
1	21.2	0.18	7227	30.5	0.13	3078	620	0.16	7227
2	20	0.18	7200	28.9	0.12	3087	658	0.16	7200
3	19.7	0.17	7487	27.6	0.11	3698	631	0.17	7487
4	19.2	0.27	7632	25.1	0.21	3789	765	0.16	7632
14	14.9	0.2	5580	18.6	0.15	2097	824	0.15	5580
15	14.7	0.2	6507	18	0.16	2979	854	0.14	6507
16	16.5	0.14	5787	22.4	0.1	2268	780	0.13	5787
17	16.7	0.15	6183	23.1	0.12	3087	747	0.14	6183
18	16.8	0.14	6039	23	0.13	2952	775	0.13	6039
19	16.4	0.14	5868	22.3	0.11	2277	754	0.13	5868
20	18.3	0.16	6363	25.8	0.14	3195	682	0.18	6363
21	16.6	0.15	6804	23.4	0.12	3177	711	0.16	6804
22	17.6	0.16	6822	24.6	0.12	3321	705	0.15	6822
23	17.1	0.24	6255	21.3	0.2	3267	778	0.17	6255
24	24.8	0.13	10179	38.6	0.15	4923	500	0.15	10179
25	22.8	0.15	10287	35	0.14	4986	632	0.16	10287
26	32.7	0.49	10304	57.5	0.4	4959	595	0.21	10304
27	38.1	0.23	10482	65.7	0.18	5084	480	0.16	10482
28	38.8	0.23	10485	67.6	0.16	5049	483	0.17	10485
29	32.5	0.29	10465	55.5	0.22	5047	565	0.18	10465
30	28.9	0.24	10480	46.6	0.2	5062	584	0.17	10480
31	34.2	0.19	10556	56.2	0.12	5121	481	0.16	10556
ALL	24.3	0.42	174992	38.2	0.49	82503	640	0.24	174992

Table 5.2 Raw Data Summary (continued)

DATA SUMMARY WITH THRESHOLDS

The data that are represented in Table 5.3 are the data that have passed a simple filtering procedure: for each of the six parameters which are computed from FWD measurements an upper limit is set. Only the data which are below these upper limits are represented in the following table. This simple filtering procedure not only eliminates extreme measurement errors but also some uninteresting physical situations (like frozen soil conditions). The upper limits are set as follows

Parameter	Upper Limit
Subgrade Modulus	500 (Mpa)
Structural Number	15
Granular Equivalent	100
Benkelman Beam at 80°	100 (Mils)
Spring Benkelman Beam	100 (Mils)
Deflection Basin Area	1,500 (mm)

Table 5.3 Parameters and Limits

	Modulus (Mpa)			Structural Number			Granular Equivalent		
Section	Average	CV	Count	Average	CV	Count	Average	CV	Count
1	177	0.35	7864	6.89	0.17	8152	49	0.15	8113
2	178	0.37	7944	6.96	0.17	8148	49.3	0.14	8076
3	192	0.36	8220	7.81	0.11	8272	55.8	0.11	8270
4	134	0.42	8013	2.78	0.15	8847	19.8	0.15	8847
14	177	0.42	6135	3.56	0.13	6804	25.5	0.13	6804
15	170	0.41	7024	3.76	0.12	7731	26.9	0.12	7731
16	176	0.36	6638	7.5	0.09	6660	53.5	0.09	6660
17	179	0.33	6974	7.49	0.12	7227	53.5	0.12	7227
18	158	0.36	6920	6.33	0.17	7163	44.6	0.1	7087
19	193	0.31	6630	7.56	0.13	6878	53.8	0.12	6852
20	187	0.29	7100	7.09	0.15	7392	50.6	0.15	7386
21	184	0.34	7591	6.56	0.14	7848	46.9	0.14	7848
22	158	0.36	7676	5.6	0.22	8046	39.9	0.21	8039
23	155	0.5	6992	4.27	0.19	7459	30.5	0.19	7459
24	136	0.3	12423	1.62	0.14	12587	11.6	0.14	12587
25	128	0.36	12420	1.8	0.14	12717	12.8	0.14	12717
26	101	0.58	12166	1.72	0.17	12743	12.3	0.17	12743
27	91	0.58	12628	2.22	0.24	12939	15.8	0.24	12939
28	87	0.53	12696	2.45	0.31	13140	17.5	0.31	13140
29	90	0.5	12526	2.69	0.26	12939	19.2	0.26	12939
30	100	0.45	12524	3.09	0.25	12946	22.1	0.25	12946
31	106	0.41	12606	2.94	0.29	13026	21	0.29	13026
ALL	139	0.49	201710	4.18	0.56	209664	29.8	0.56	209436

Table 5.4 Data Summary with Thresholds

	BB at 80° (Mils)			Spring BB (Mils)			Deflection Area (mm)		
Section	Average	CV	Count	Average	CV	Count	Average	CV	Count
1	20.9	0.2	8379	30.3	0.13	3240	622	0.16	8379
2	19.7	0.2	8424	28.7	0.13	3249	659	0.16	8424
3	19.3	0.19	8720	27.3	0.12	3860	637	0.17	8720
4	18.9	0.28	8847	25	0.21	3951	778	0.17	8847
14	14.6	0.21	6804	18.5	0.15	2259	833	0.15	6804
15	14.4	0.2	7731	17.9	0.16	3141	866	0.14	7730
16	16.3	0.16	7020	22.2	0.11	2430	783	0.14	7020
17	16.5	0.17	7407	23	0.12	3249	747	0.14	7407
18	16.5	0.15	7263	22.8	0.14	3105	773	0.13	7263
19	16.2	0.16	7074	22.2	0.11	2421	752	0.13	7073
20	18	0.18	7578	25.6	0.14	3357	685	0.18	7577
21	16.3	0.16	8028	23.2	0.13	3339	713	0.15	8028
22	17.4	0.17	8046	24.4	0.13	3483	703	0.15	8046
23	16.8	0.25	7459	21.1	0.2	3429	788	0.18	7459
24	25	0.13	12587	38.3	0.16	5085	507	0.15	12587
25	22.5	0.15	12717	34.7	0.15	5148	648	0.16	12717
26	31.7	0.45	12689	52.9	0.32	4815	617	0.21	12743
27	38.7	0.25	12939	65.3	0.18	5246	486	0.18	12939
28	40.2	0.27	13140	67.3	0.17	5211	485	0.2	13140
29	32.5	0.29	12939	55.1	0.22	5209	577	0.2	12939
30	29.1	0.25	12946	46.4	0.2	5224	596	0.18	12946
31	35.4	0.23	13026	55.8	0.13	5278	488	0.19	13026
ALL	24.5	0.44	211763	37.5	0.48	85729	645	0.24	211814

Table 5.5 Data Summary with Thresholds (continued)

COMPARISON BETWEEN VARIOUS MEASURES

This section presents the relationships between some of the six FWD parameters. Each data value corresponds to one section. The strongest correlation exists between the Benkelman Beam at 80° and Spring Benkelman Beam (see Figure 5.5). This means that for comparison purposes between sections the spring correction of the Benkelman Beam at 80° is not relevant.

Another interesting correlation exists between the Benkelman Beam parameters and the Deflection Basin Area. It appears that the value of the Deflection Basin Area may be estimated with reasonable precision if Benkelman Beam at 80° or Spring Benkelman beam are available. However, this correlation is not as good as in the previous case and the Deflection Basin Area should be considered as an independent parameter. Similar correlations also exist between the Subgrade Modulus and the Benkelman Beam parameters.

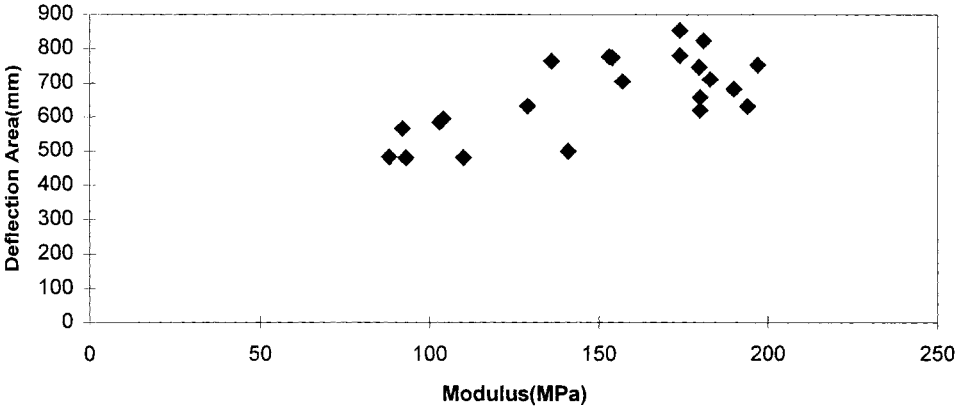

Figure 5.1 Deflection Area Versus Modulus

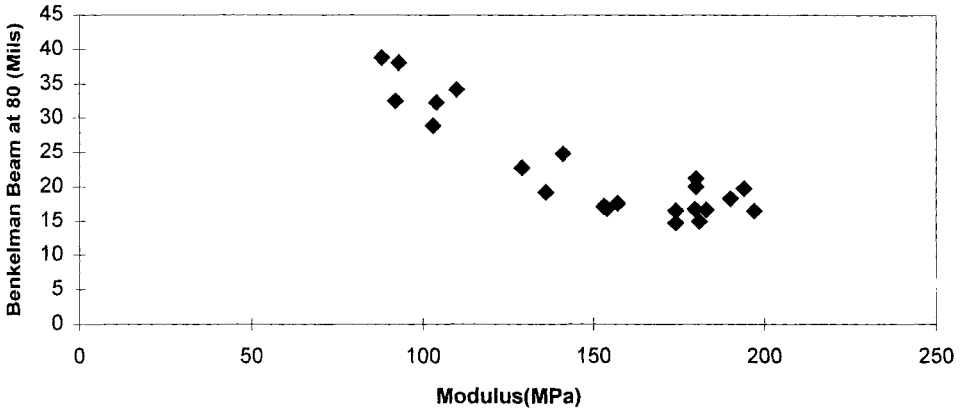

Figure 5.2 Benkelman Beam at 80° Versus Modulus

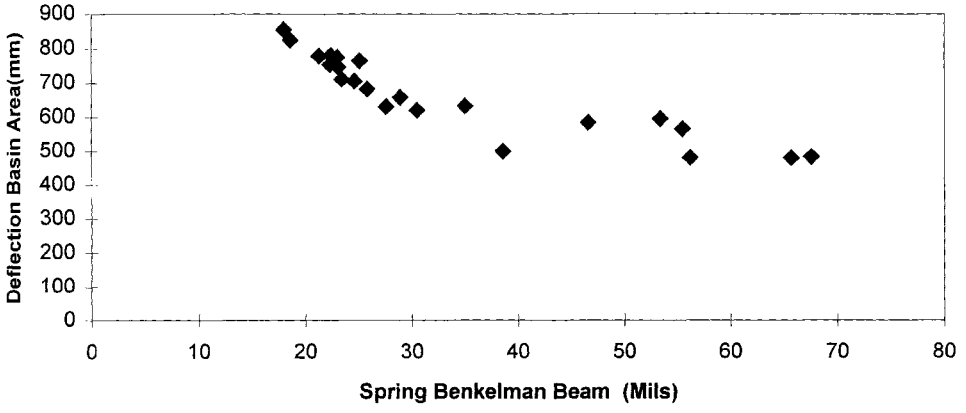

Figure 5.3 Deflection Basin Area Versus Spring Benkelman Beam

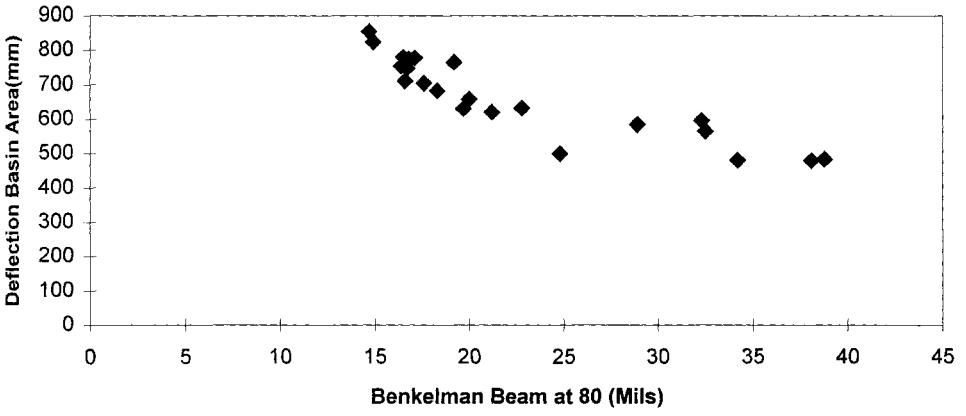

Figure 5.4 Deflection Basin Area Versus Benkelman Beam at 80°

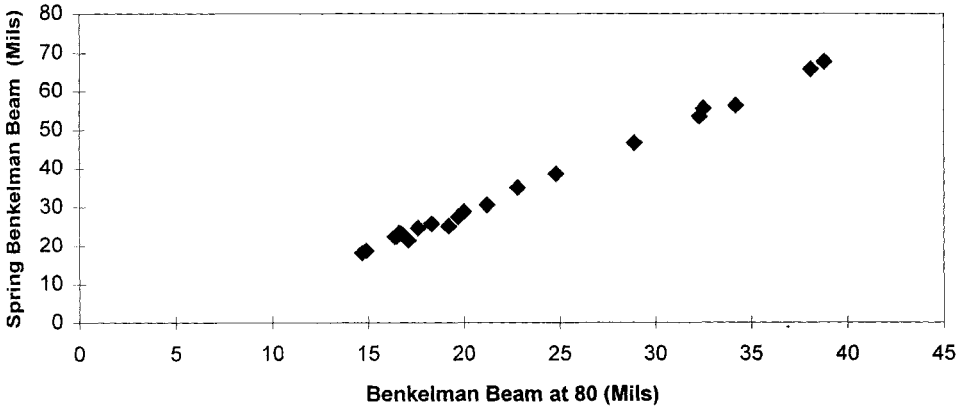

Figure 5.5 Spring Benkelman Beam Versus Benkelman Beam at 80°

SPATIAL ANALYSIS

The spatial analysis is performed for each of the six FWD parameters on the section-by-section basis. The basic tools for use in this analysis are the variograms of these parameters. For each parameter and for all sections, the variograms show a lack of any spatial correlation between the neighboring measurements. This is demonstrated on the variogram plots for the Section 19. The variograms for are other sections are comparable.

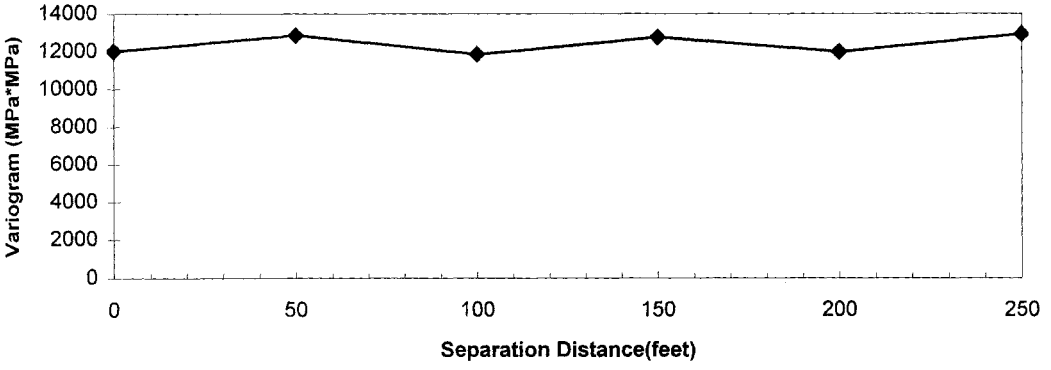

Figure 5.6 Modulus Variogram for Section 19

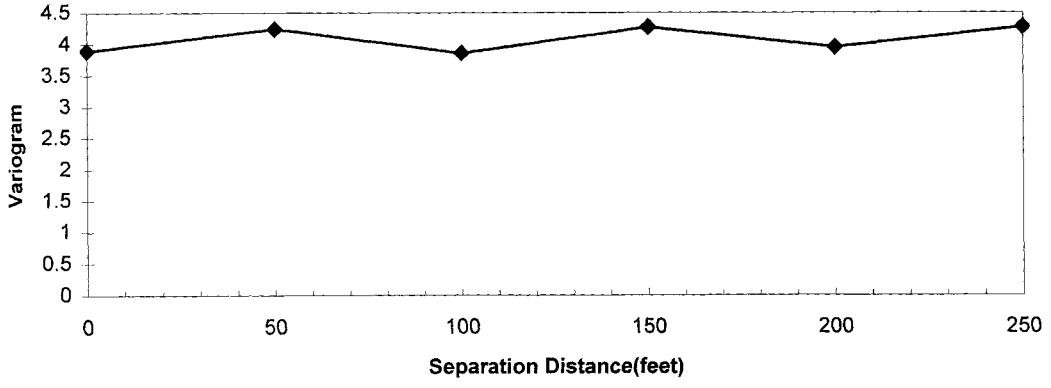

Figure 5.7 Structural Number Variogram for Section 19

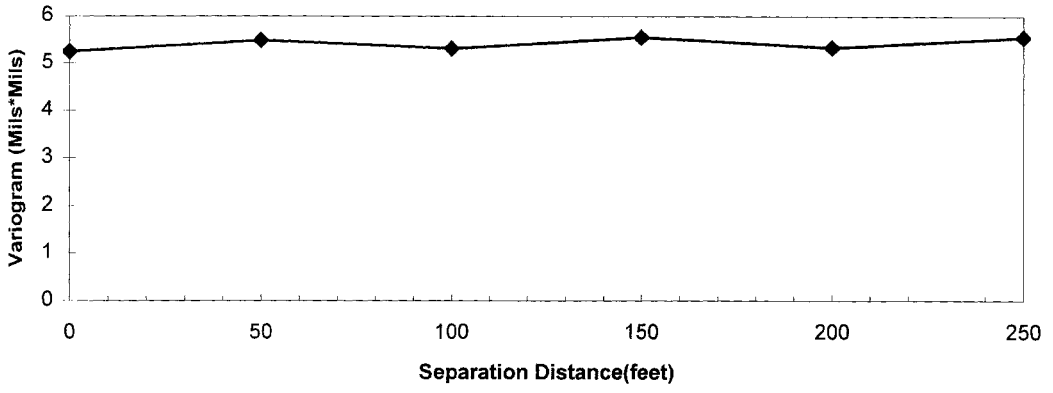

Figure 5.8 Benkelman Beam Variogram for Section 19

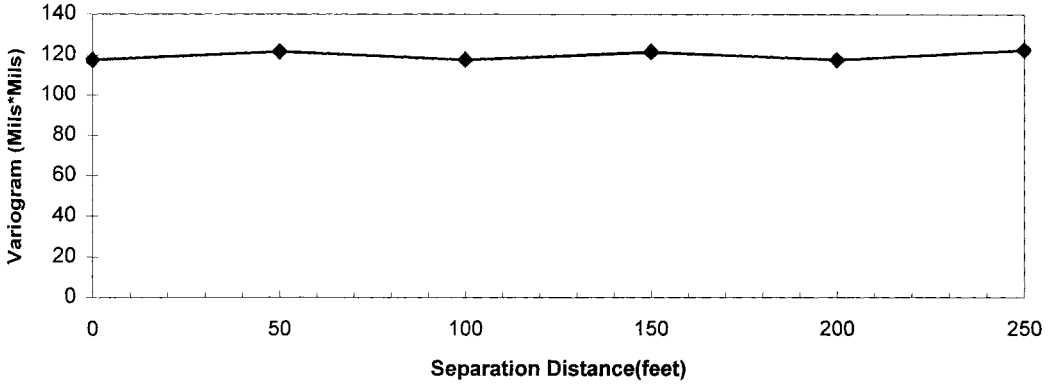

Figure 5.9 Spring Benkelman Beam Variogram for Section 19

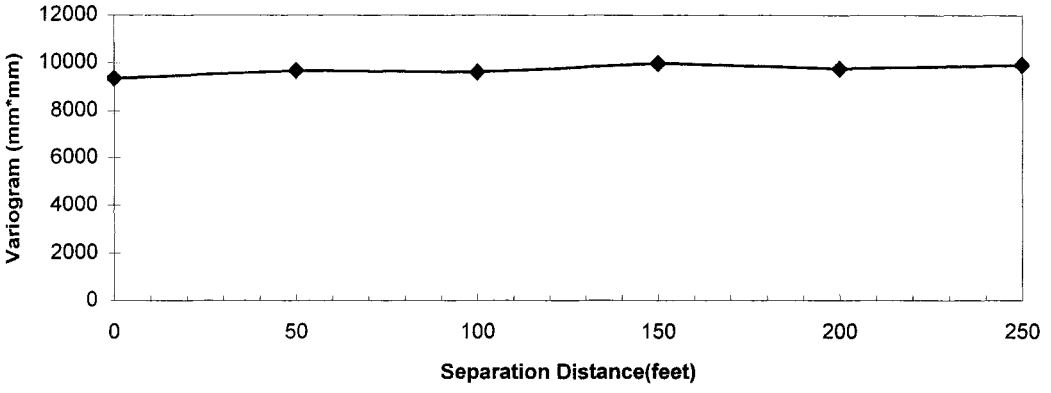

Figure 5.10 Deflection Basin Area Variogram for Section 19

Because of the lack of spatial correlation of FWD parameters, these parameters may be treated as simple random variables of the given mean and standard deviation. The distribution of these parameters appears to follow the lognormal distribution closely.

CHAPTER 6

LOAD AND ENVIRONMENTAL FACTORS

APPLIED LOADS

Tables 6.1 and 6.2 present the summary statistics for the monthly accumulation of the standard *equivalent uniform axle loads* (ESAL). The underlying ESAL computations are based upon the formulae presented in the 1993 AASHTO Guide for Design [4]. Due to the data collection design and censor placement, it is assumed that vehicles entering the test area in Lane 1 remain in Lane 1 along the entire length of the test; similarly, vehicles entering the test area in Lane 2 are assumed to remain in Lane 2.

As can be seen from these summary statistics the applied loads in Lane 1 are significantly higher than the applied load in Lane 2 (about four times higher). This is due to the propensity of the heavier truck traffic to use Lane 1.

The following 14 figures show the time history of the applied loads on the 14 mainline sections under study. These load histories are presented as monthly accumulations. As can be seen from these figures the applied loads are remarkably uniform for each section. Over the period of this study there are no discernable trends or patterns in the applied loads. This is not surprising given the stability of the economy during the study (thus, there are no significant changes in interstate or intrastate haulage patterns).

Section	Minimum	Maximum	Average	Standard Deviation
1	8,135	52,129	37,972	10,860
2	8,120	52,066	37,914	10,846
3	8,313	52,919	38,670	11,033
4	9,031	56,580	41,563	11,775
14	8,641	54,530	39,984	11,365
15	8,585	54,234	39,756	11,307
16	8,322	52,962	38,707	11,042
17	8,334	53,023	38,757	11,054
18	8,225	52,528	38,328	10,947
19	8,334	53,023	38,757	11,054
20	8,360	53,143	38,860	11,080
21	8,211	52,466	38,272	10,934
22	8,214	52,477	38,281	10,936
23	8,424	53,442	39,116	11,144

Table 6.1 Summary Statistics of the Monthly Cumulative ESAL's for Lane 1 (July 1994 through June 1997)

Section	Minimum	Maximum	Average	Standard Deviation
1	2,723	15,776	9,503	3,075
2	2,718	15,744	9,483	3,069
3	2,772	16,103	9,698	3,135
4	2,998	17,564	10,562	3,399
14	2,889	16,864	10,150	3,273
15	2,889	16,864	10,150	3,273
16	2,791	16,225	9,770	3,157
17	2,796	16,253	9,787	3,162
18	2,766	16,057	9,670	3,126
19	2,791	16,225	9,770	3,157
20	2,800	16,281	9,804	3,167
21	2,748	15,940	9,600	3,105
22	2,740	15,888	9,569	3,096
23	2,807	16,325	9,830	3,175

Table 6.2 Summary Statistics of the Monthly Cumulative ESAL's for Lane 2 (July 1994 through June 1997)

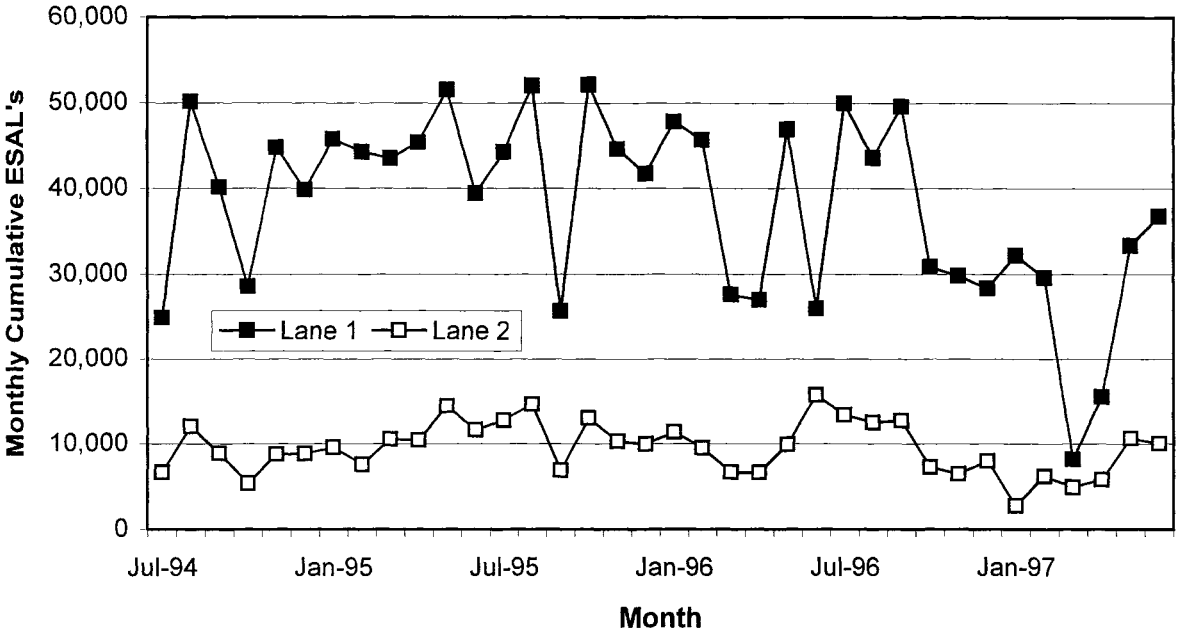

Figure 6.1 ESAL's for Section 1

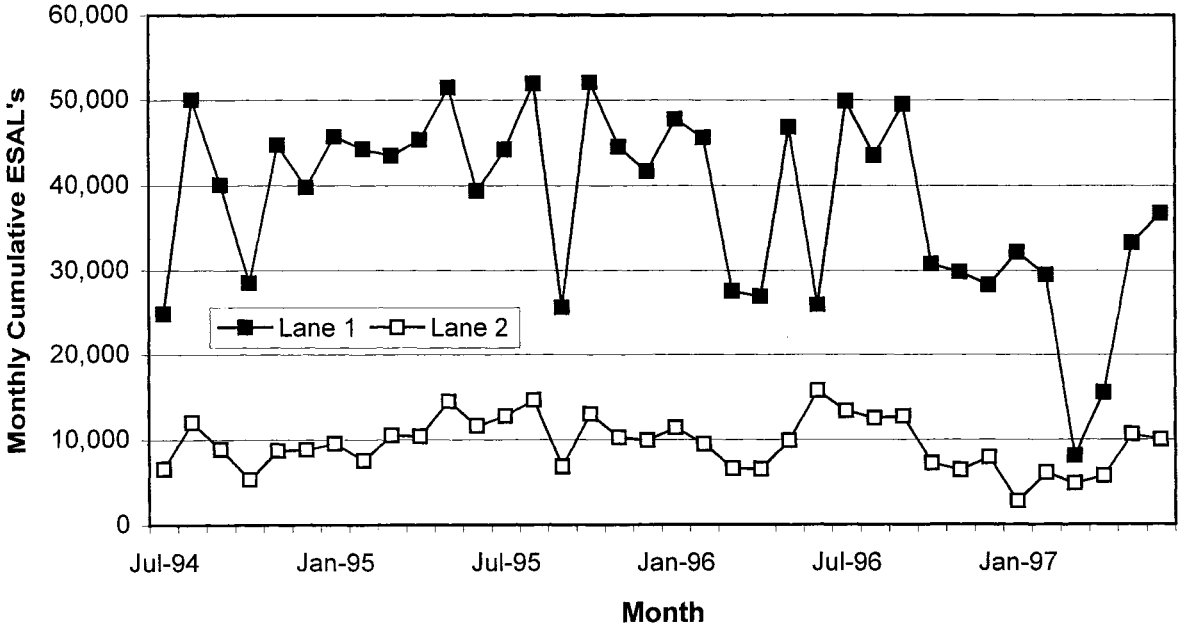

Figure 6.2 ESAL's for Section 2

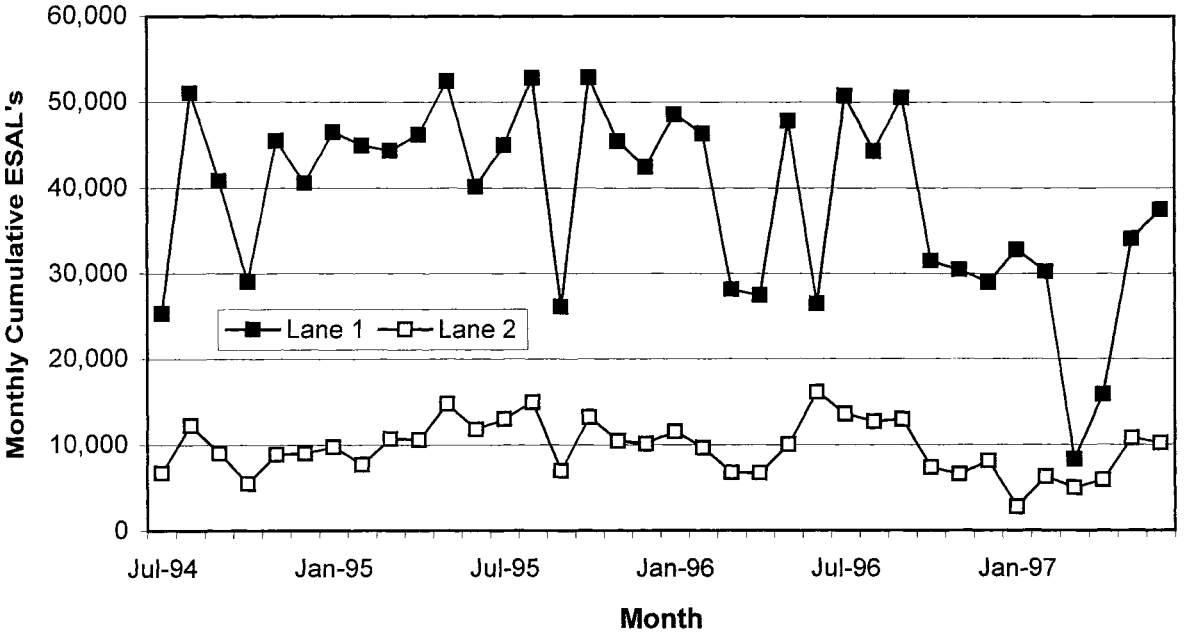

Figure 6.3 ESAL's for Section 3

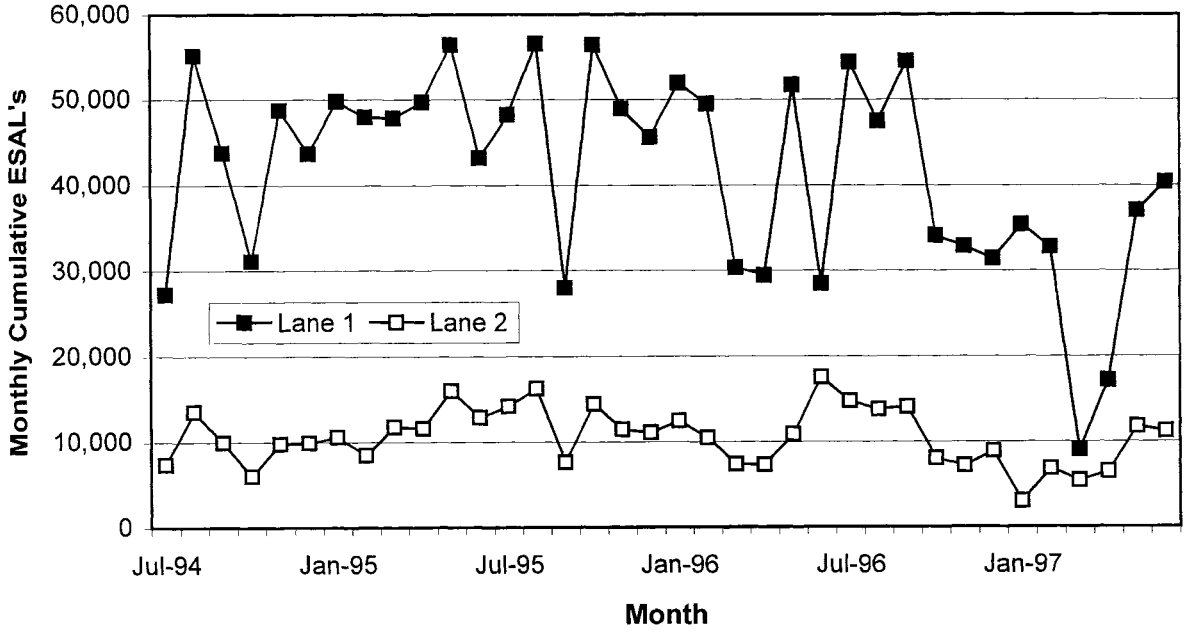

Figure 6.4 ESAL's for Section 4

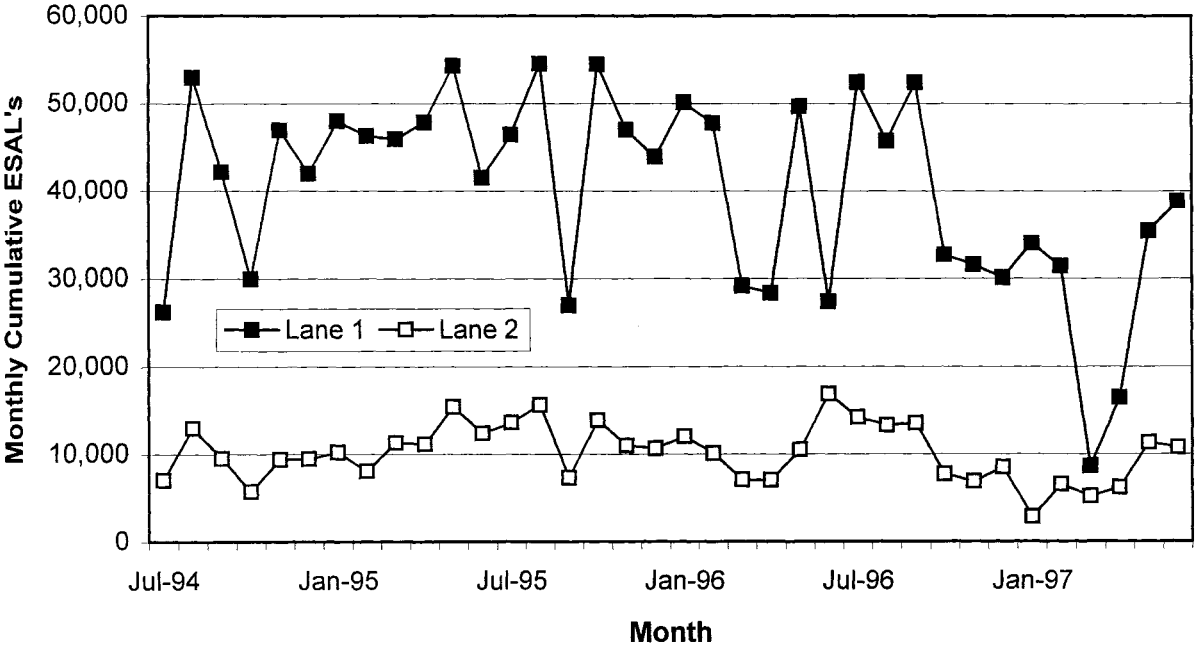

Figure 6.5 ESAL's for Section 14

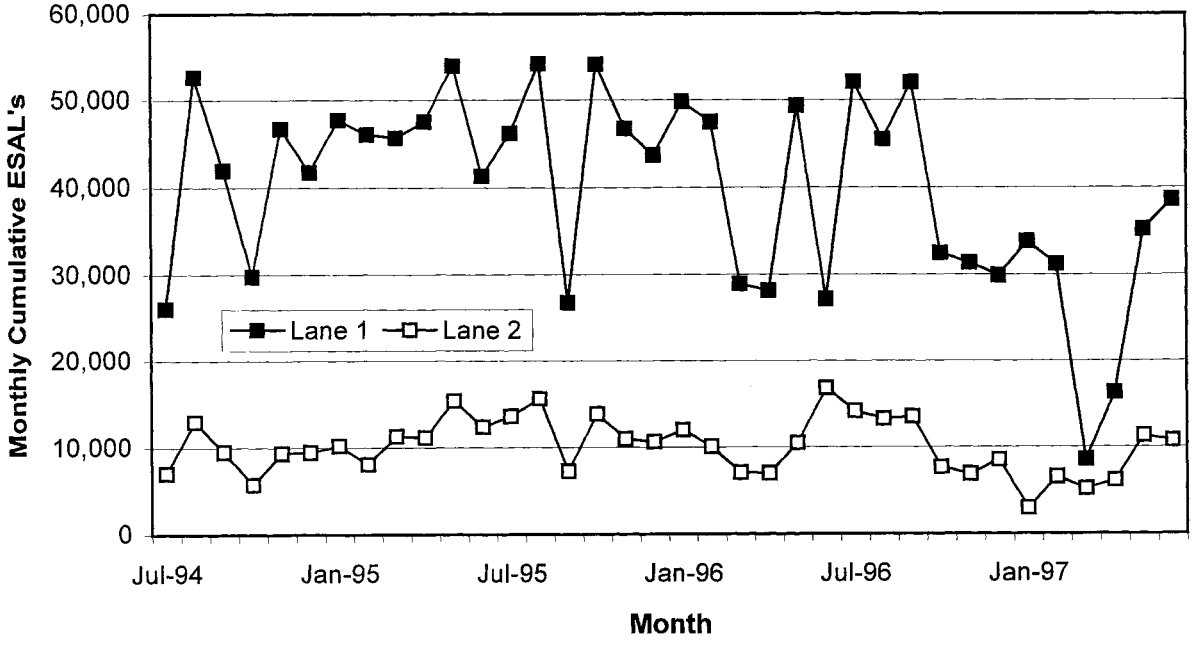

Figure 6.6 ESAL's for Section 15

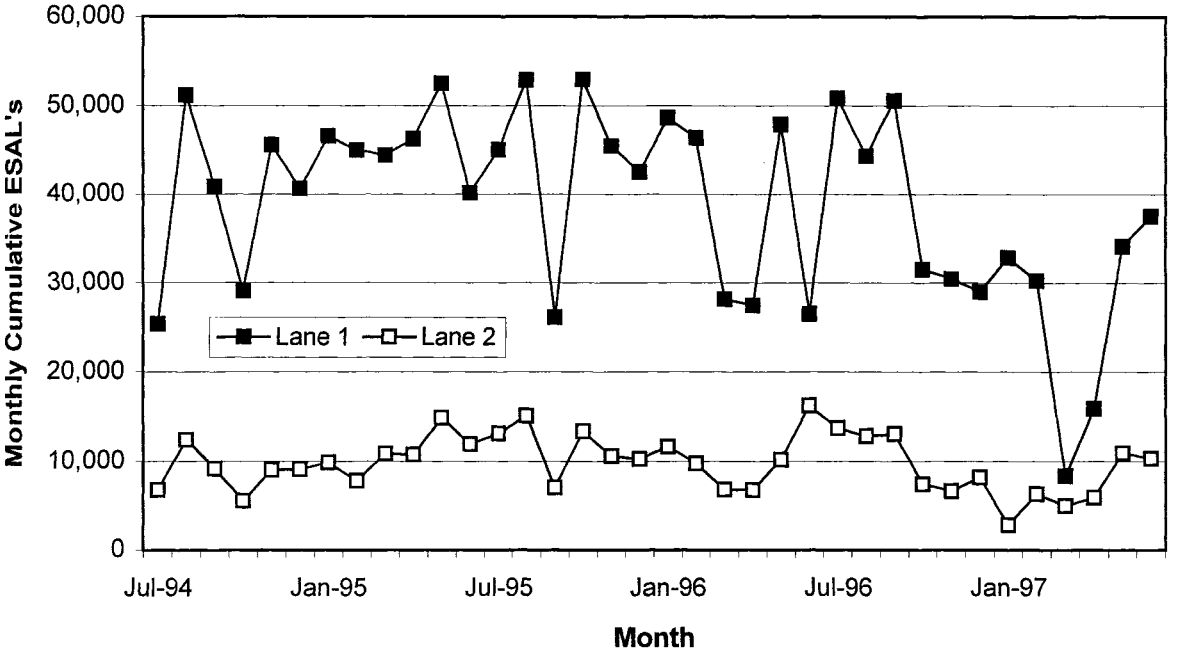

Figure 6.7 ESAL's for Section 16

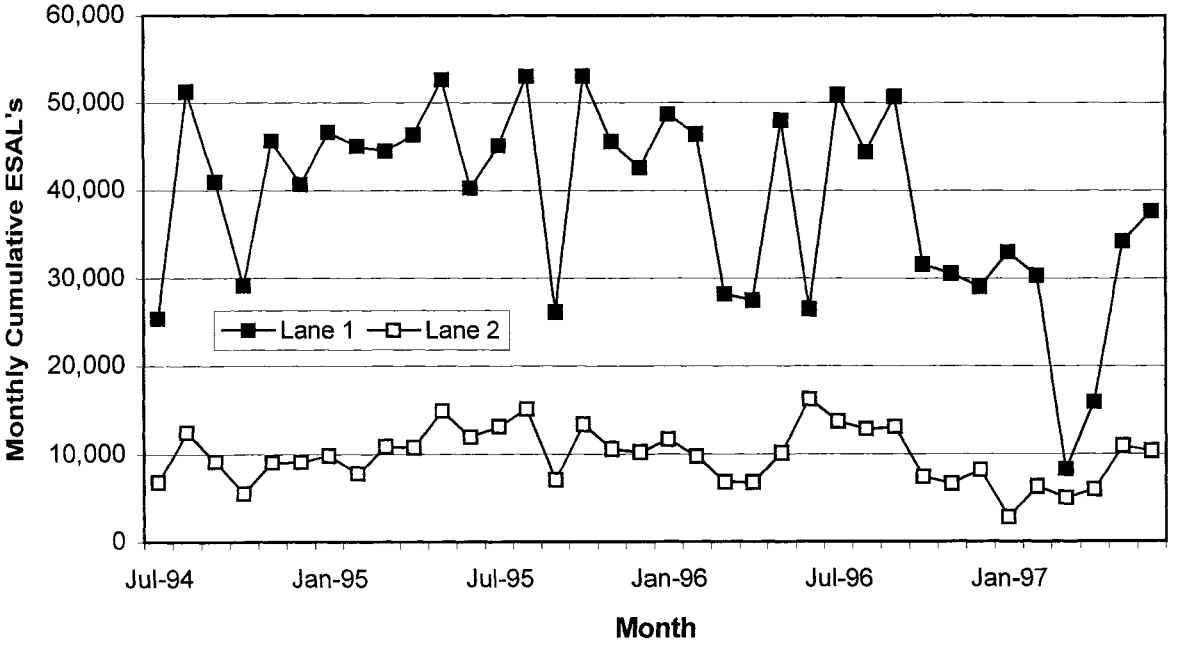

Figure 6.8 ESAL's for Section 17

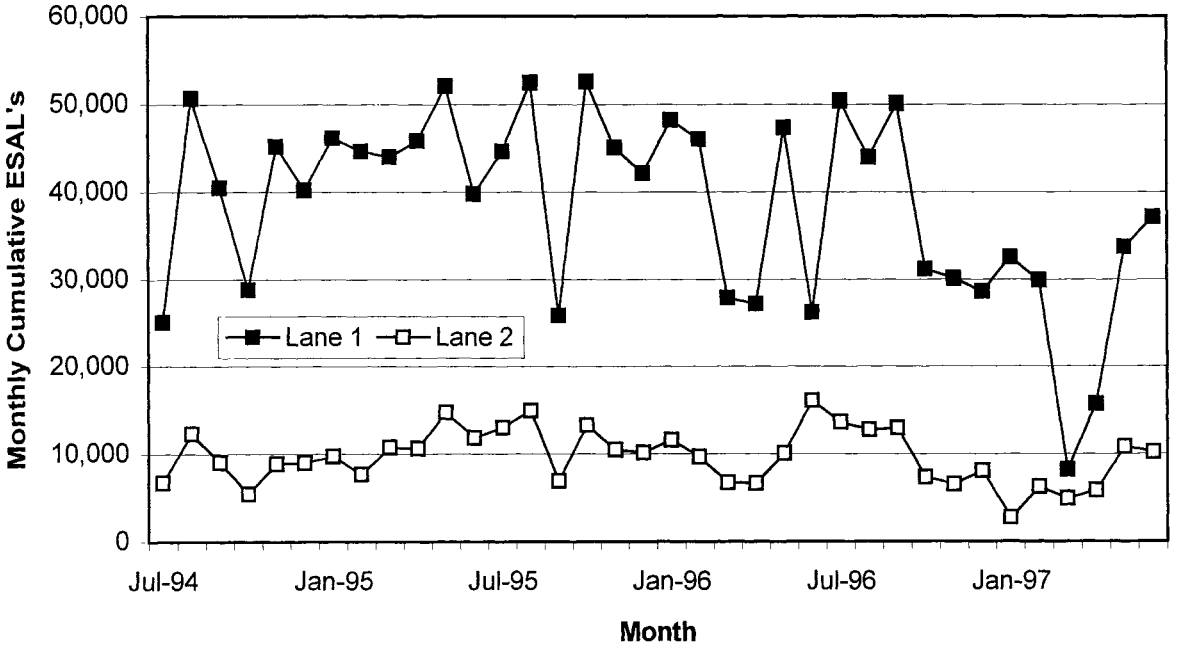

Figure 6.9 ESAL's for Section 18

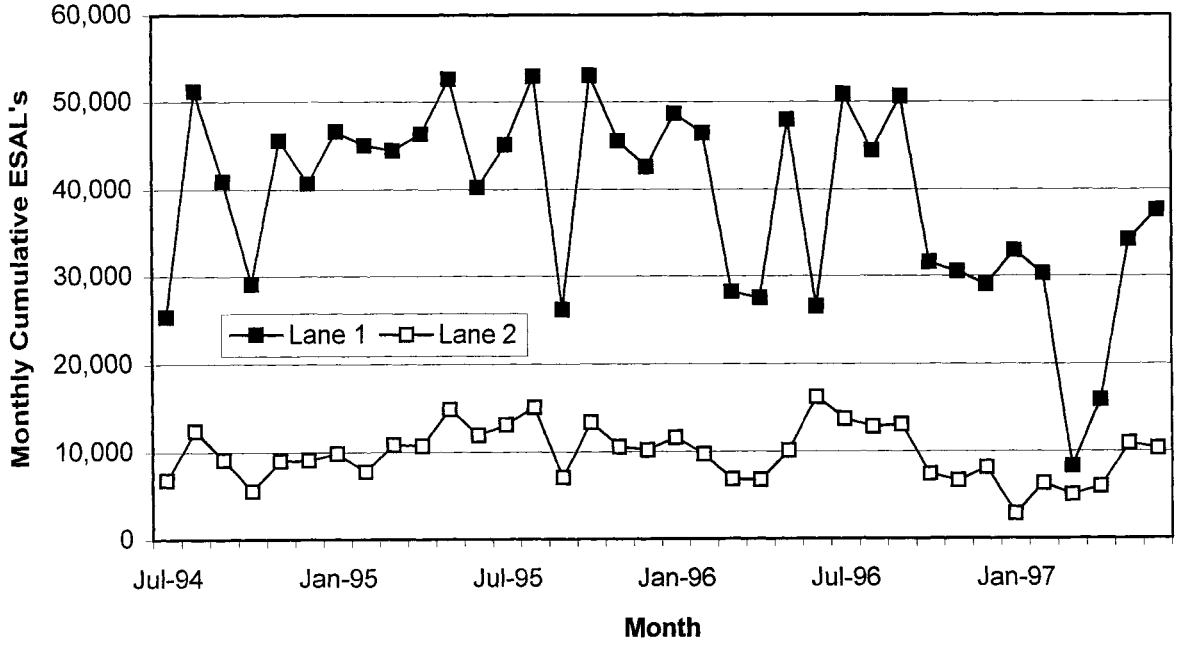

Figure 6.10 ESAL's for Section 19

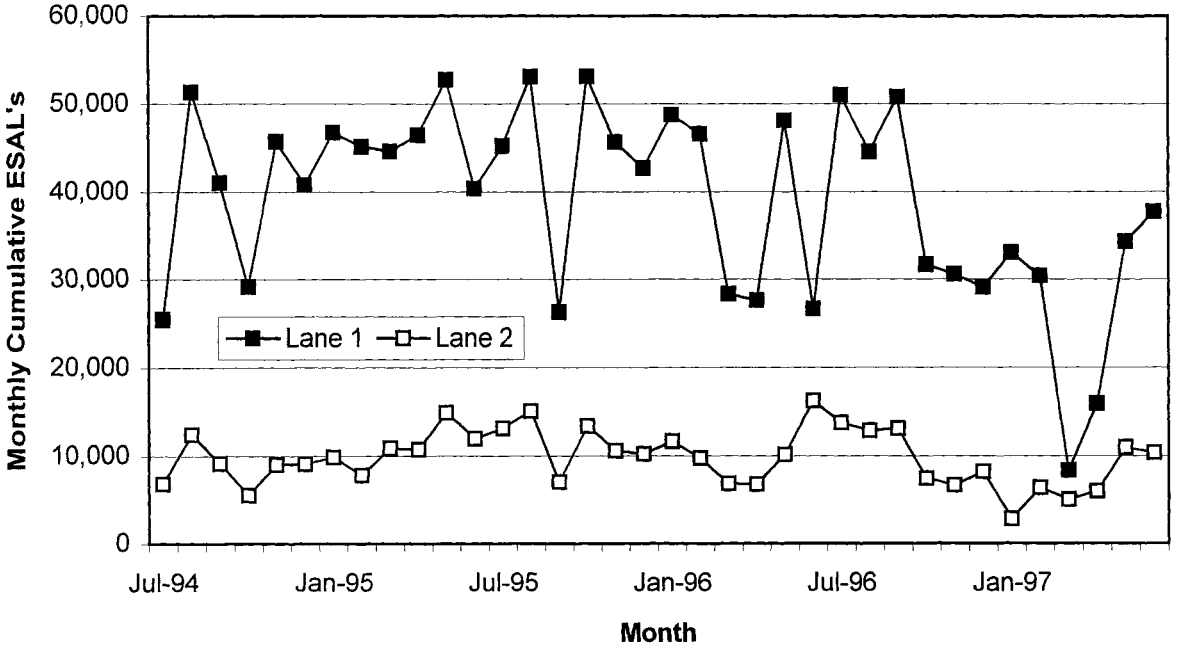

Figure 6.11 ESAL's for Section 20

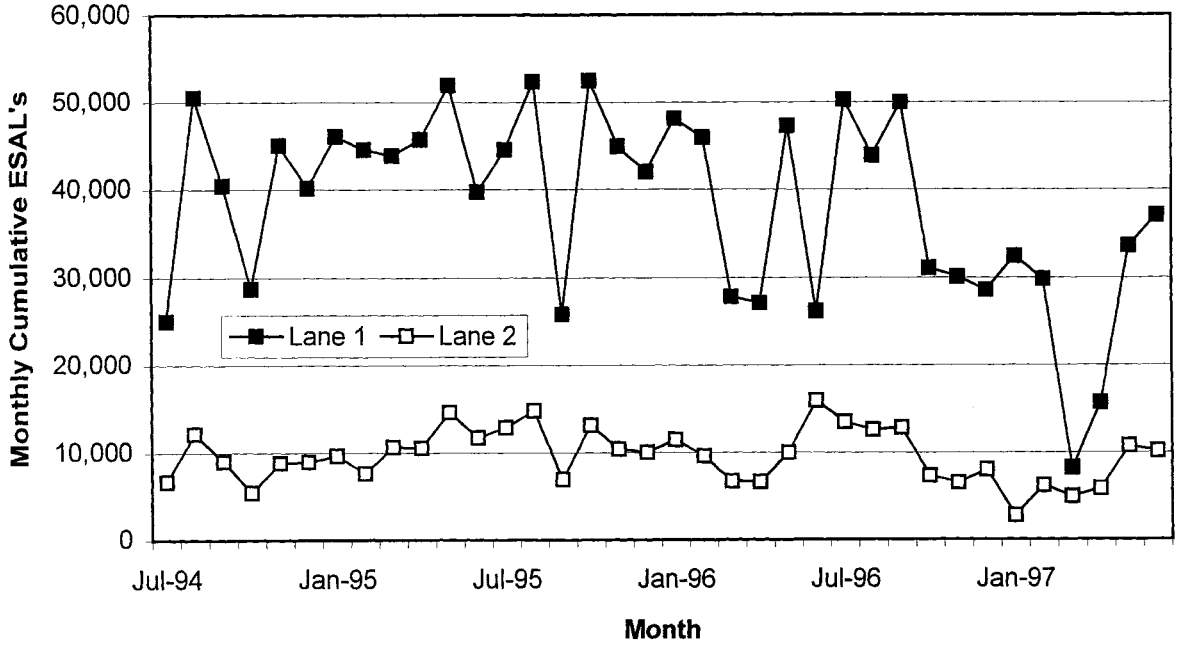

Figure 6.12 ESAL's for Section 21

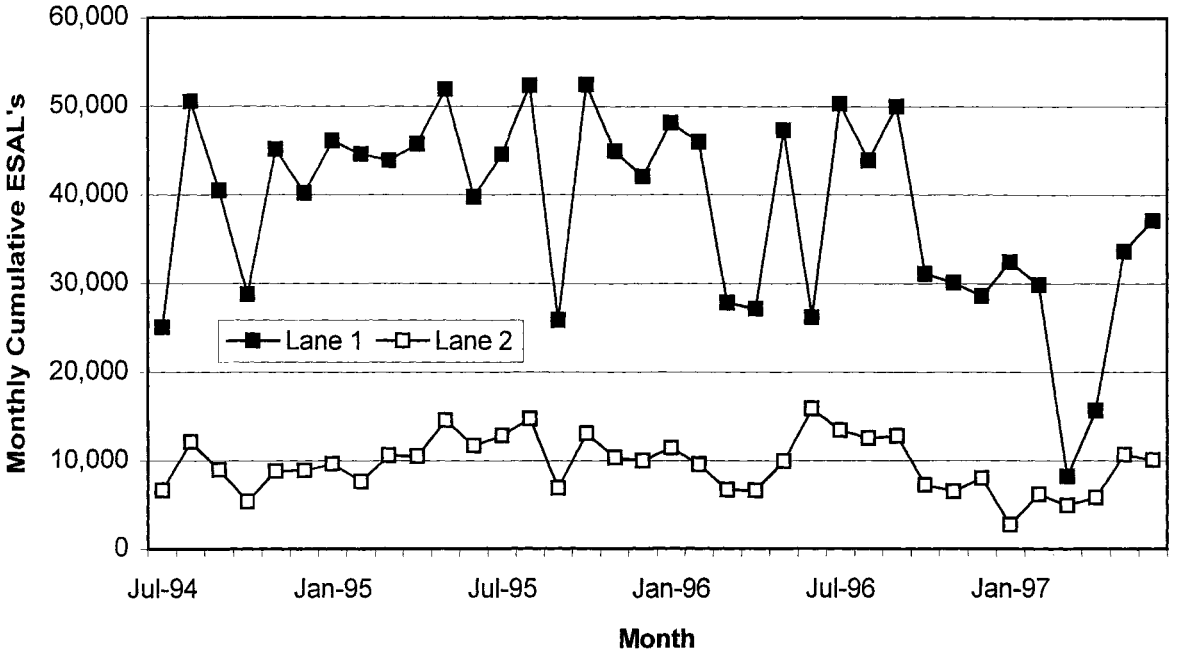

Figure 6.13 ESAL's for Section 22

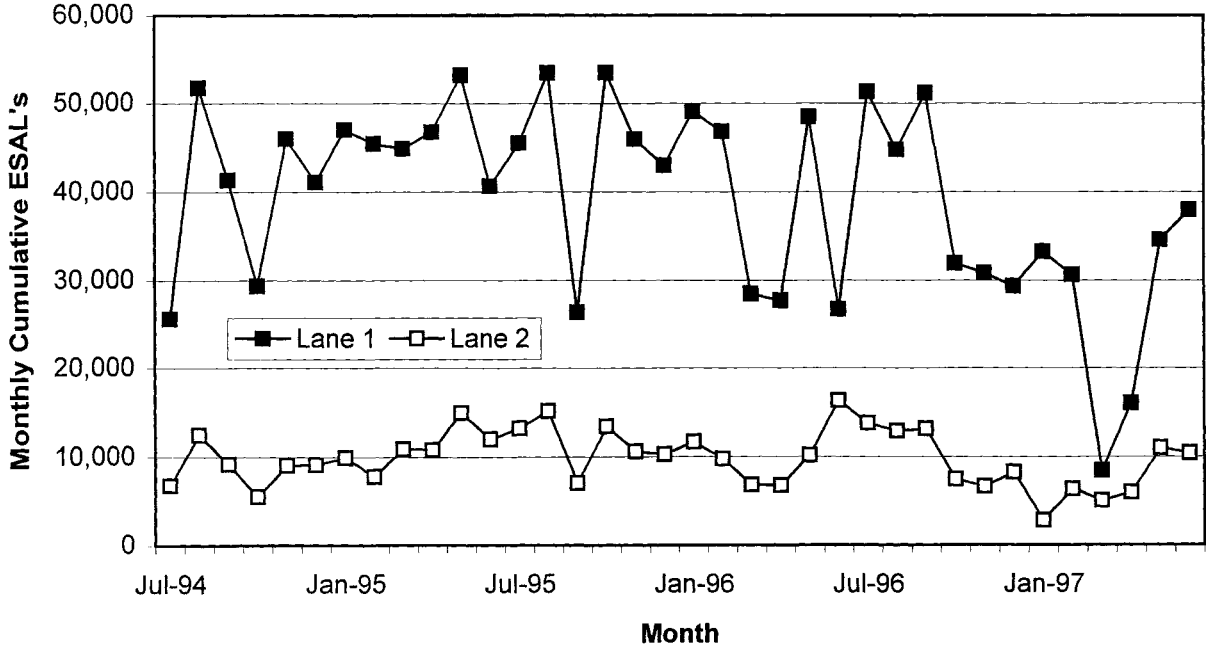

Figure 6.14 ESAL's for Section 23

GROUNDWATER DEPTH

This section presents the groundwater depths as functions of time for each of the 22 sections. The maximum measurable depth is 4.27 meters (14 feet). Where the water table is more than 4.27 meters (14 feet) below the surface, a value of 4.27 meters (14 feet) is assigned.

Some sections show the typical seasonal variations in water elevations (e.g., Section 1). In three sections (25, 26 and 30) a persistent trend of a raising water table (depths becoming smaller) seems to exist. This is probably due to the transient effects caused by the construction of sections. The rising water table may have an effect on the performance degradation of these cells.

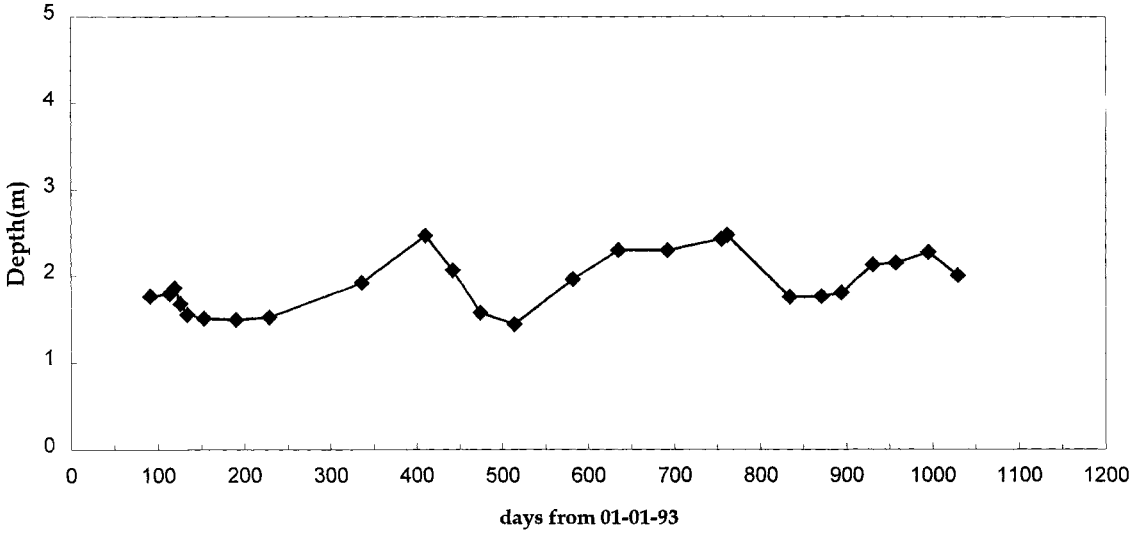

Figure 6.15 Groundwater Depth for Section 1

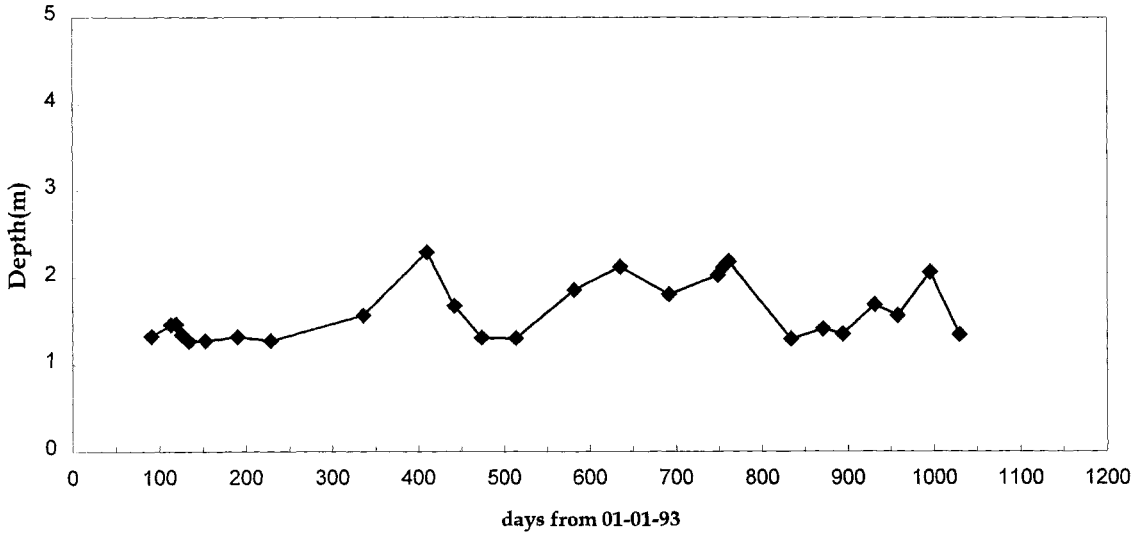

Figure 6.16 Groundwater Depth for Section 2

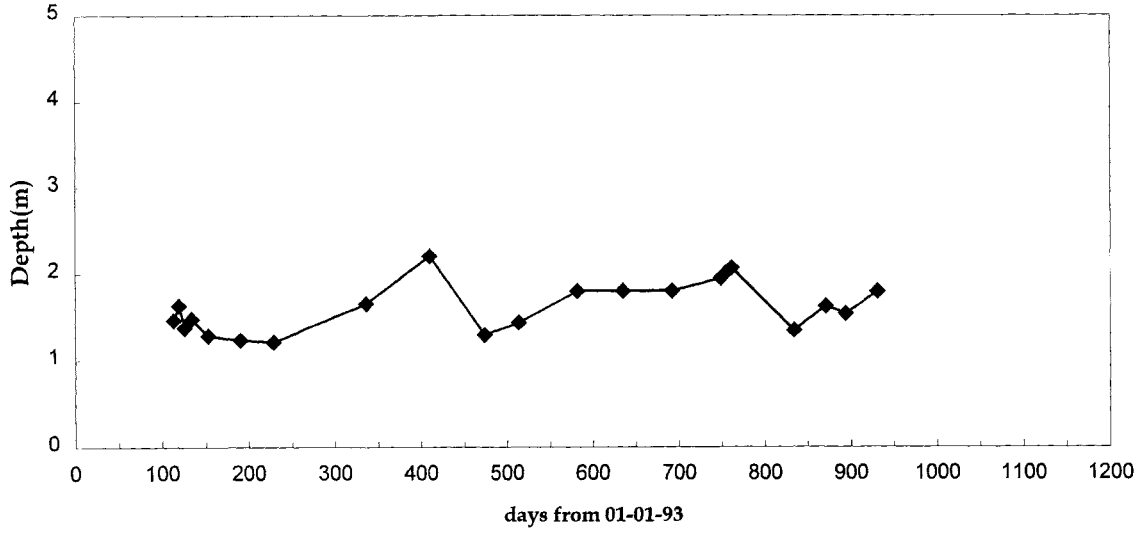

Figure 6.17 Groundwater Depth for Section 3

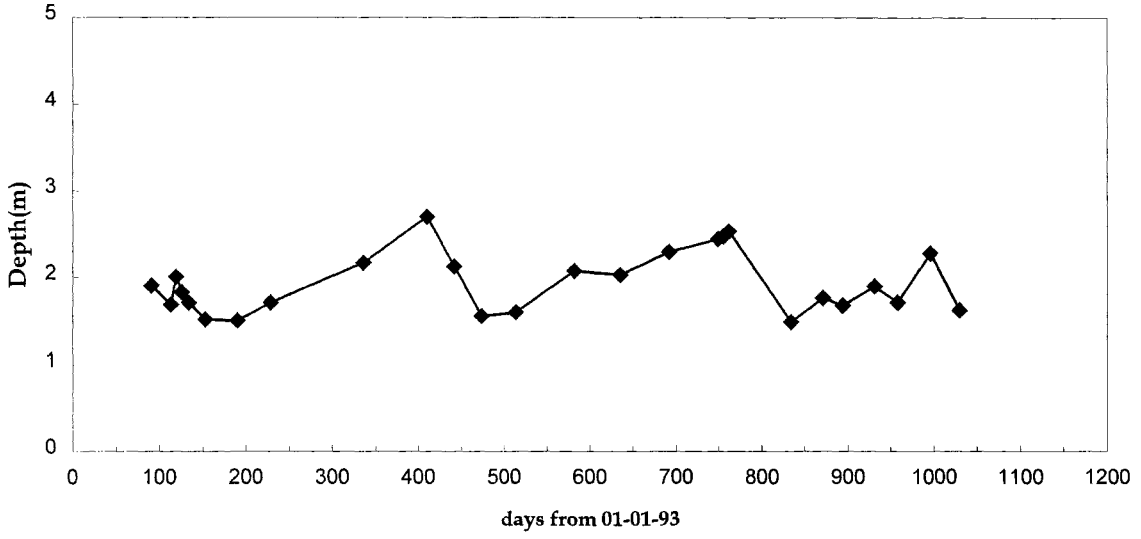

Figure 6.18 Groundwater Depth for Section 4

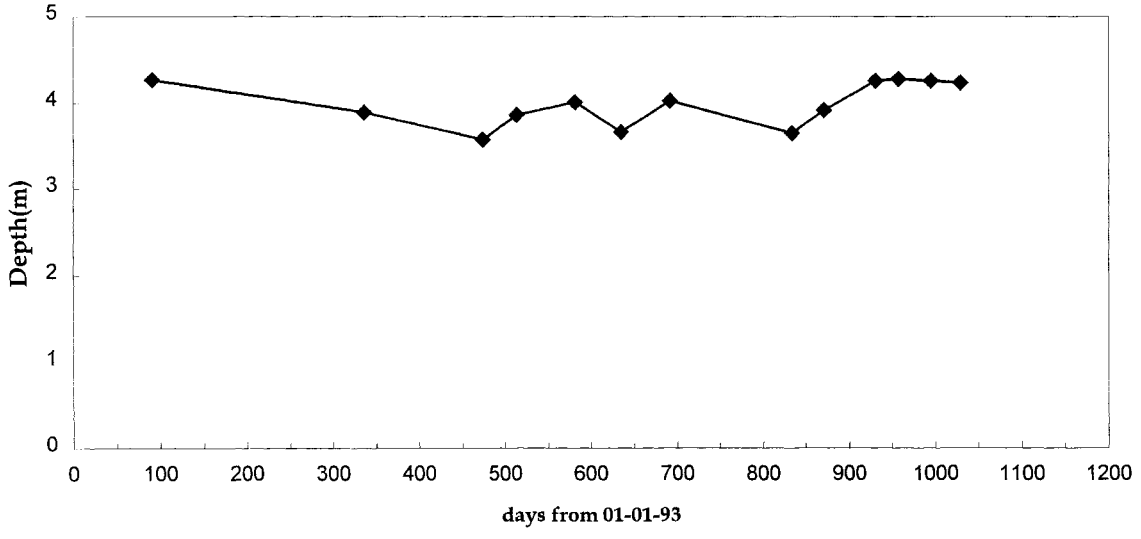

Figure 6.19 Groundwater Depth for Section 14

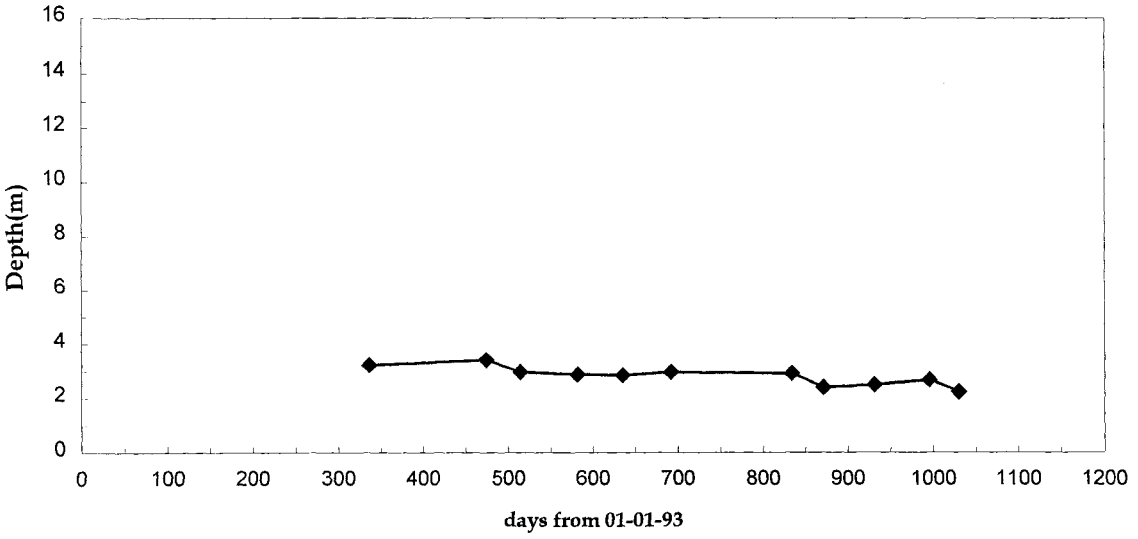

Figure 6.20 Groundwater Depth for Section 15

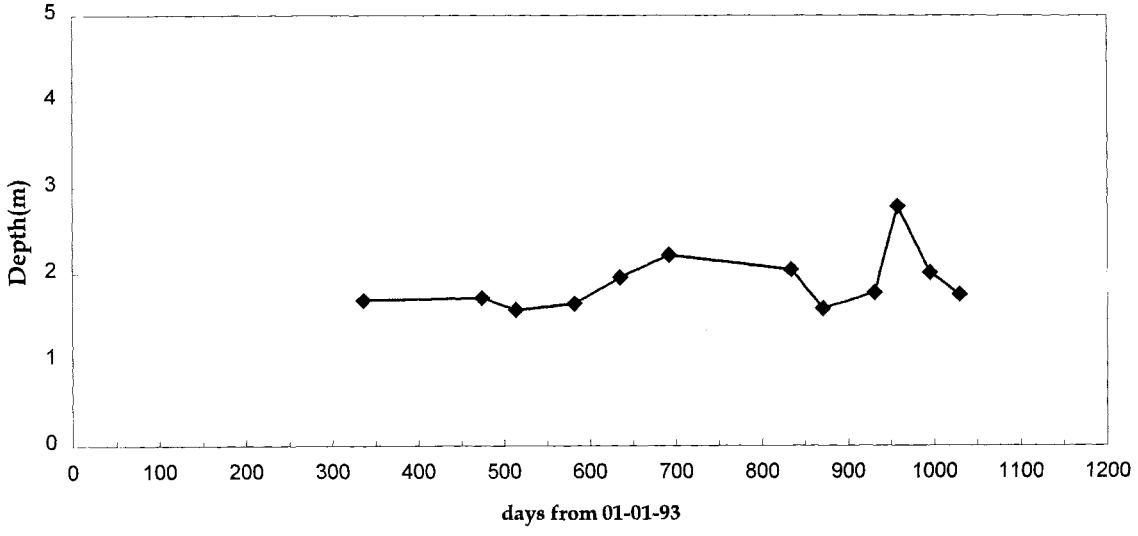

Figure 6.21 Groundwater Depth for Section 16

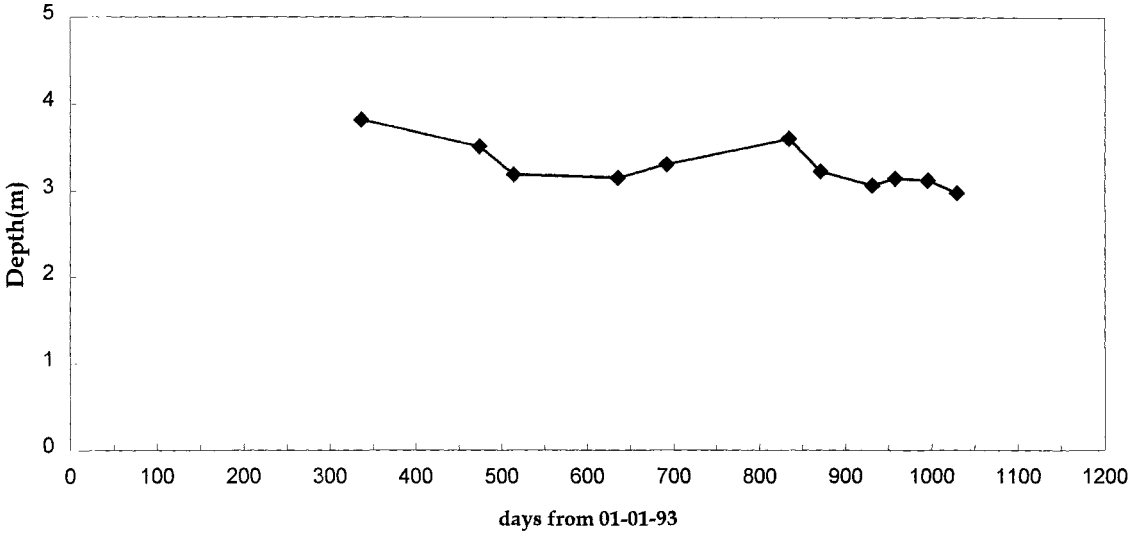

Figure 6.22 Groundwater Depth for Section 17

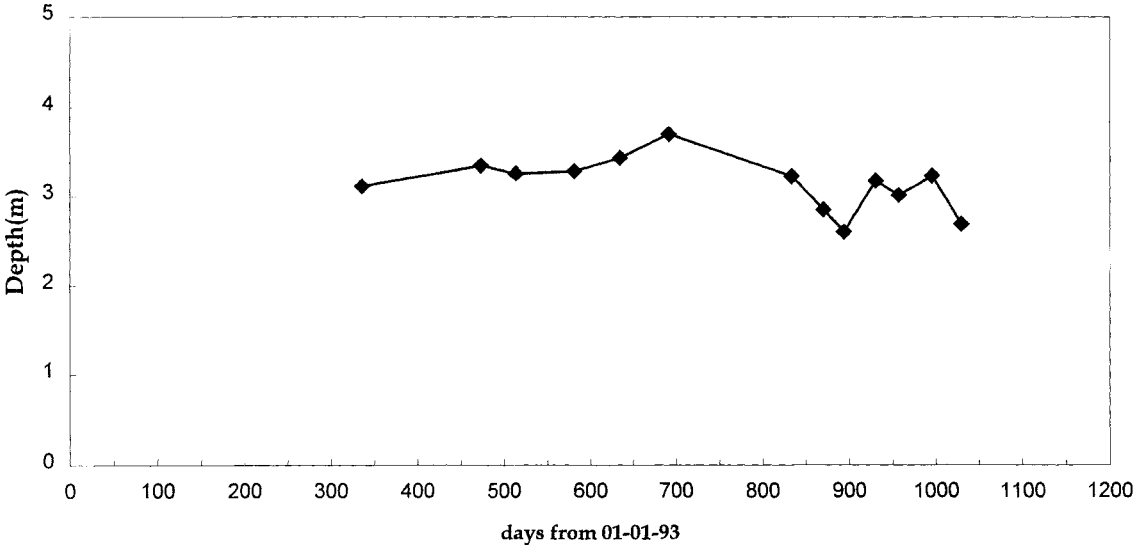

Figure 6.23 Groundwater Depth for Section 18

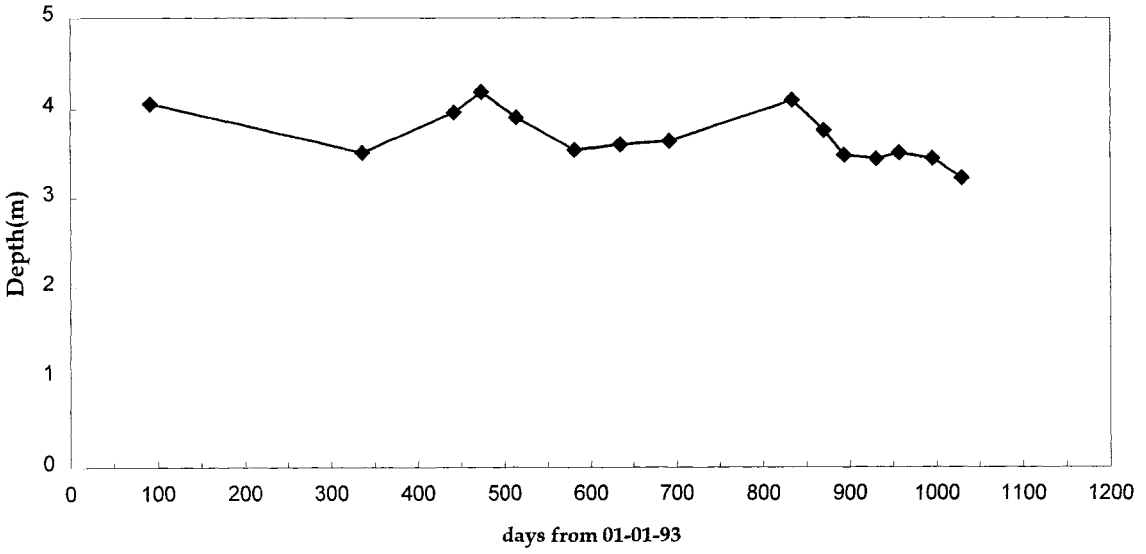

Figure 6.24 Groundwater Depth for Section 19

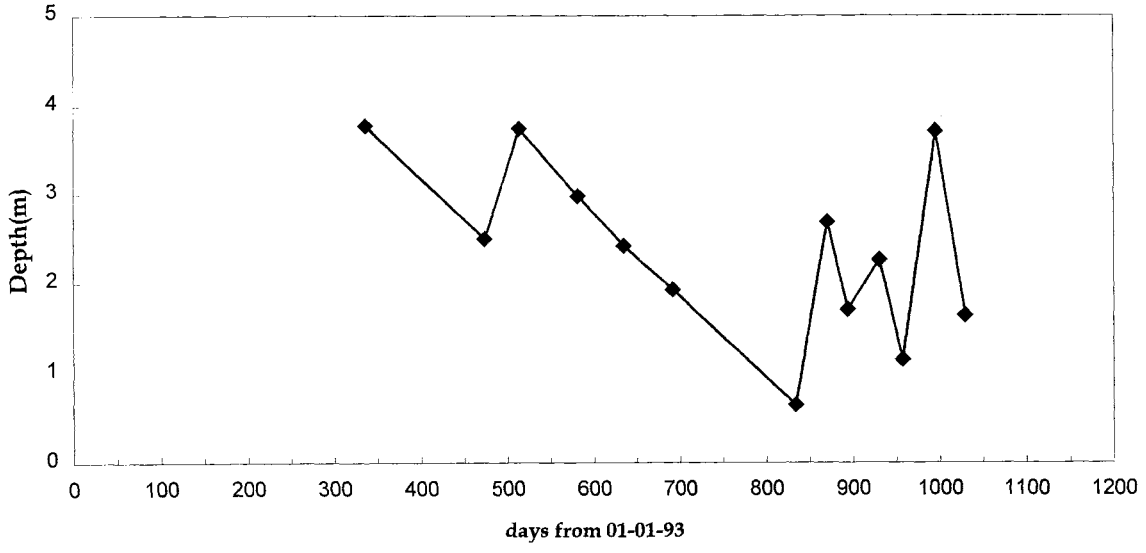

Figure 6.25 Groundwater Depth for Section 20

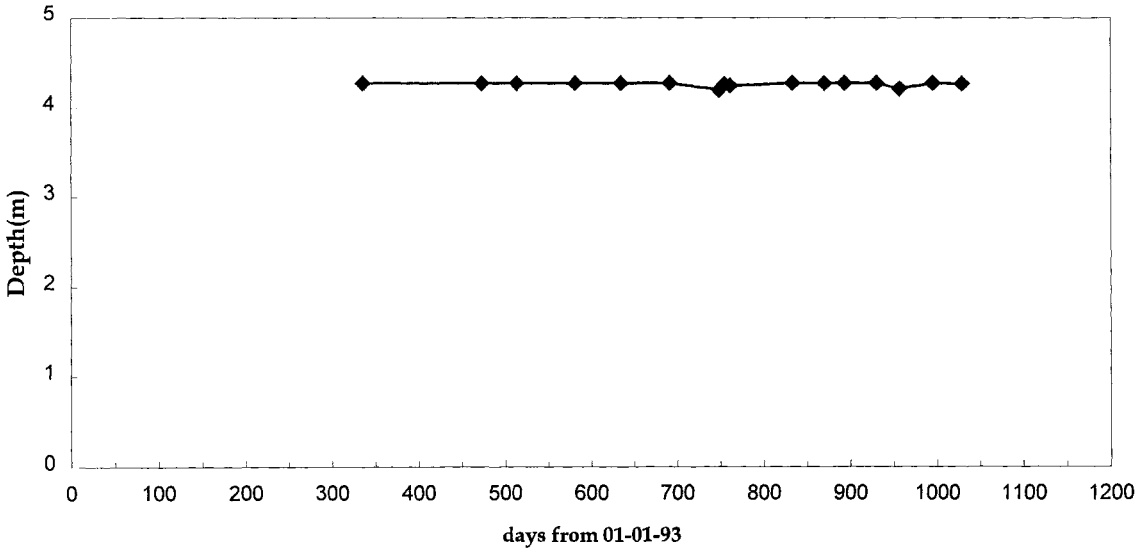

Figure 6.26 Groundwater Depth for Section 21

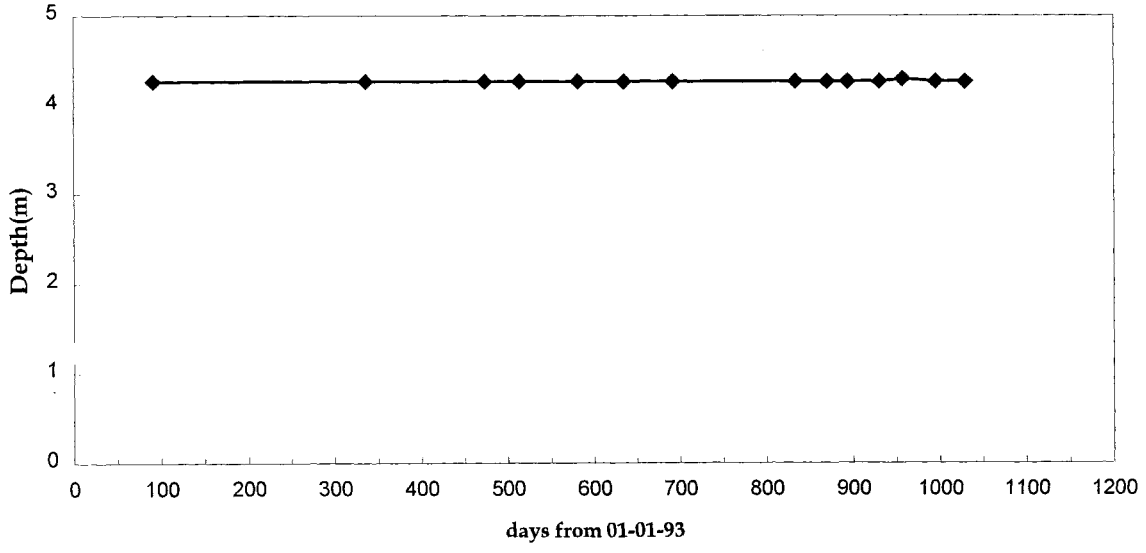

Figure 6.27 Groundwater Depth for Section 22

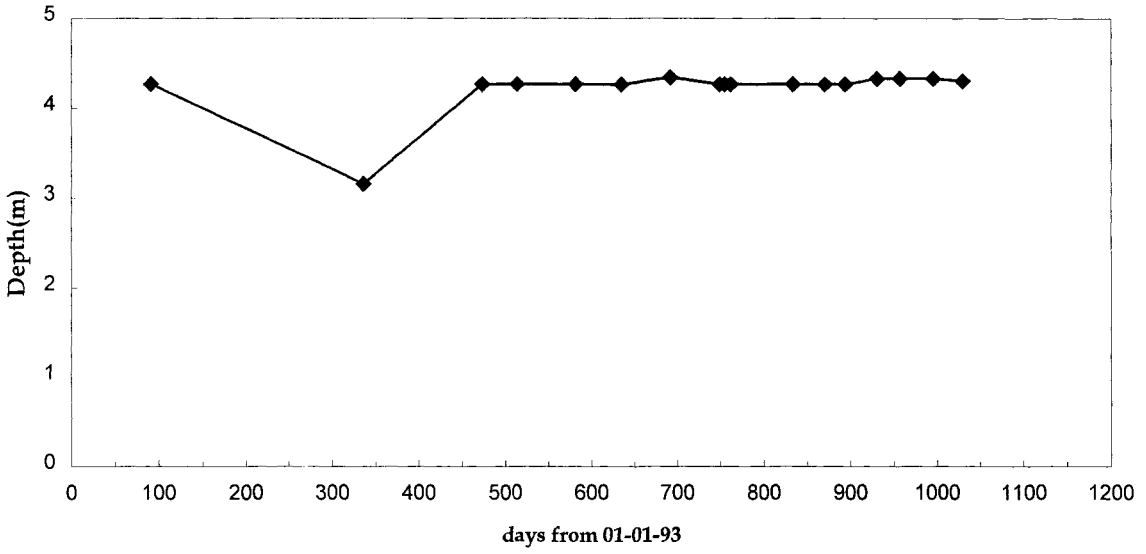

Figure 6.28 Groundwater Depth for Section 23

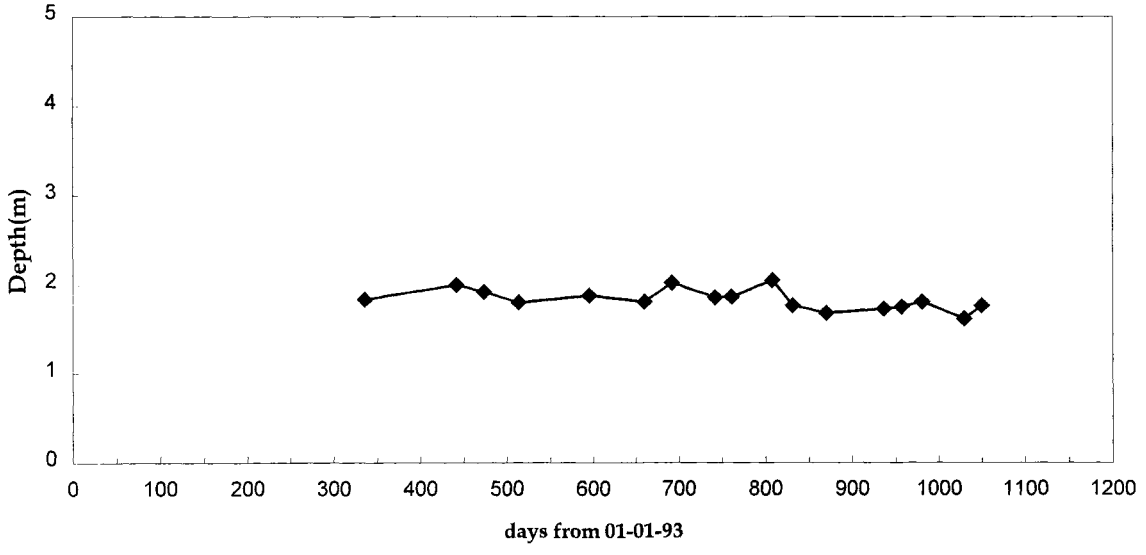

Figure 6.29 Groundwater Depth for Section 24

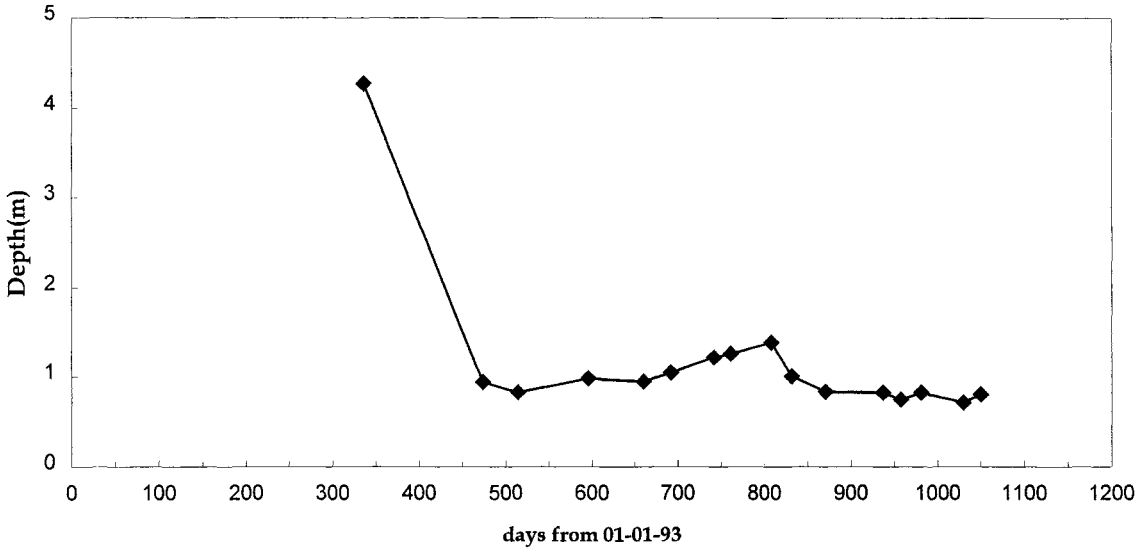

Figure 6.30 Groundwater Depth for Section 25

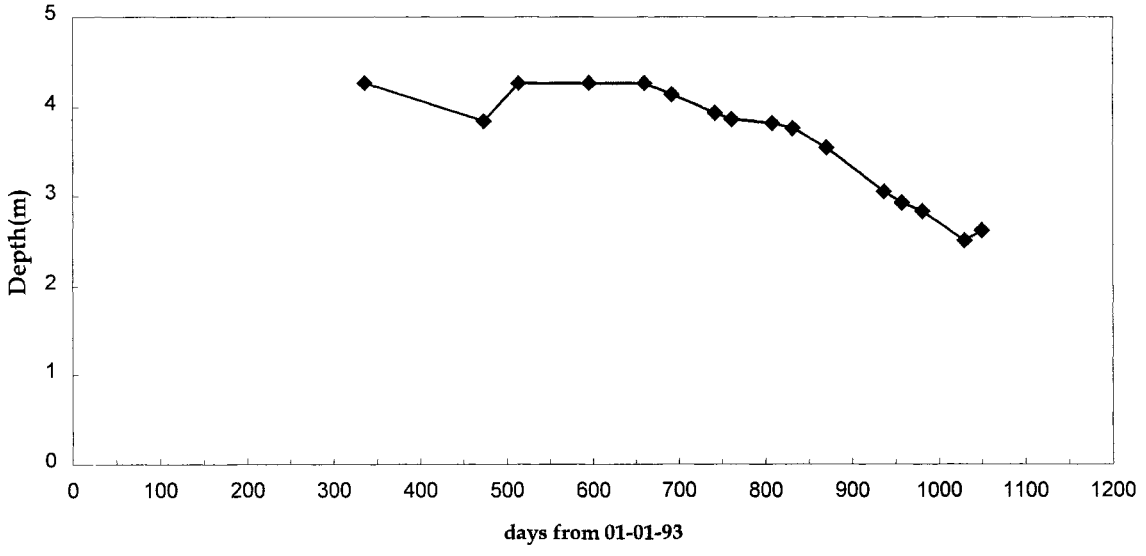

Figure 6.31 Groundwater Depth for Section 26

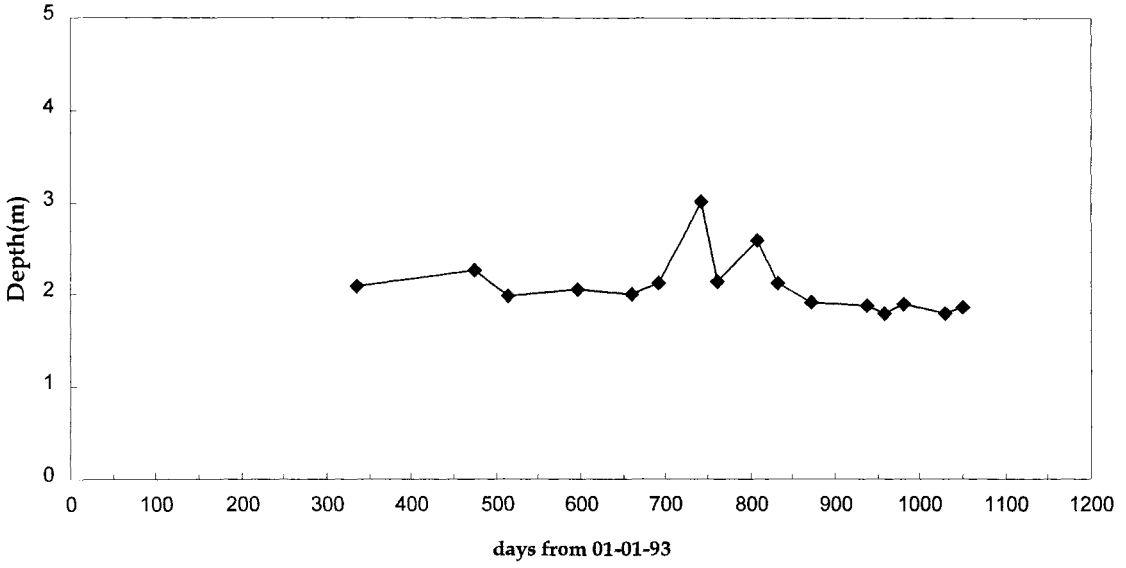

Figure 6.32 Groundwater Depth for Section 27

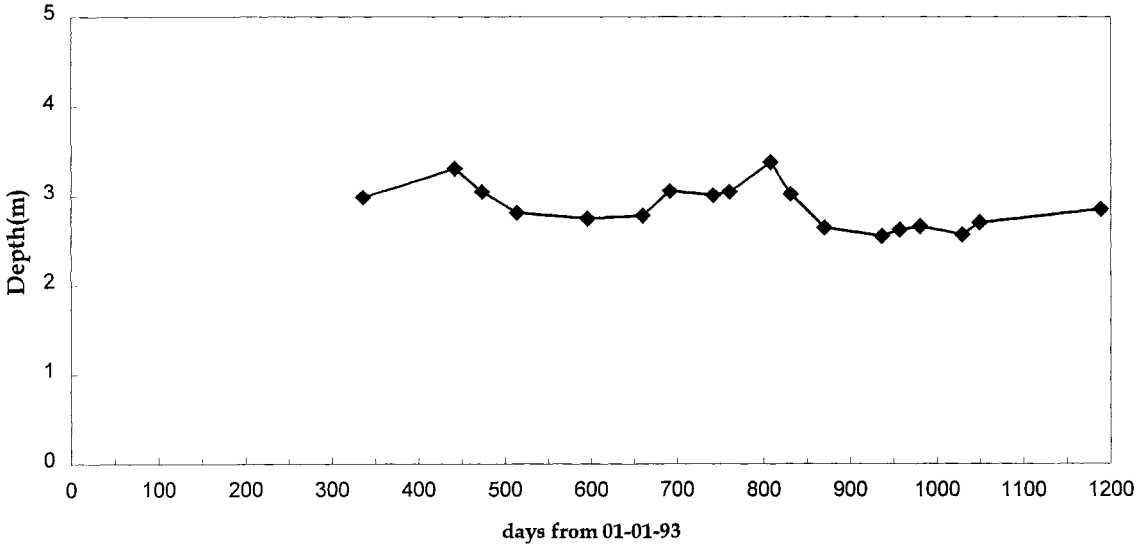

Figure 6.33 Groundwater Depth for Section 28

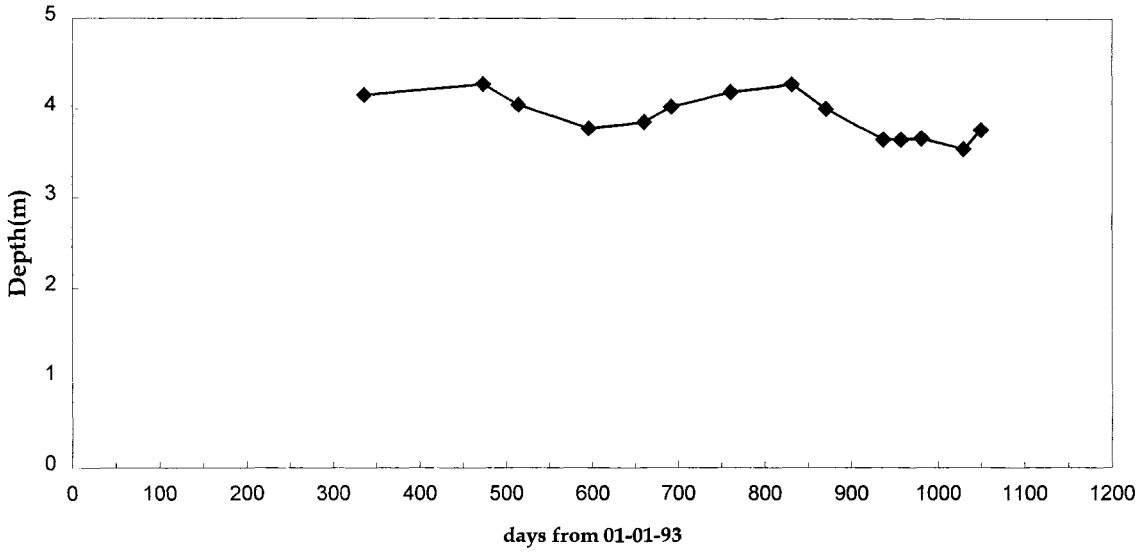

Figure 6.34 Groundwater Depth for Section 29

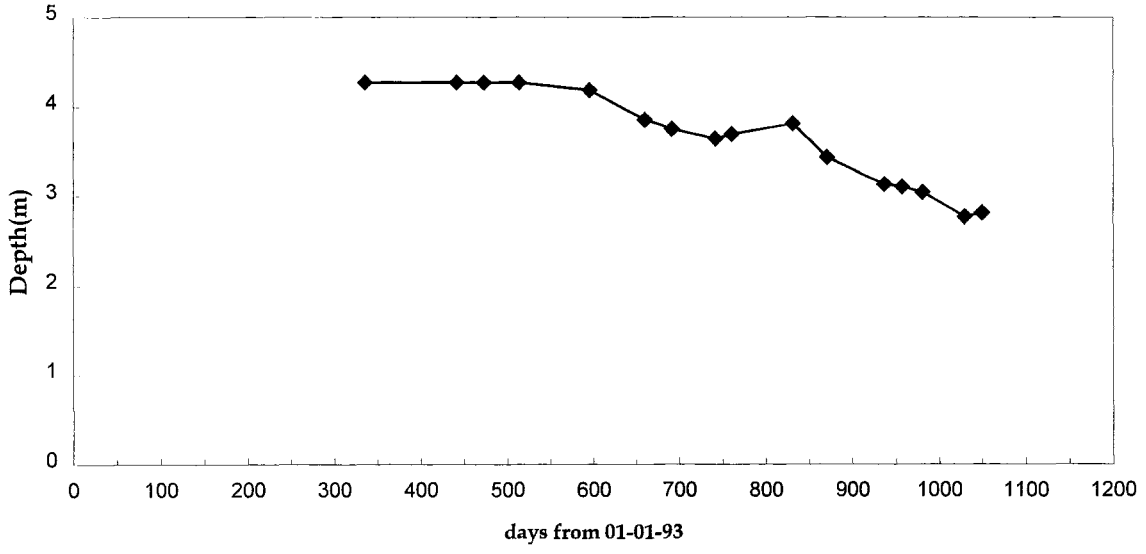

Figure 6.35 Groundwater Depth for Section 30

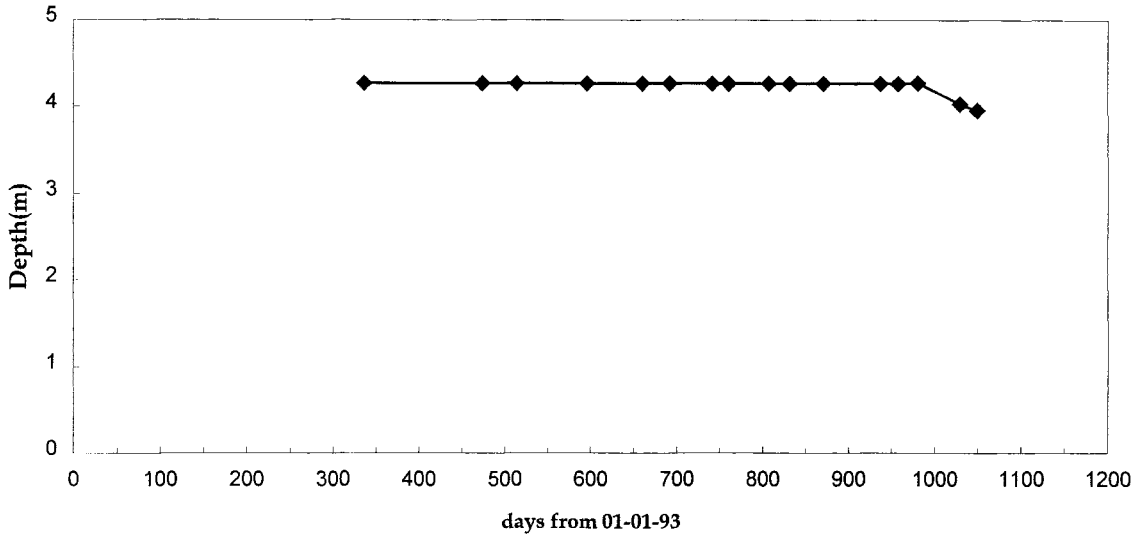

Figure 6.36 Groundwater Depth for Section 31

PORE WATER PRESSURE AND VOLUMETRIC MOISTURE CONTENT

Most of the data available for this project are of high quality. This is especially true for the FWD measurements, where just a few records out of more than 200,000 could not be used due to typographical errors. The exceptions to this rule are the volumetric moisture content data and pore pressure data. Many volumetric moisture content records show the readings near the value of 1, which is physically impossible. The upper limit for the volumetric moisture content is the porosity, which is typically in the 0.25 to 0.35 range.

Similarly, the pore pressure data also seem to suffer from quality problems. The pore pressure should increase with depth (due to gravity). However, in many records the pore pressure is actually decreasing with depth. The problems with moisture content data and pore pressure data follow. Because of these problems, these data are not used in other sections of this report.

TEMPERATURE

Because the temperature variations between the sections are insignificant, the temperature data can not be used for comparison purposes. As such, the influence of this parameter can not be clearly identified based on the available data collected on the Mn/ROAD site.

CHAPTER 7

PERFORMANCE STATISTICS

INTERNATIONAL ROUGHNESS INDEX

Introduction

This section presents the International Roughness Index (IRI) measurements for all sections. For each mainline section, both the north lane (right lane) and the south lane (left lane) measurements are presented as functions of time. For the low volume road sections, both the outer lane (102,000 lane) and inner lane (80,000 lane) measurements are presented as functions of time. For each section the linear model (time vs. IRI) is fitted for both lanes. It appears that he anomalous peaks in the IRI plots are due to winter-time freezing, which induces pavement roughness.

Mainline Data Summary

The mainline section data summaries are presented in the following figures. In general, the IRI values for the south lane (left lane) are higher than the north lane (right lane). Considering all of the mainline sections, the differences between the IRI for the north lane and for the south lane are statistically significant at any practical level: i.e. in more than 80 percent of the paired measurements (157 out of 196) the south lane IRI is higher than the north lane IRI. However, the magnitude of the differences are not large.

The IRI values for almost all mainline sections seem to be increasing over time. This phenomenon is quantified later in this section. Besides this long-term trend, seasonal variations in IRI values also appear, as can be seen from the following figures. (The last data points shown in figures 7.1 through 7.14, day 1151, are anomalous and unsubstantiated by subsequent data.)

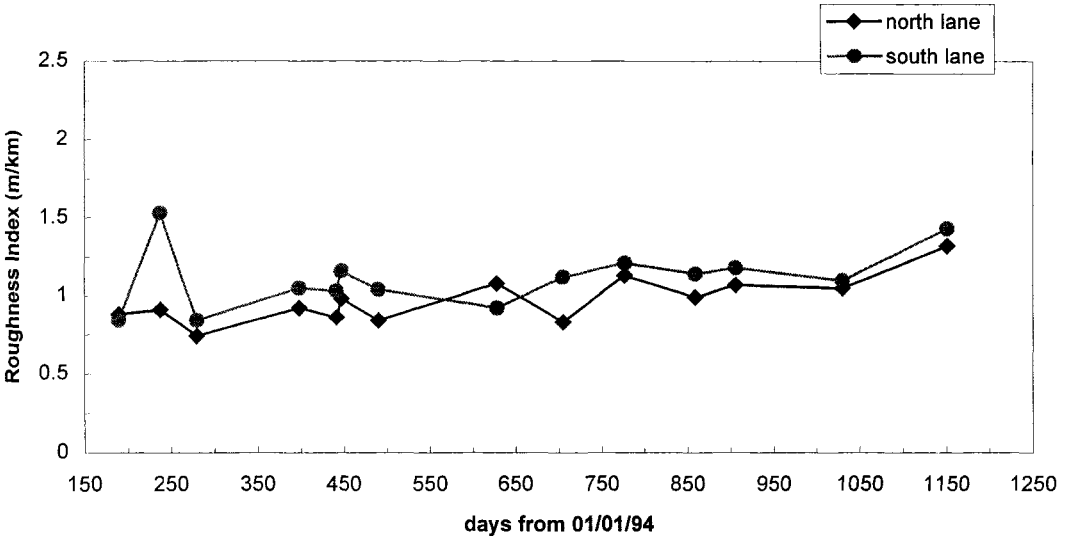

Figure 7.1 IRI for Mainline Section 1

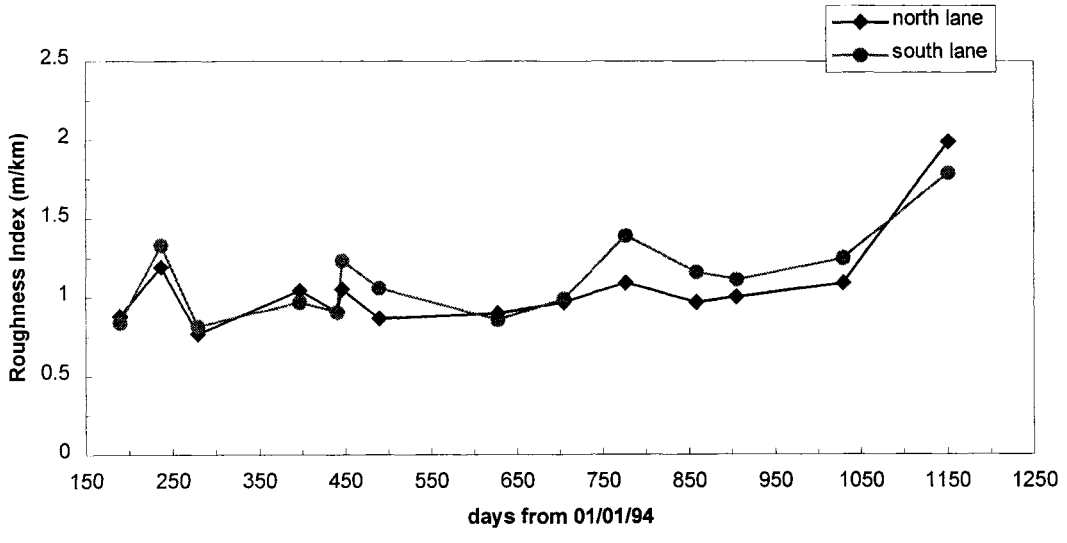

Figure 7.2 IRI for Mainline Section 2

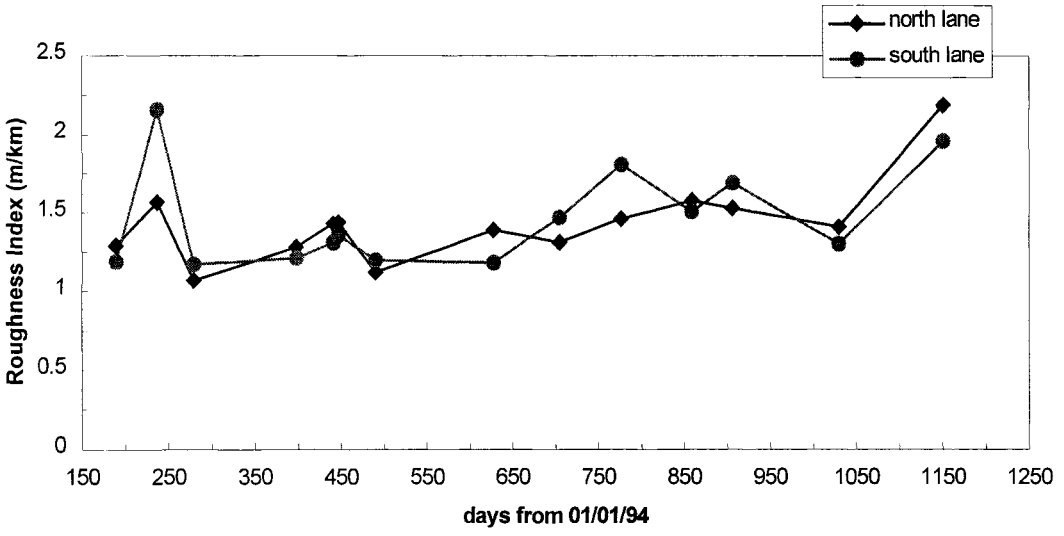

Figure 7.3 IRI for Mainline Section 3

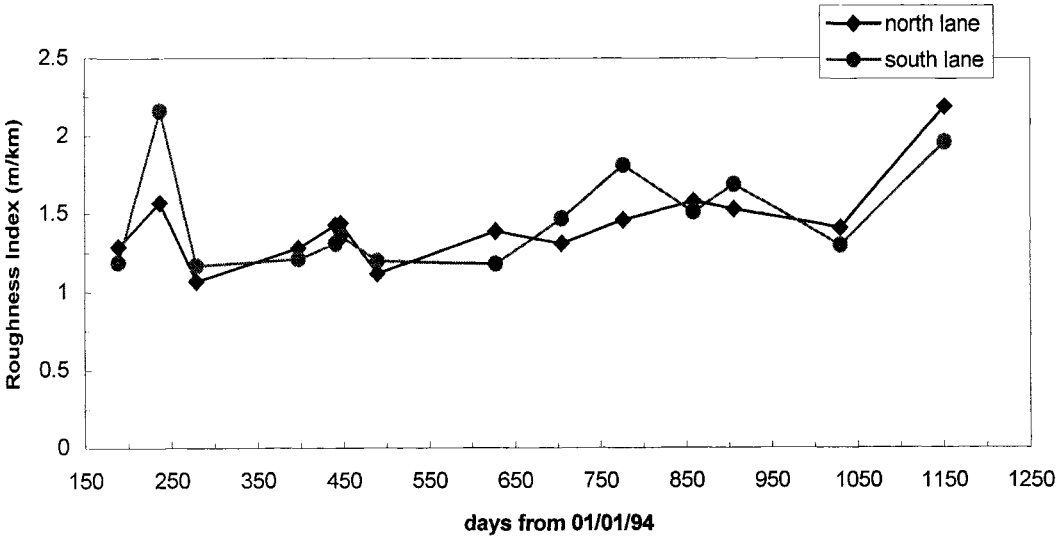

Figure 7.4 IRI for Mainline Section 4

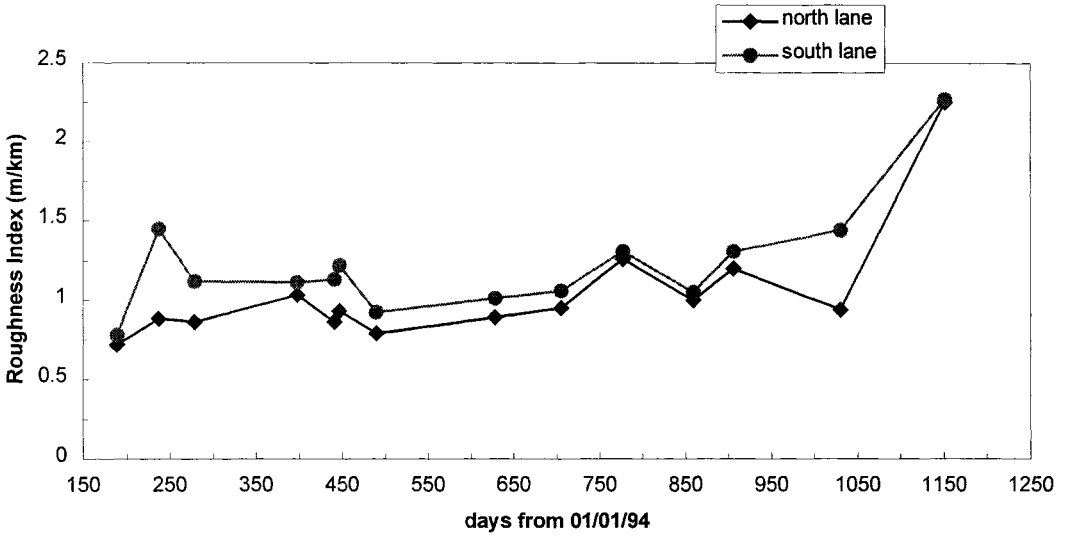

Figure 7.5 IRI for Mainline Section 14

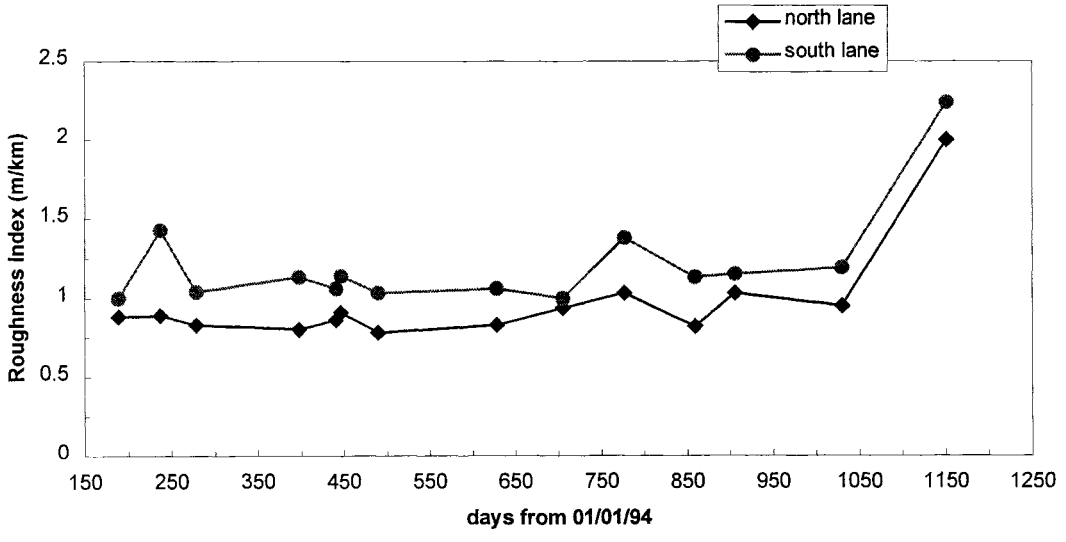

Figure 7.6 IRI for Mainline Section 15

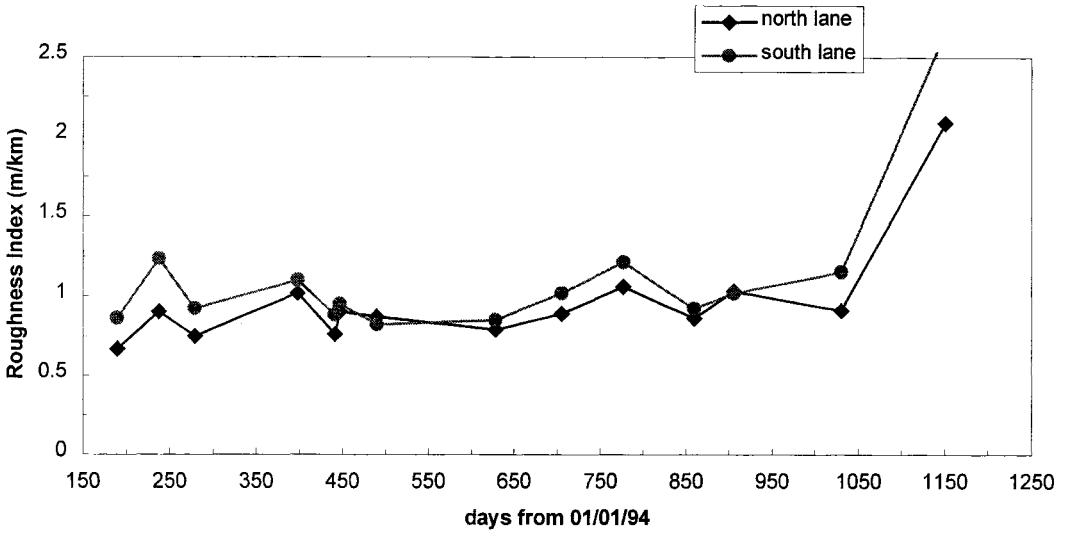

Figure 7.7 IRI for Mainline Section 16

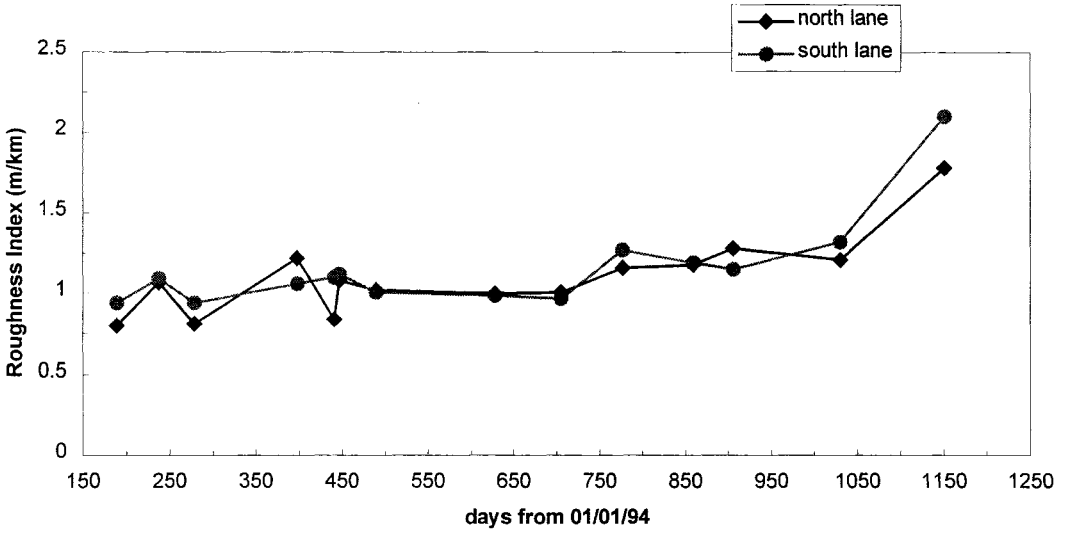

Figure 7.8 IRI for Mainline Section 17

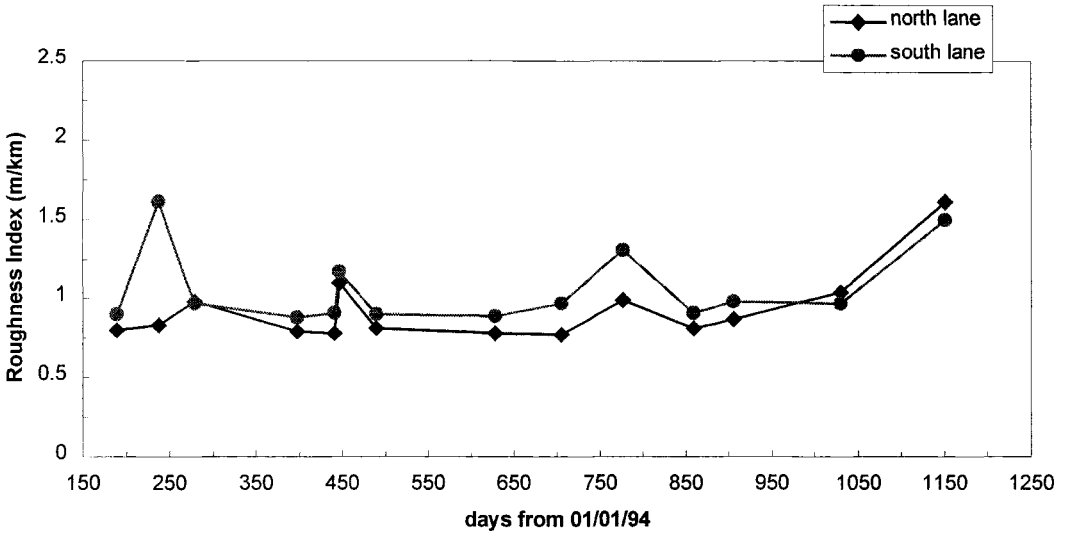

Figure 7.9 IRI for Mainline Section 18

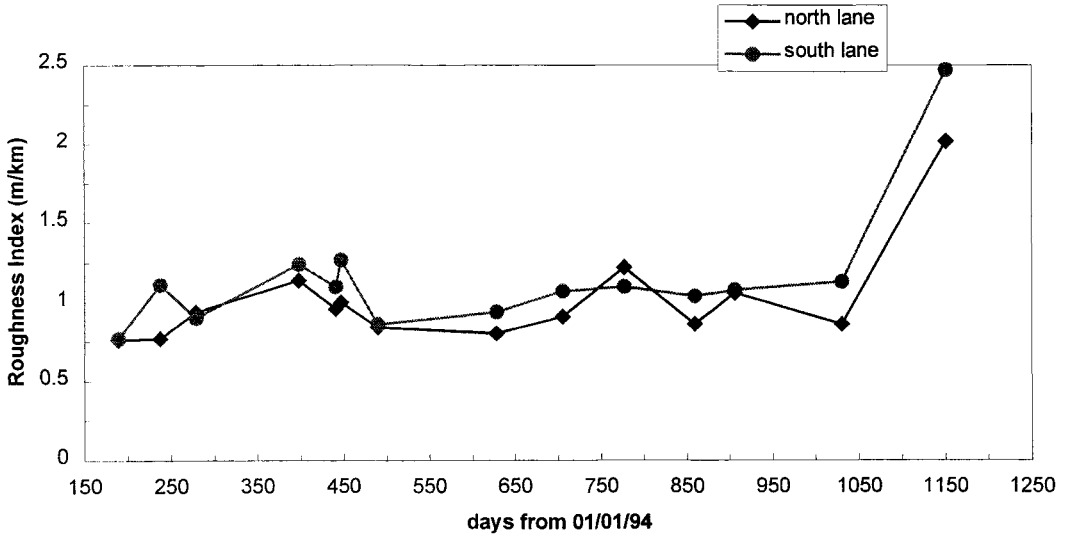

Figure 7.10 IRI for Mainline Section 19

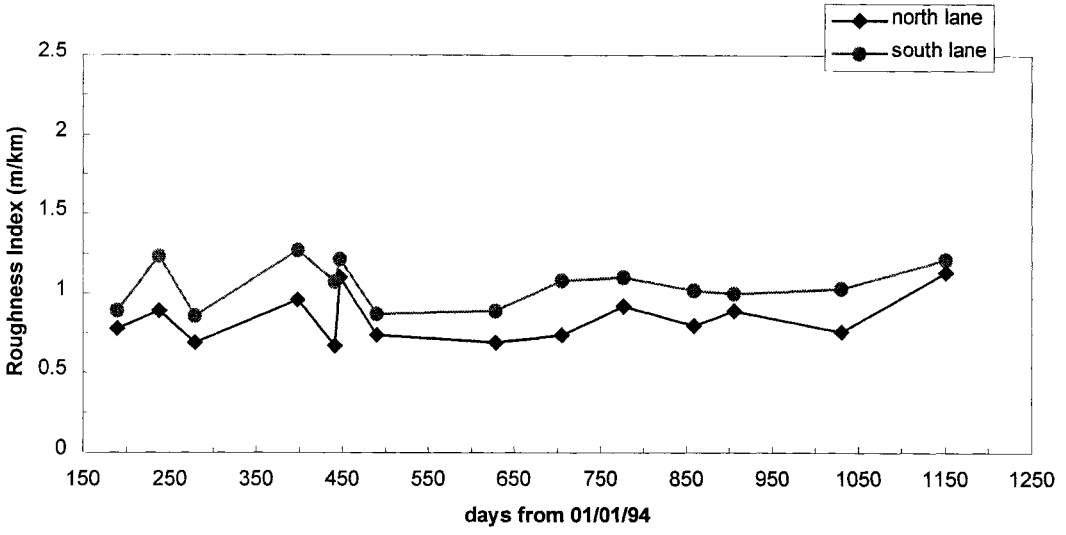

Figure 7.11 IRI for Mainline Section 20

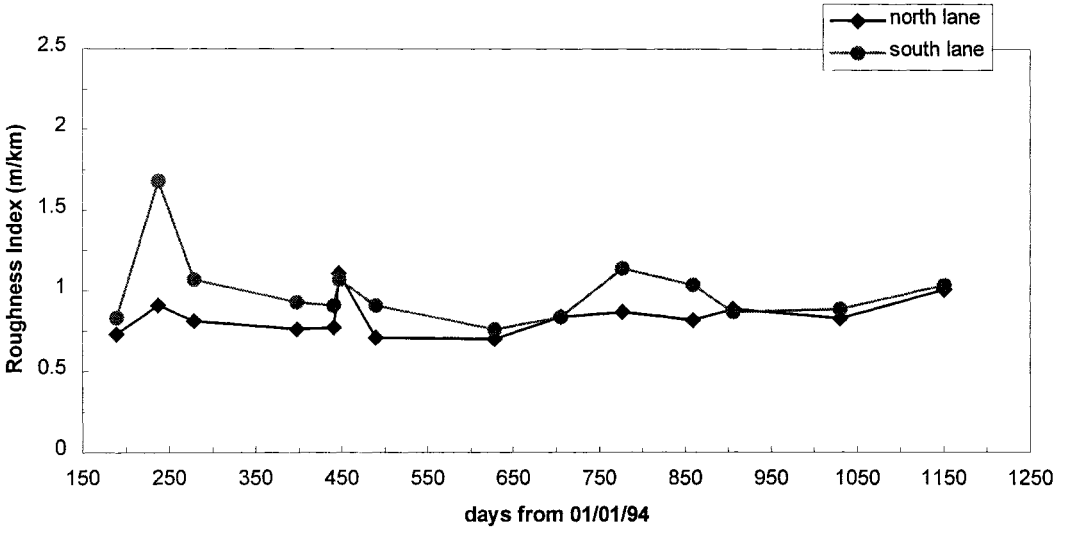

Figure 7.12 IRI for Mainline Section 21

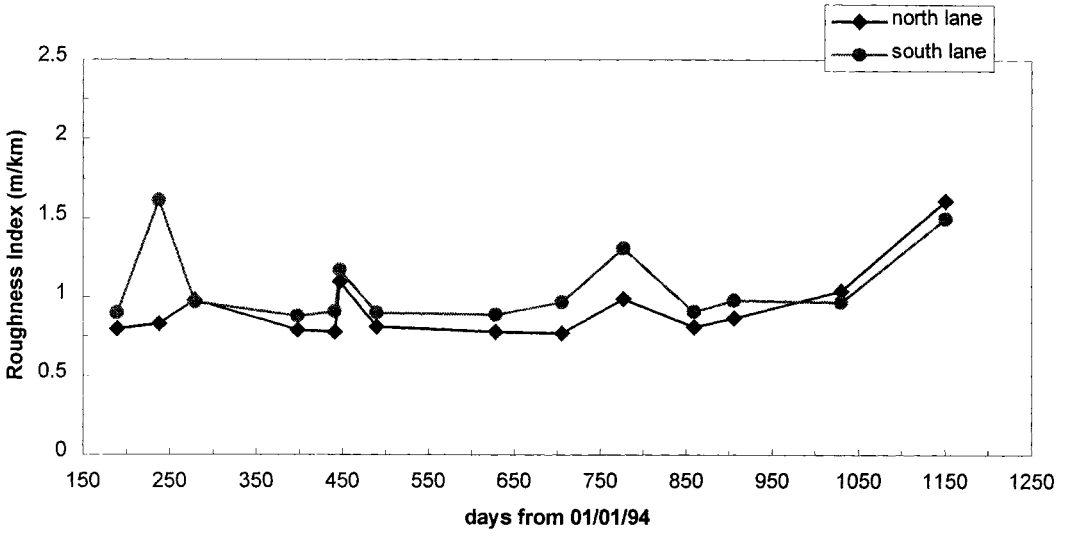

Figure 7.13 IRI for Mainline Section 22

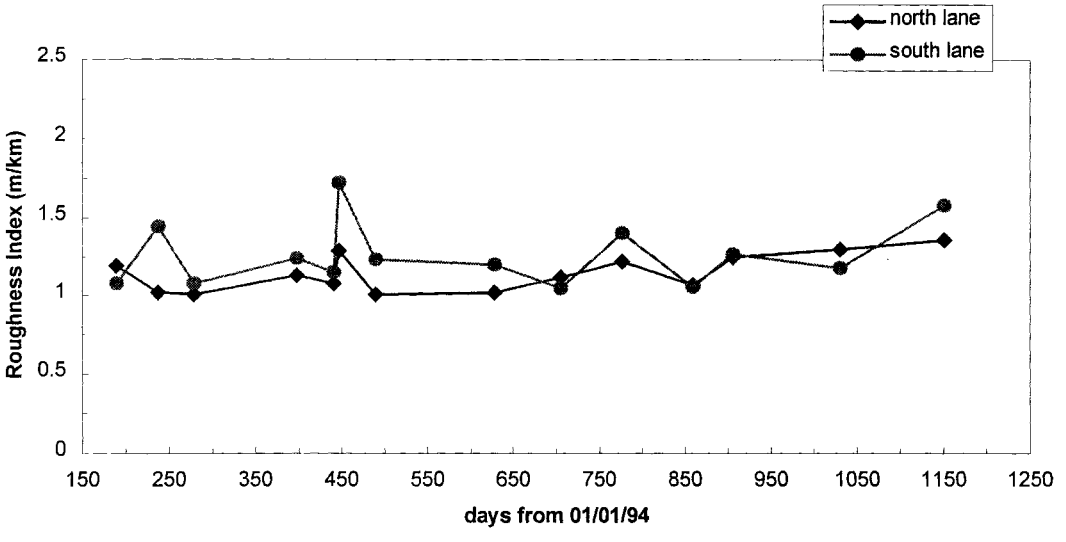

Figure 7.14 IRI for Mainline Section 23

Low Volume Road Data Summary

The low-volume section data summaries are presented in the following figures. In general, the IRI values for the outer lane (102,000 lane) are higher than the IRI values inner lane (80,000 lane). Hence, the very heavy load in the outer lane seems to deteriorate the pavement surface, as measured by the IRI.

The IRI values for almost all low-volume road sections seem to be increasing over time. This phenomenon is quantified later in this section. Besides this long-term trend, an apparent seasonal variations of IRI values can be seen in the following figures.

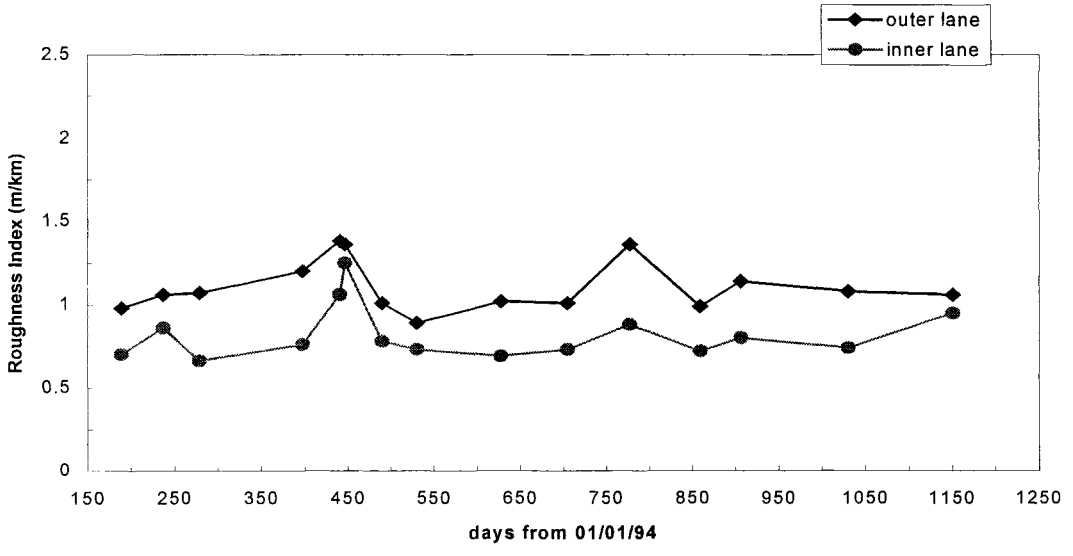

Figure 7.15 IRI for Low Volume Section 24

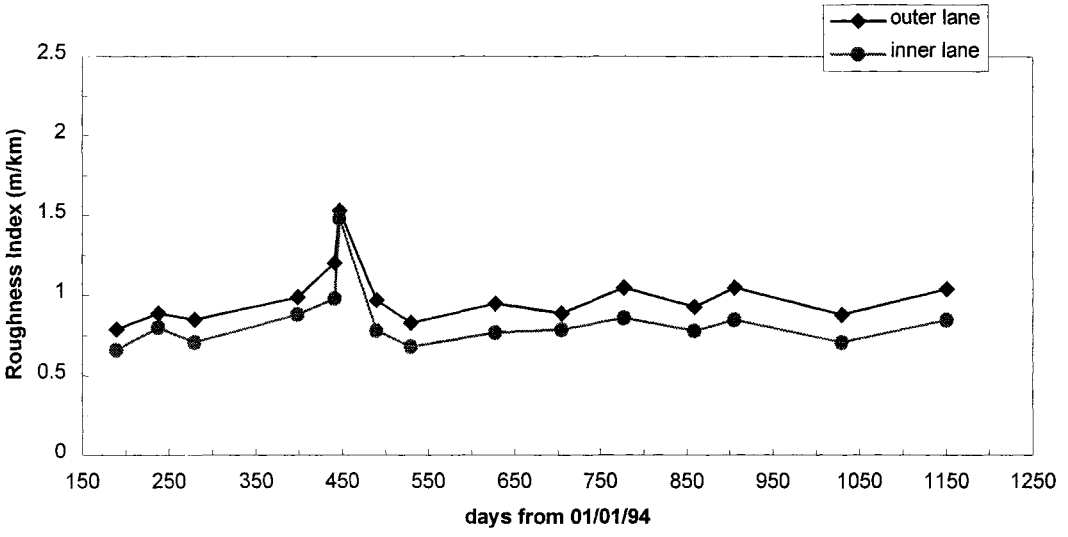

Figure 7.16 IRI for Low Volume Section 25

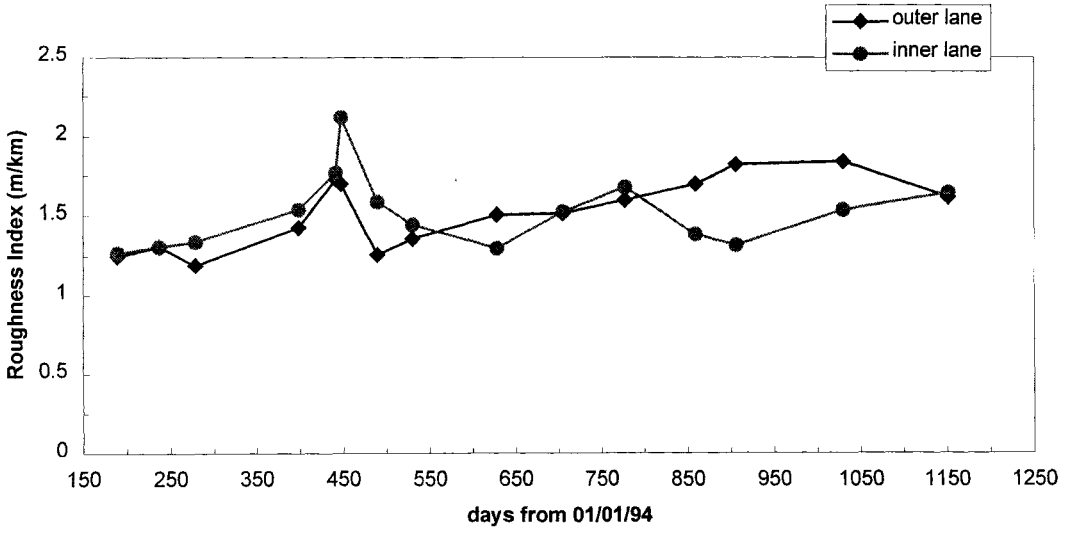

Figure 7.17 IRI for Low Volume Section 26

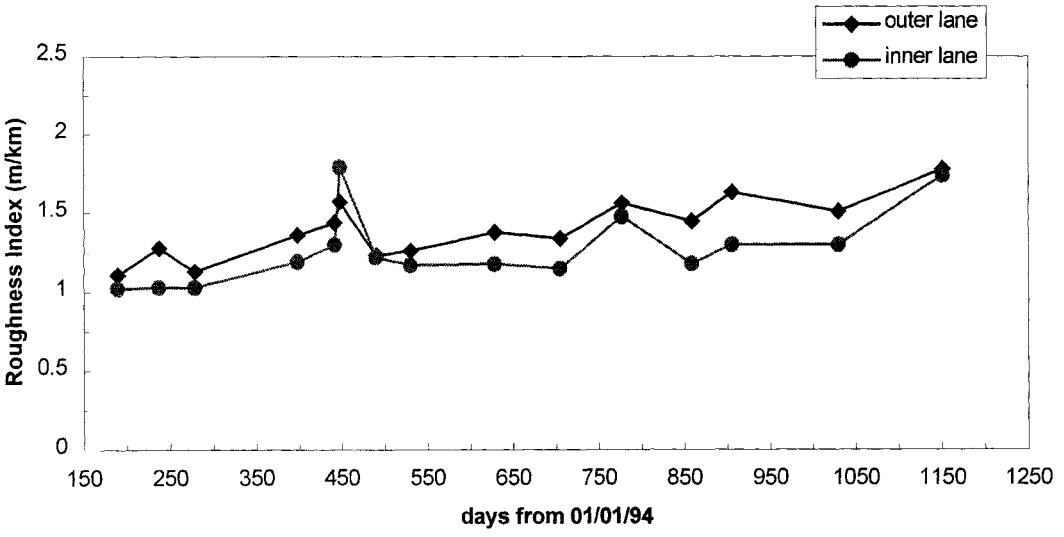

Figure 7.18 IRI for Low Volume Section 27

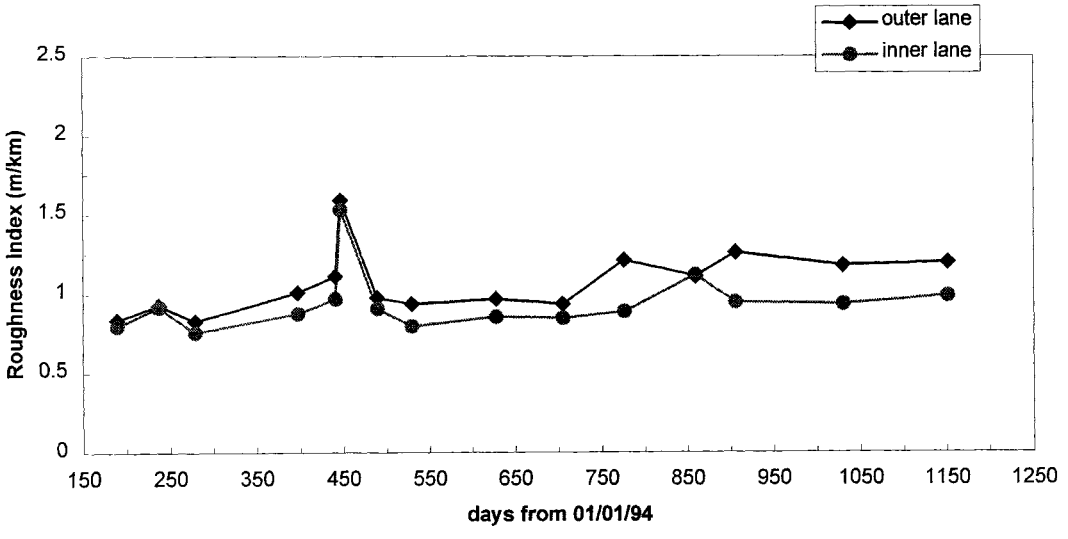

Figure 7.19 IRI for Low Volume Section 28

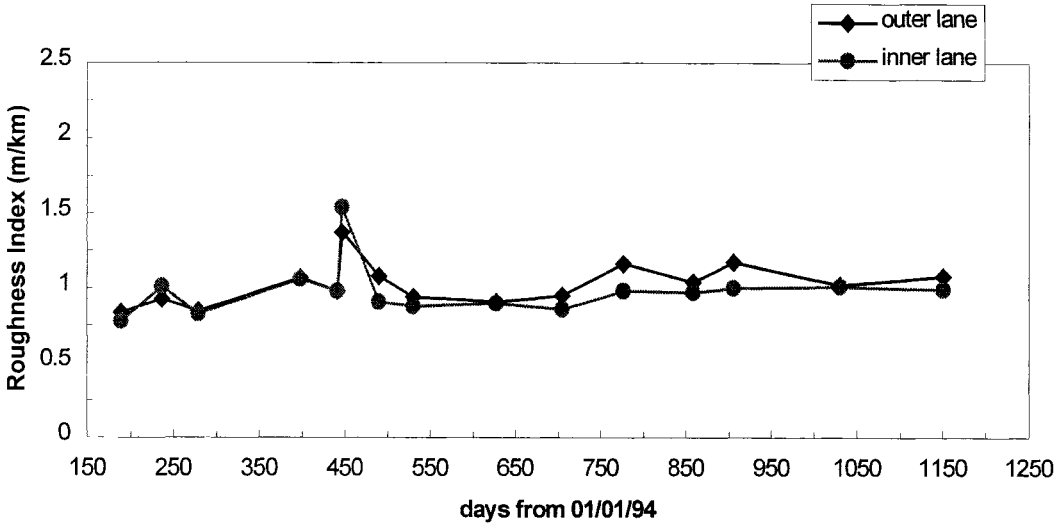

Figure 7.20 IRI for Low Volume Section 29

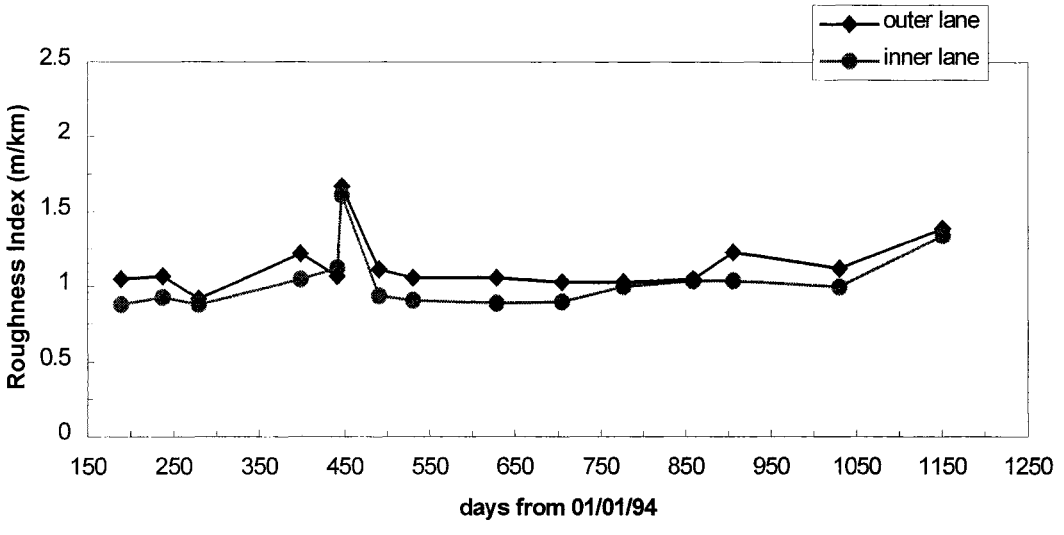

Figure 7.21 IRI for Low Volume Section 30

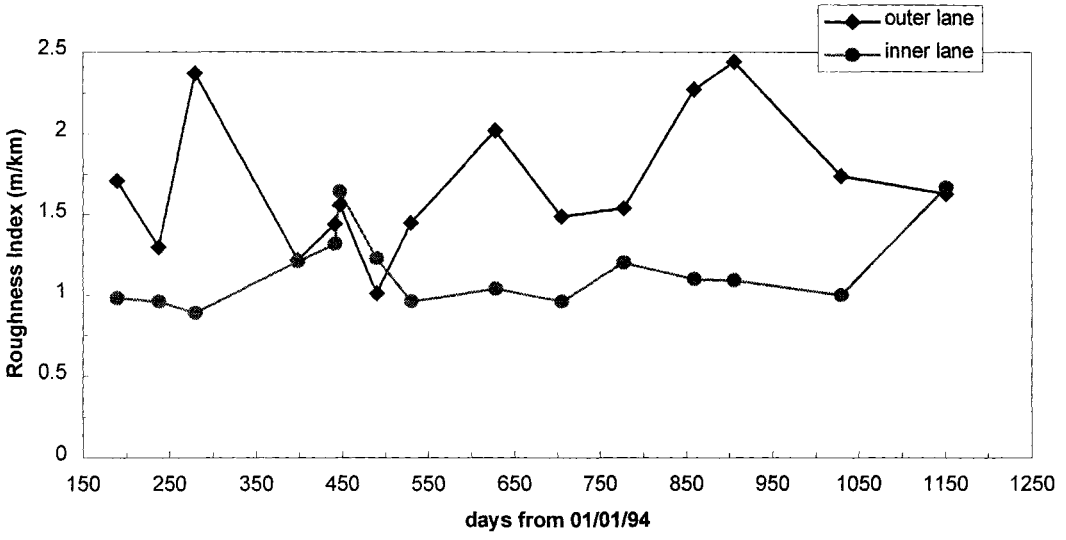

Figure 7.22 IRI for Low Volume Section 31

Linear Regression Model

This section quantifies the pavement surface deterioration (as measured by IRI) for all asphalt sections at Mn/ROAD. For each lane in every section, a linear model (i.e. IRI equals *intercept* plus *slope* multiplied by day). that describes changes of IRI over time is fitted to the available data and the results are presented in following two tables: 7.1 and 7.2.

Mainline Section	Right Lane			Left Lane		
	Intercept (m/km)	Slope (m/km/day)	Pearson R^2	Intercept (m/km)	Slope (m/km/day)	Pearson R^2
1	0.74	3.8E-04	0.58	0.97	2.4E-04	0.14
2	0.72	5.4E-04	0.32	0.79	5.4E-04	0.38
3	1.02	3.8E-04	0.55	0.99	4.0E-04	0.42
4	1.10	5.5E-04	0.39	1.26	3.4E-04	0.11
14	0.65	6.0E-04	0.38	0.99	2.6E-04	0.06
15	0.59	6.1E-04	0.37	0.88	5.5E-04	0.26
16	0.53	7.1E-04	0.39	0.60	8.4E-04	0.30
17	0.72	6.3E-04	0.59	0.74	6.9E-04	0.50
18	0.53	8.4E-04	0.46	0.79	7.1E-04	0.37
19	0.65	5.9E-04	0.31	0.69	7.5E-04	0.32
20	0.76	1.3E-04	0.07	1.02	6.1E-05	0.02
21	0.77	1.1E-04	0.08	1.11	-1.9E-04	0.06
22	0.68	4.0E-04	0.29	1.00	1.1E-04	0.02
23	1.00	2.35E-04	0.35	1.20	9.6E-05	0.02

Table 7.1 IRI Versus Time Regression Fit for the Mainline Sections

The slope of this linear model is a measure that can be used to quantify and compare the deterioration of the pavement surface (as measured by the IRI) between different sections at the Mn/ROAD site. However, as can be seen from the associated Pearson product moment correlation coefficient, the R^2 statistic, the regressions are unimpressively poor (values close to 1.0 indicate an unambiguous linear fit).

Low Volume Road Section	102,000 Lane			80,000 Lane		
	Intercept (m/km)	Slope (m/km/day)	Pearson R^2	Intercept (m/km)	Slope (m/km/day)	Pearson R^2
24	1.12	-1.6E-05	0.00	0.82	6.4E-06	0.00
25	0.97	3.6E-05	0.00	0.86	-3.9E-05	0.00
26	1.20	5.3E-04	0.52	1.47	8.9E-05	0.01
27	1.09	5.1E-04	0.64	1.03	4.1E-04	0.26
28	0.89	3.0E-04	0.20	0.89	9.1E-05	0.02
29	0.92	1.7E-04	0.13	0.96	3.3E-05	0.00
30	1.06	1.3E-04	0.04	0.94	1.6E-04	0.06
31	1.43	4.1E-04	0.08	1.00	2.4E-04	0.09

Table 7.2 IRI Versus Time Regression Fit for the Low Volume Road Sections

For most sections, this linear model visually fit the data well. An example is presented for the case of the north (right) lane of Section 1, but there is no significant predictive power. The conclusion drawn is that the study period is insufficient in length and the accumulated damage is to small.

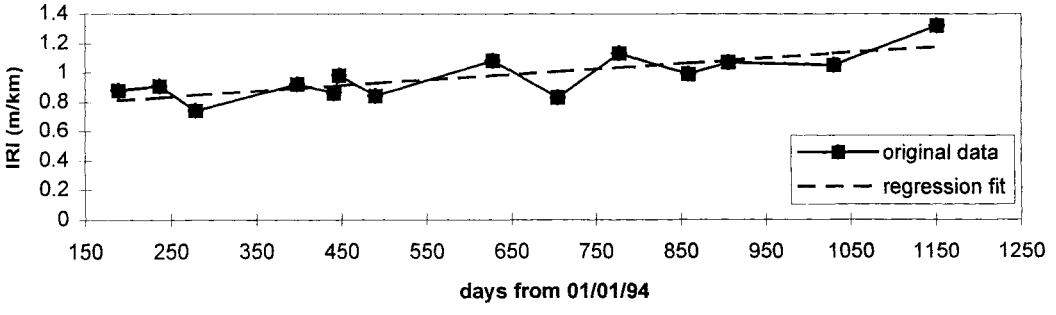

Figure 7.23 IRI for Mainline Section 1 (right lane)

RUTTING DEPTHS

Introduction

The 6-foot straight edge rutting depth data were manually collected (using a straight edge and a scale) for all sections by MN/DOT personnel. These data are presented as average rutting edge data: for every wheel path in every section one datum value was available for each of the years (1994, 1995 and 1996). For a given year, these data are presented for all sections on the same plot. These data are then presented separately for each section as a plot of rutting depths vs. time.

In general, the mainline right (north) lane is more rutted than the left (south) lane for most of the sections. This is believed to be due to the larger traffic volumes in the right lane. In the mainline left lane, the rutting depths for the left wheel path are lager than for the right wheel path; it is conjectured that this is due to a reduction in strength at edge of the road.

On low-volume road sections, the rutting values for the inside lane are higher than the rutting values for the outside lane. This is probably due to the larger number of load repetitions in the inside lane.

Average Rutting Depth Data

The following observations are made based upon the 6-foot straight edge rutting depths. These observations are substantiated by the following figures. The mainline right lane (north lane) has more severe rutting than the left lane; it is conjectured that this is due to the larger traffic load. In the left mainline lane the left wheel path has more severe rutting that the right wheel path; it is conjectured that this is due to a reduction in strength at edge of the road.

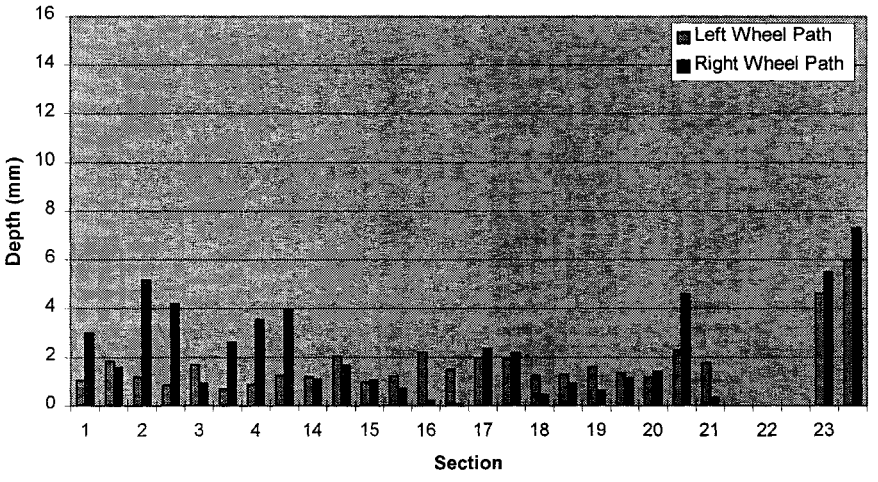

Figure 7.24 Rutting Depths for Right Lanes of the Mainline Sections, 1994

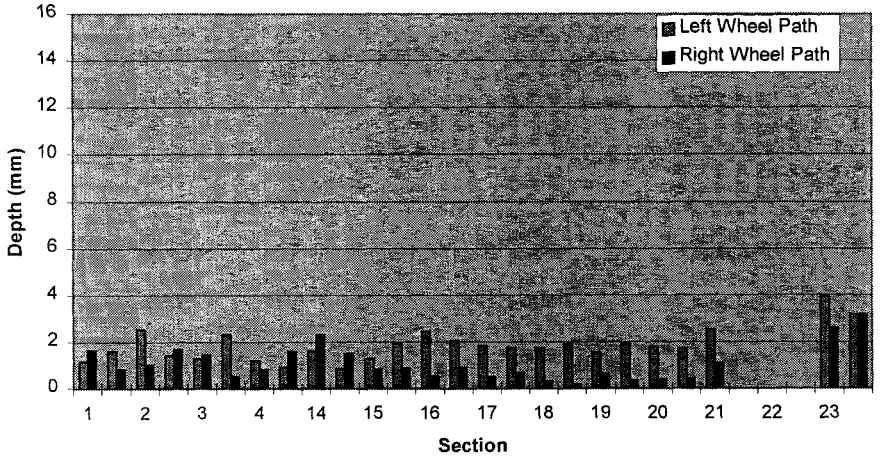

Figure 7.25 Rutting Depths for Left Lanes of Mainline Sections, 1994

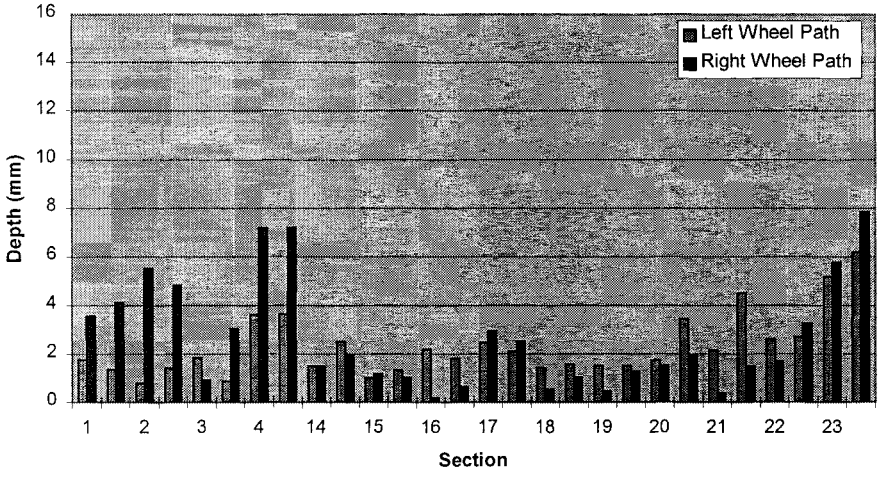

Figure 7.26 Rutting Depths for Right Lanes of Mainline Sections, 1995

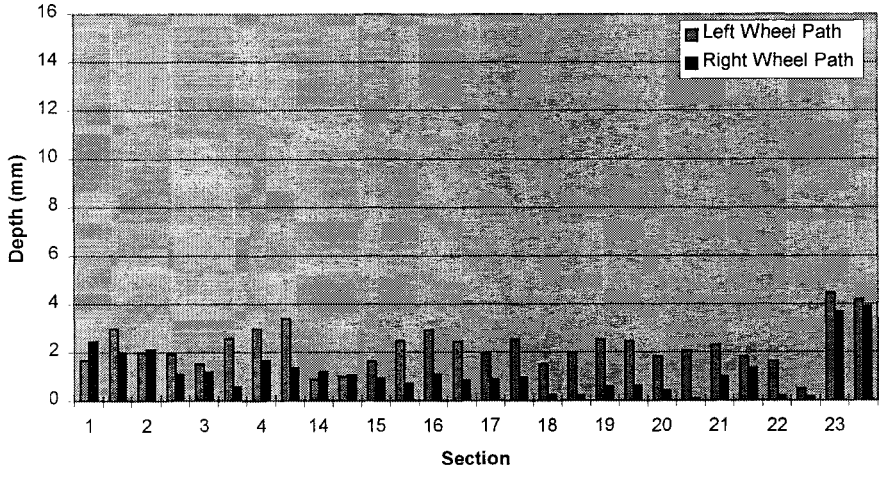

Figure 7.27 Rutting Depths for Left Lanes of Mainline Sections, 1995

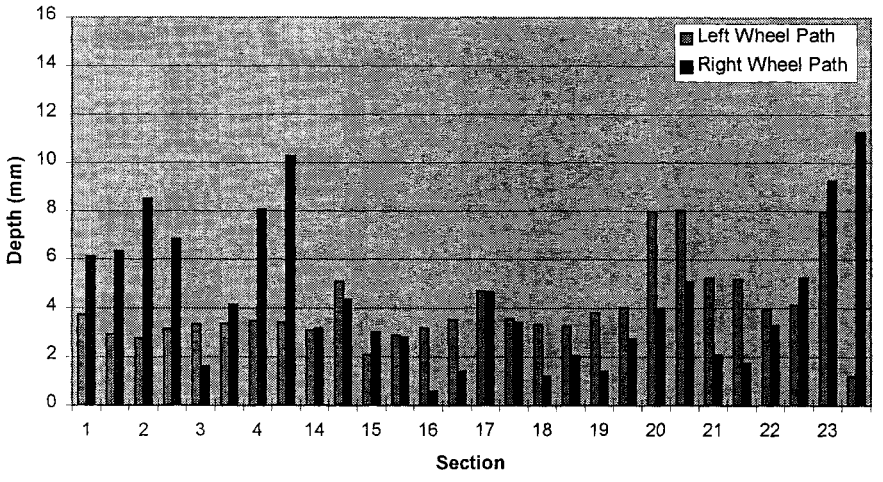

Figure 7.28 Rutting Depths for Right Lanes of Mainline Sections, 1996

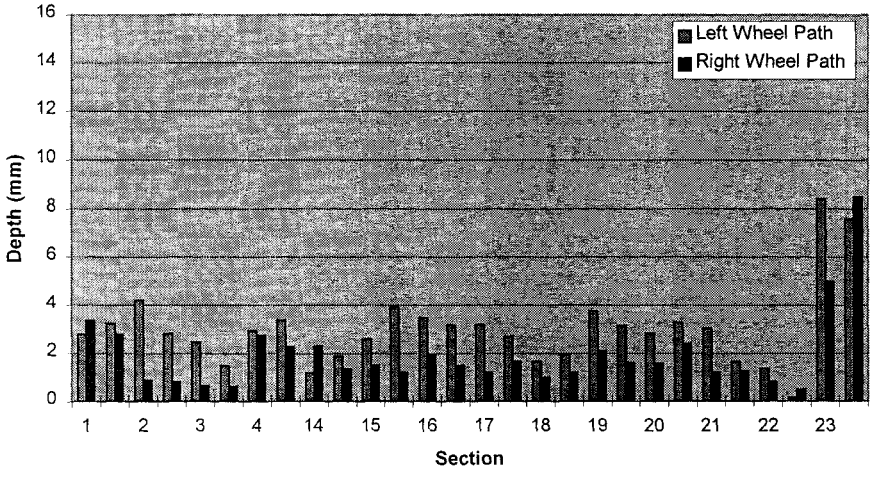

Figure 7.29 Rutting Depths for Left Lanes of Mainline Sections, 1996

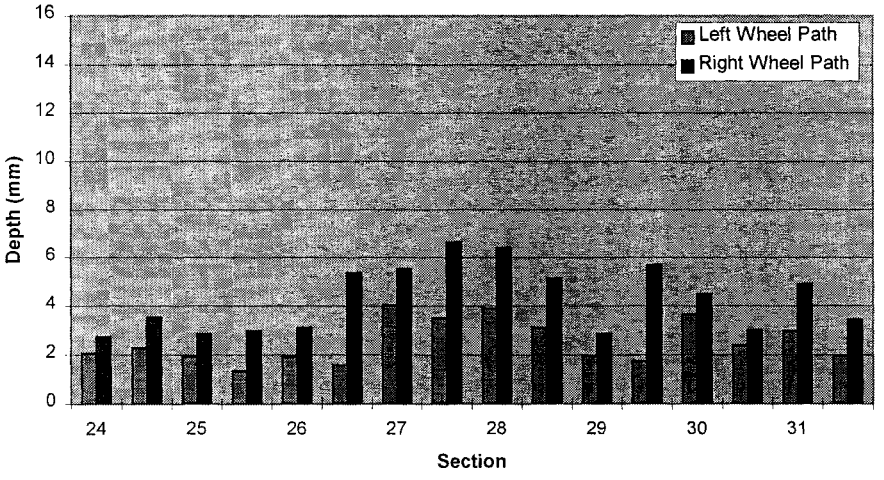

Figure 7.30 Rutting Depths for Inside Lanes of Low Volume Sections, 1994

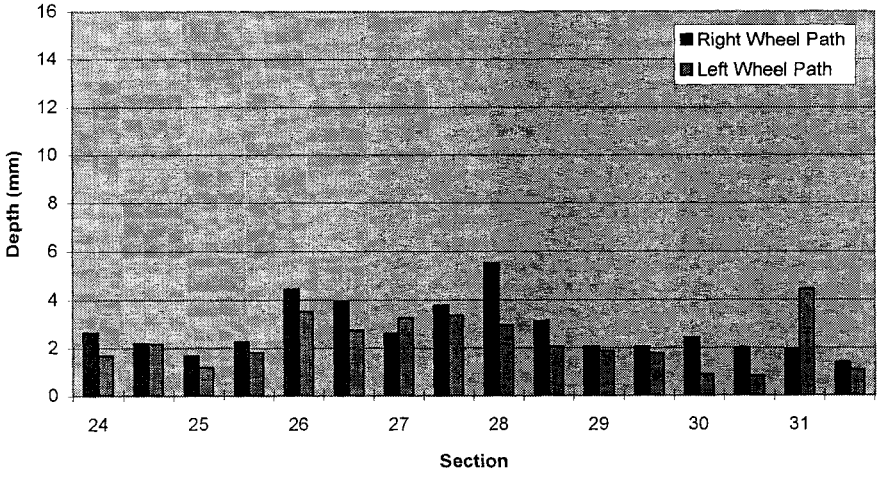

Figure 7.31 Rutting Depths for Outside Lanes of Low Volume Sections, 1994

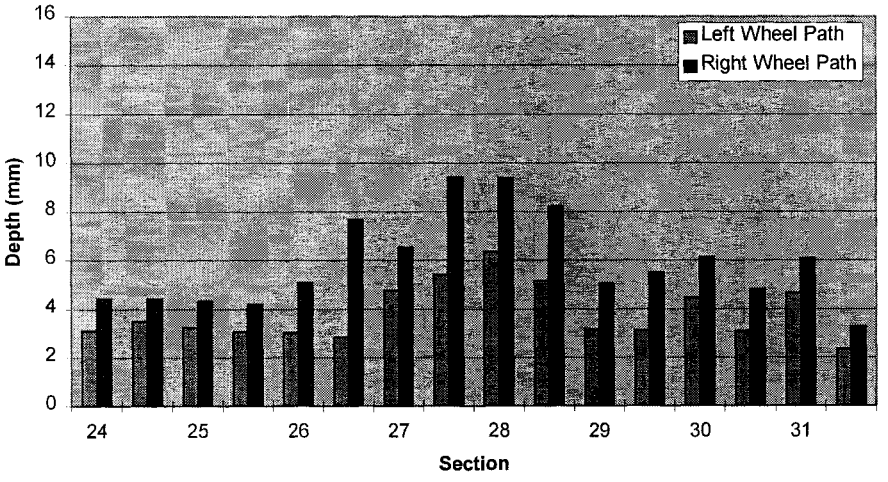

Figure 7.32 Rutting Depths for Inside Lanes of Low Volume Sections, 1995

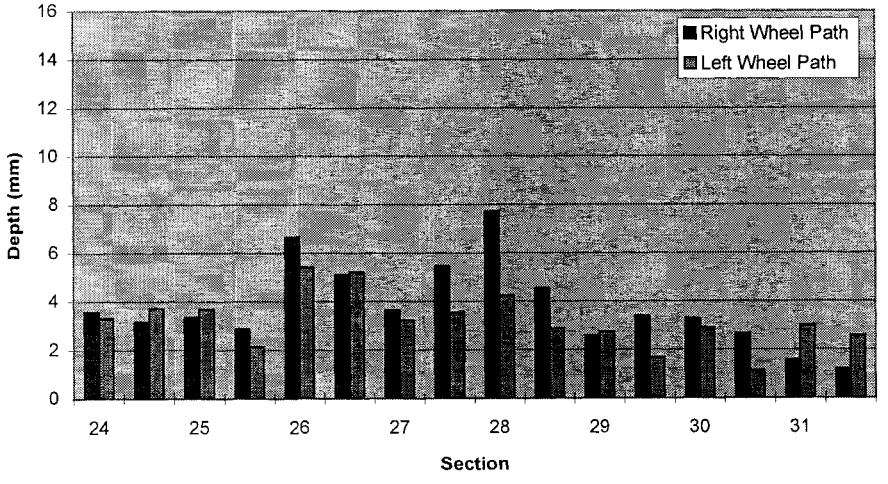

Figure 7.33 Rutting Depths for Outside Lanes of Low Volume Sections, 1995

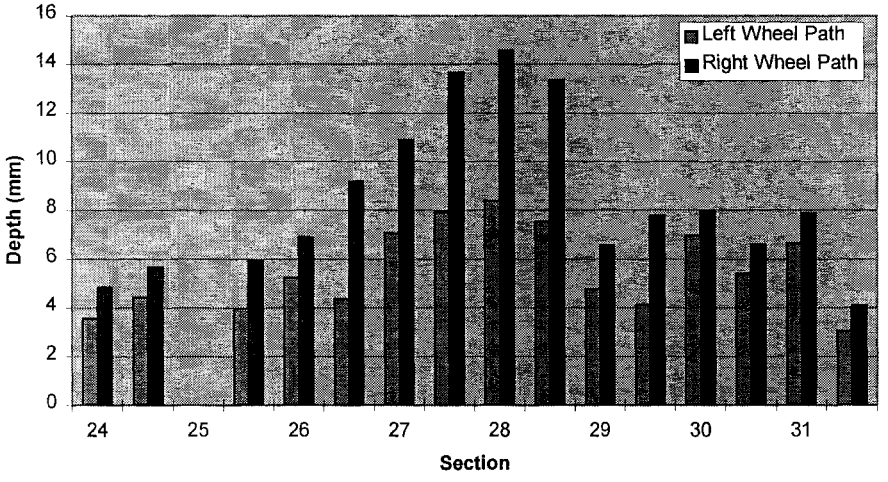

Figure 7.34 Rutting Depths for Inside Lanes of Low Volume Sections, 1996

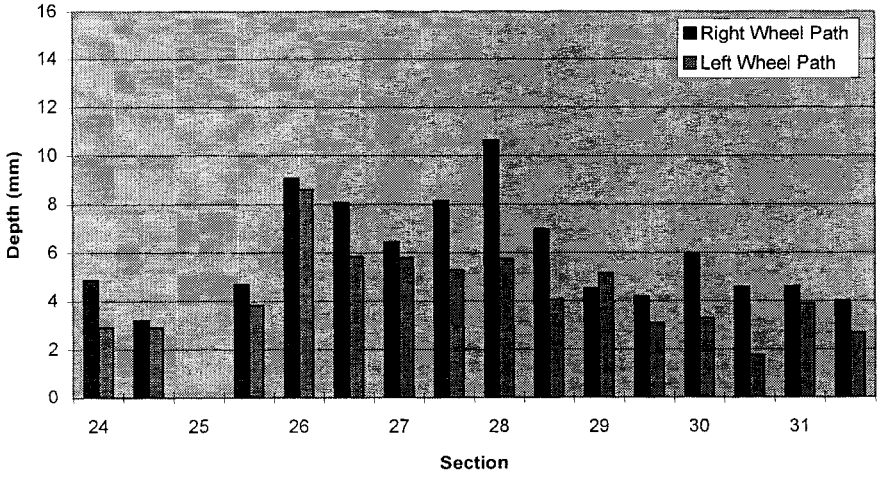

Figure 7.35 Rutting Depths for Outside Lanes of Low Volume Sections, 1996

On the low volume road, the inside lane has more severe rutting than the outside lane; it is conjectured that this is due to the additional loading on the inside lane (the inside lane has more repetitions).

Although the available data does not offer an explanation, there are some noteworthy apparent patterns in the previous set of figures. In particular, on the low volume road (Sections 24-31) the right wheel path shows greater rutting depths than the left wheel path. This observation holds for almost all section in all years, and is independent of the lane.

Temporal Variations of Rutting Depths

The following 88 figures show the change in rutting depths over time for 1994 through 1997. These plots are broken out by section, by lane, and by wheel path. Both the mainline sections and the low volume sections are presented.

A slight linearly increasing trend is present in almost all plots. The only exception is the right lane of Section 20, which shows a more marked increase in rutting depth with time.

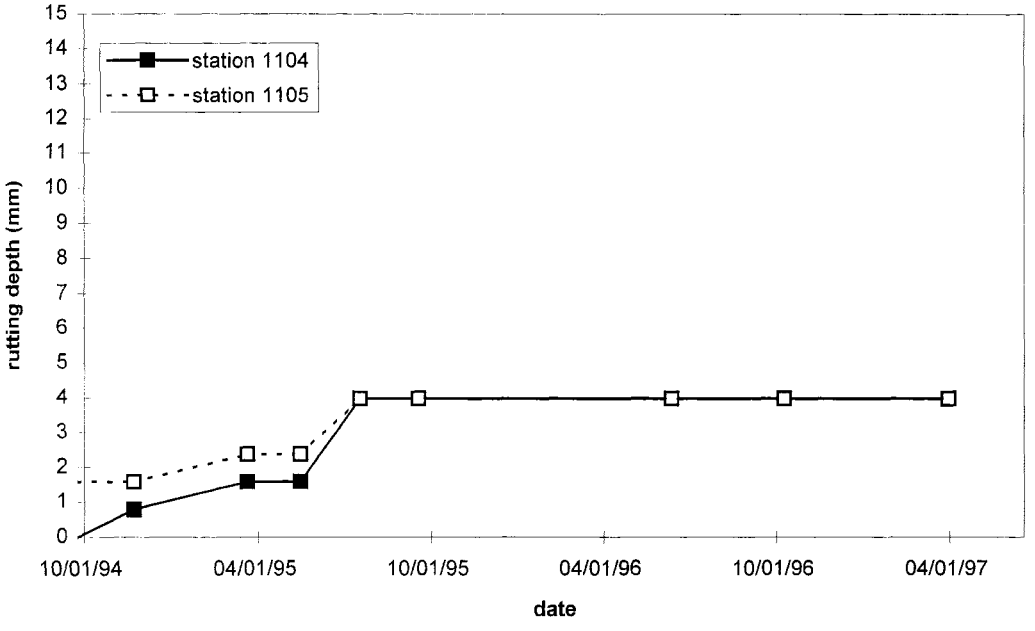

Figure 7.36 Rutting Depths, Section 1, Left Lane, Left Wheel Path

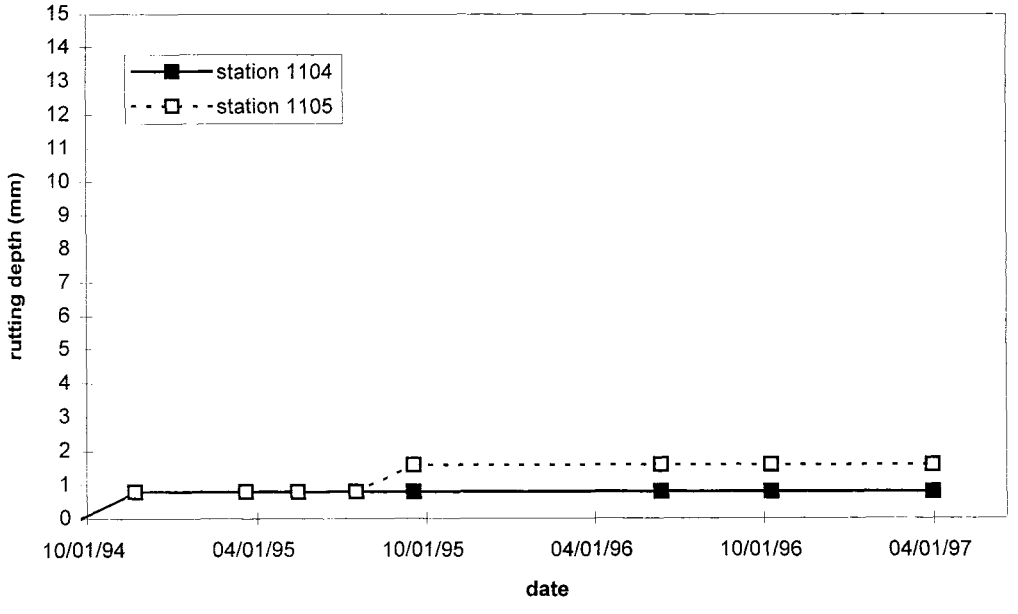

Figure 7.37 Rutting Depths, Section 1, Left Lane, Right Wheel Path

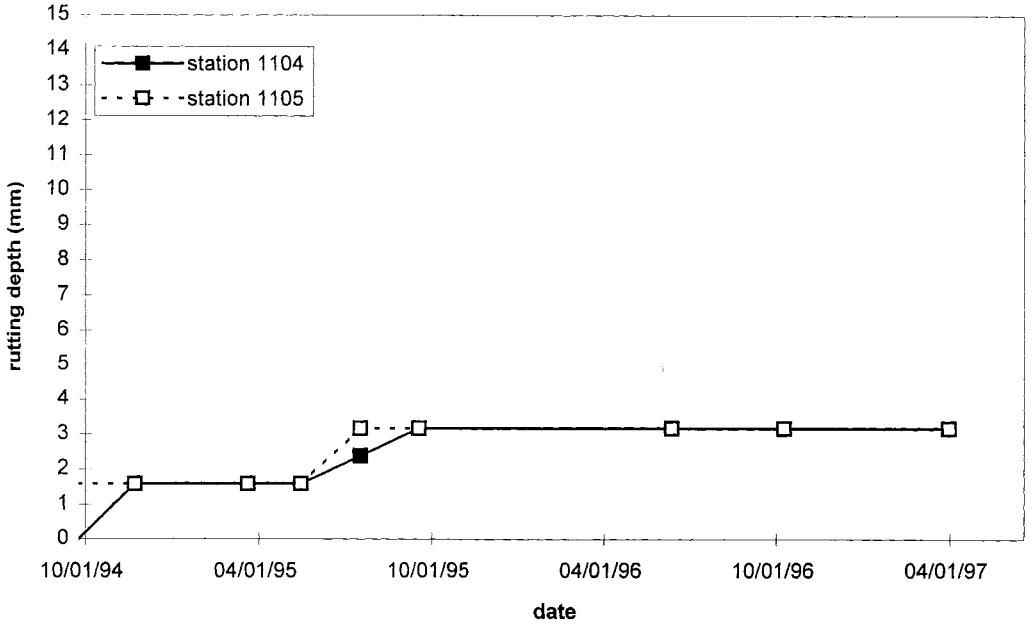

Figure 7.38 Rutting Depths, Section 1, Right Lane, Left Wheel Path

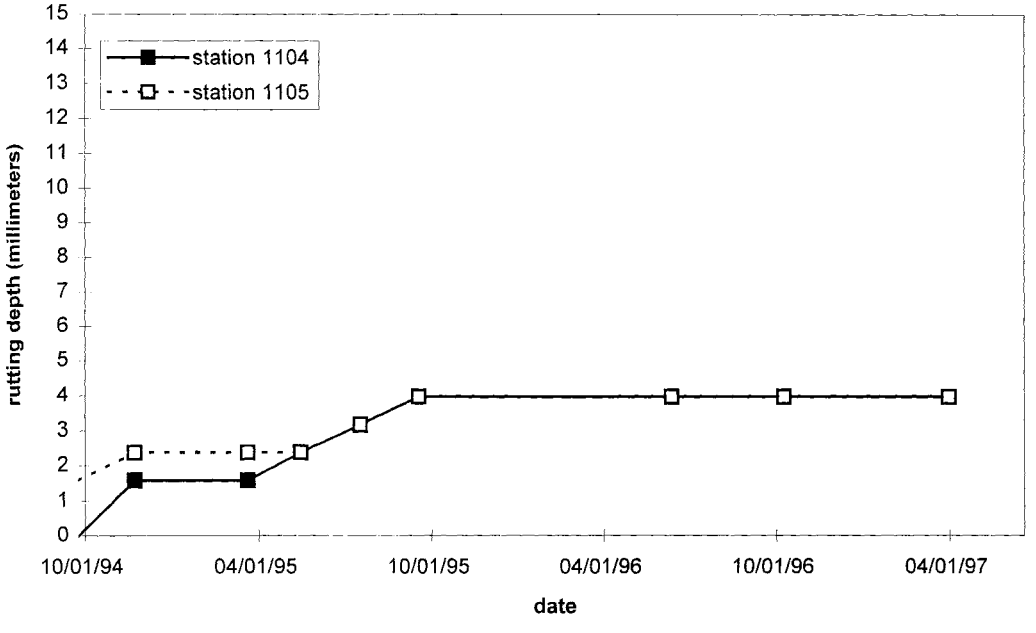

Figure 7.39 Rutting Depths, Section 1, Right Lane, Right Wheel Path

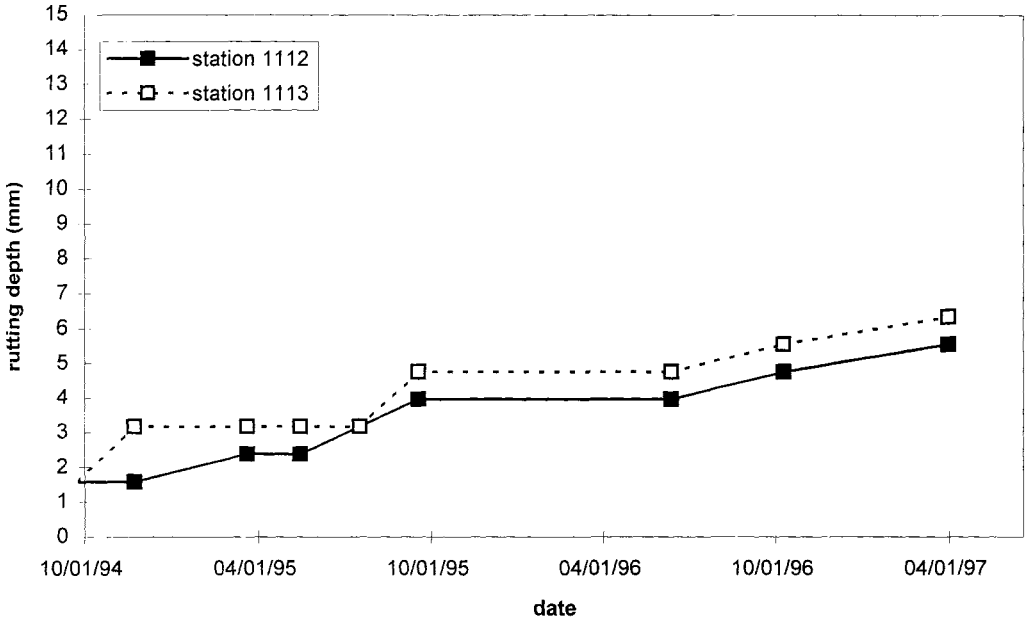

Figure 7.40 Rutting Depths, Section 2, Left Lane, Left Wheel Path

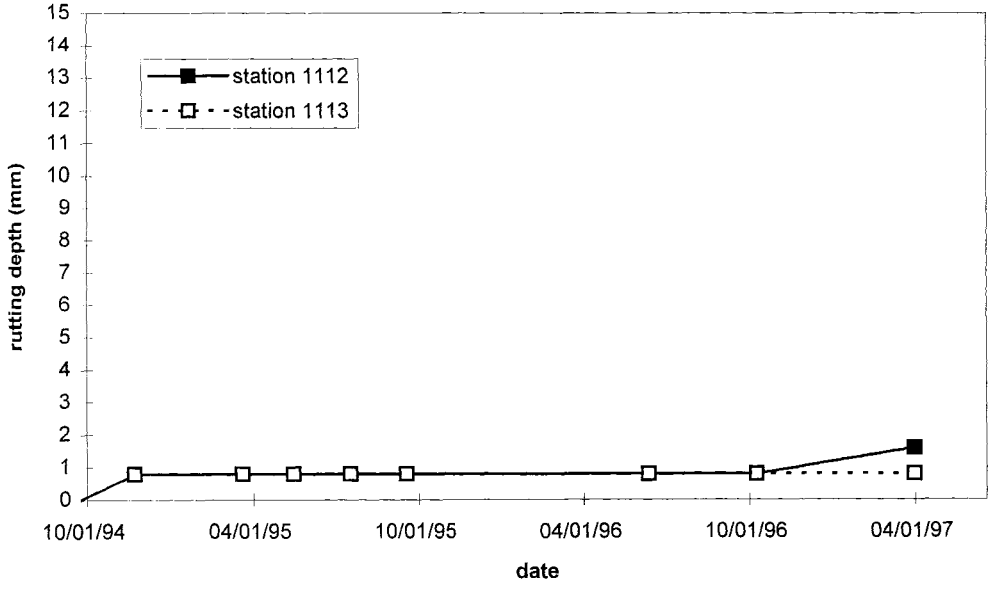

Figure 7.41 Rutting Depths, Section 2, Left Lane, Right Wheel Path

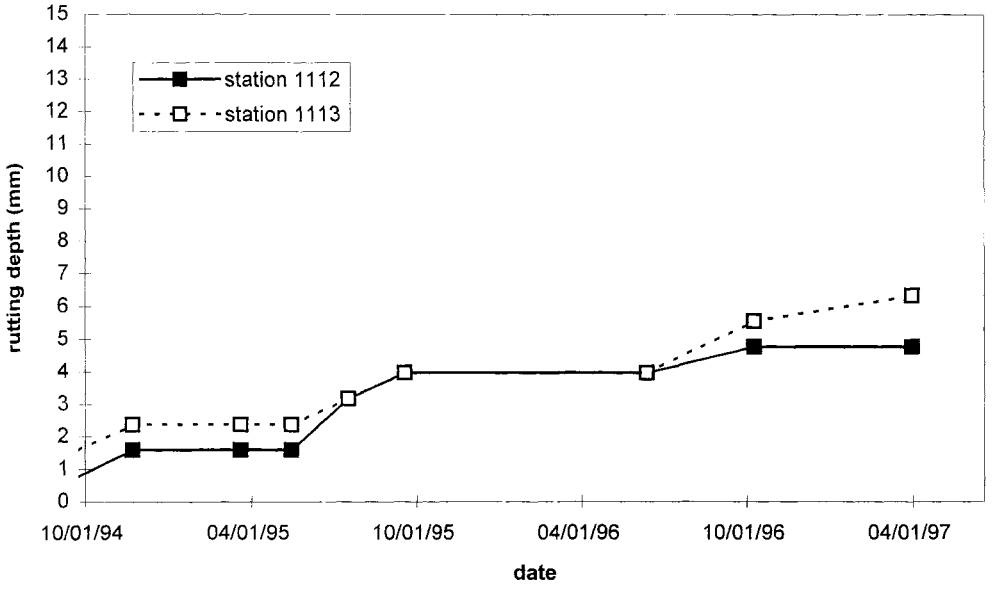

Figure 7.42 Rutting Depths, Section 2, Right Lane, Left Wheel Path

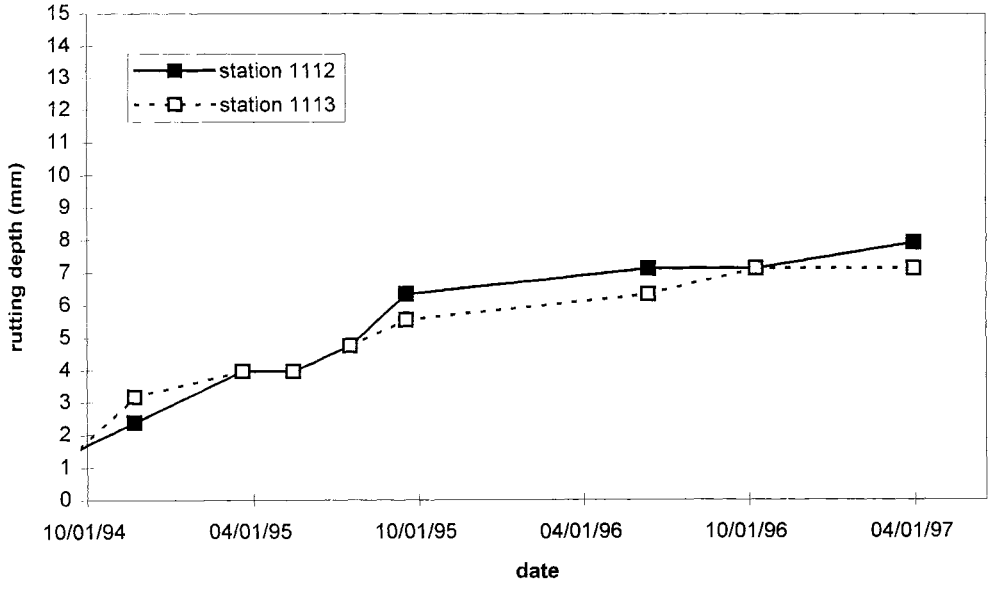

Figure 7.43 Rutting Depths, Section 2, Right Lane, Right Wheel Path

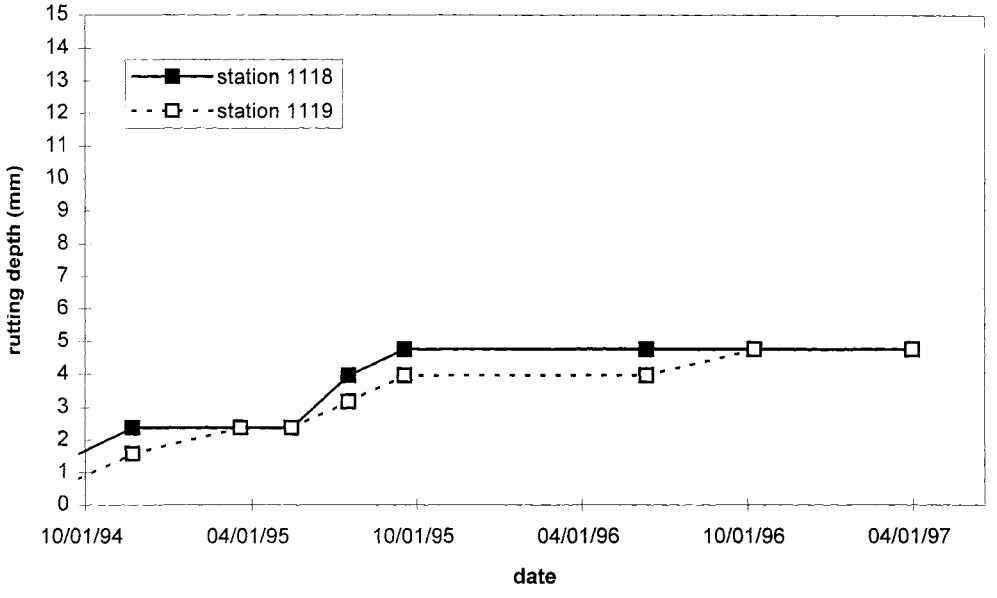

Figure 7.44 Rutting Depths, Section 3, Left Lane, Left Wheel Path

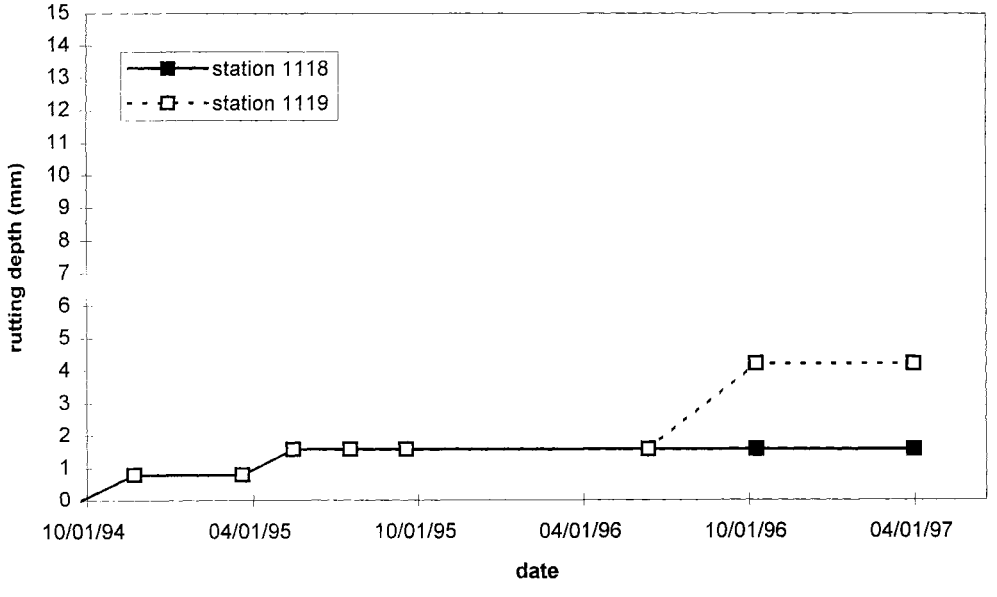

Figure 7.45 Rutting Depths, Section 3, Left Lane, Right Wheel Path

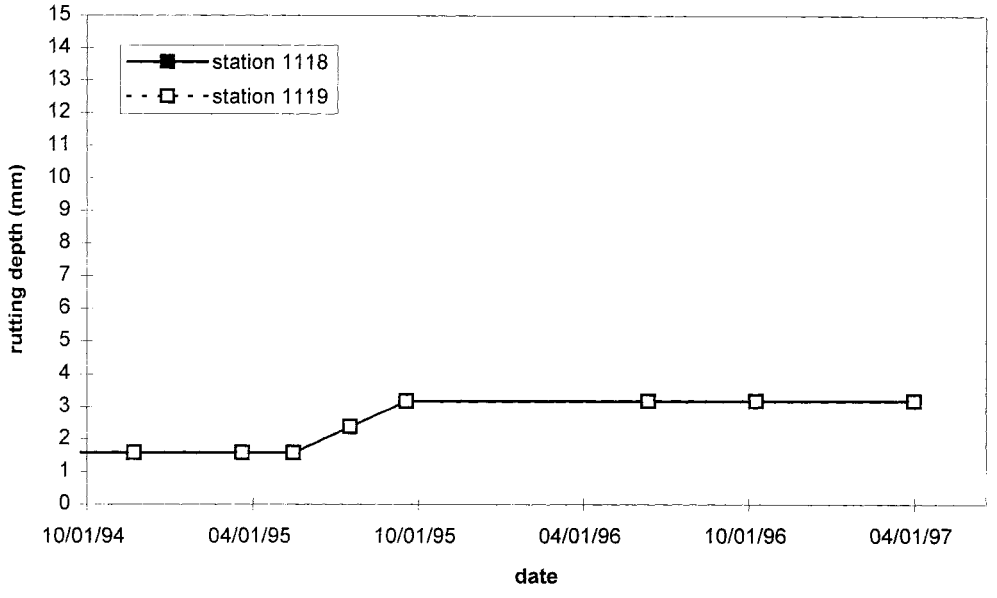

Figure 7.46 Rutting Depths, Section 3, Right Lane, Left Wheel Path

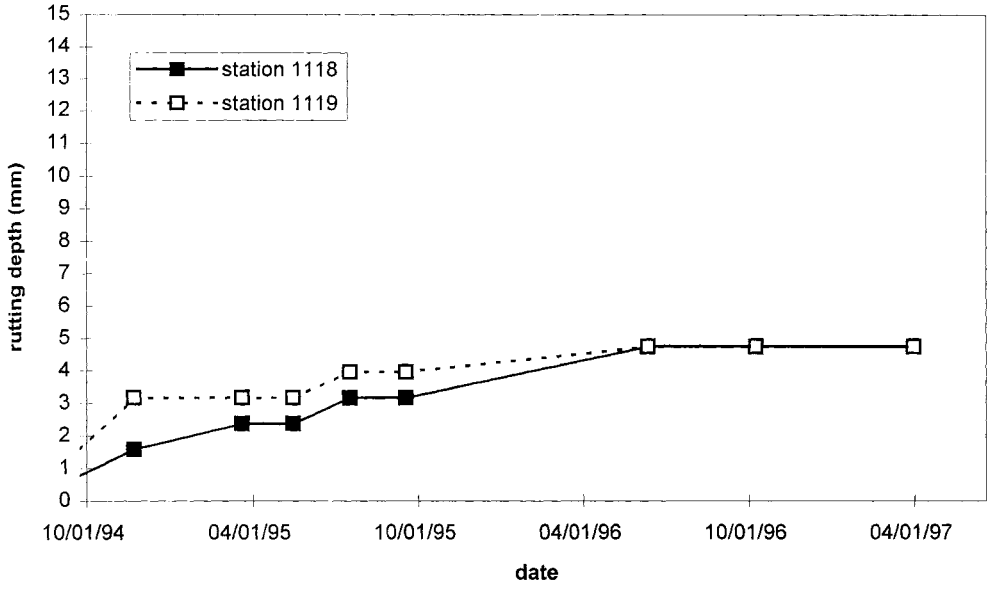

Figure 7.47 Rutting Depths, Section 3, Right Lane, Right Wheel Path

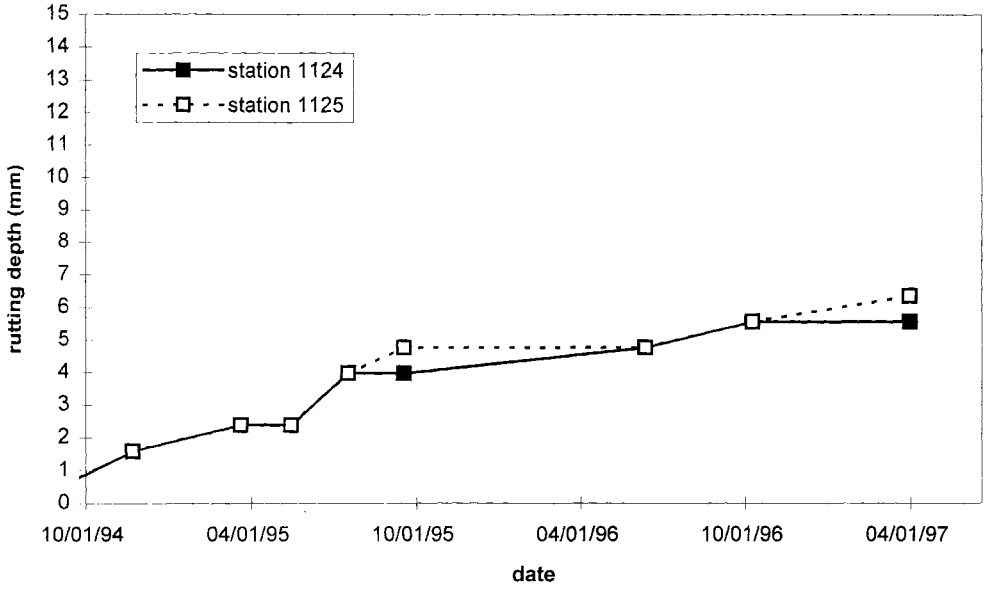

Figure 7.48 Rutting Depths, Section 4, Left Lane, Left Wheel Path

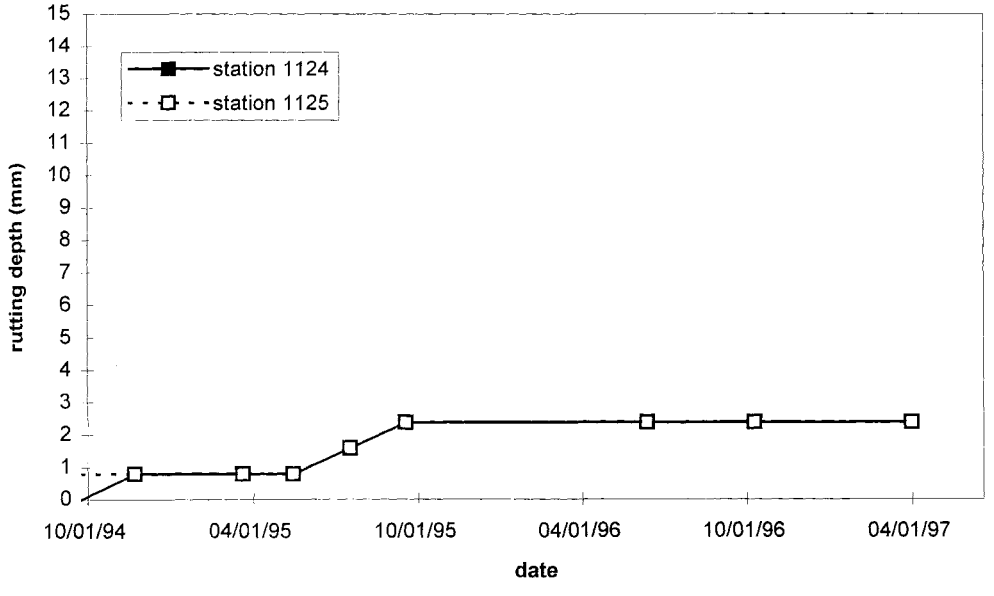

Figure 7.49 Rutting Depths, Section 4, Left Lane, Right Wheel Path

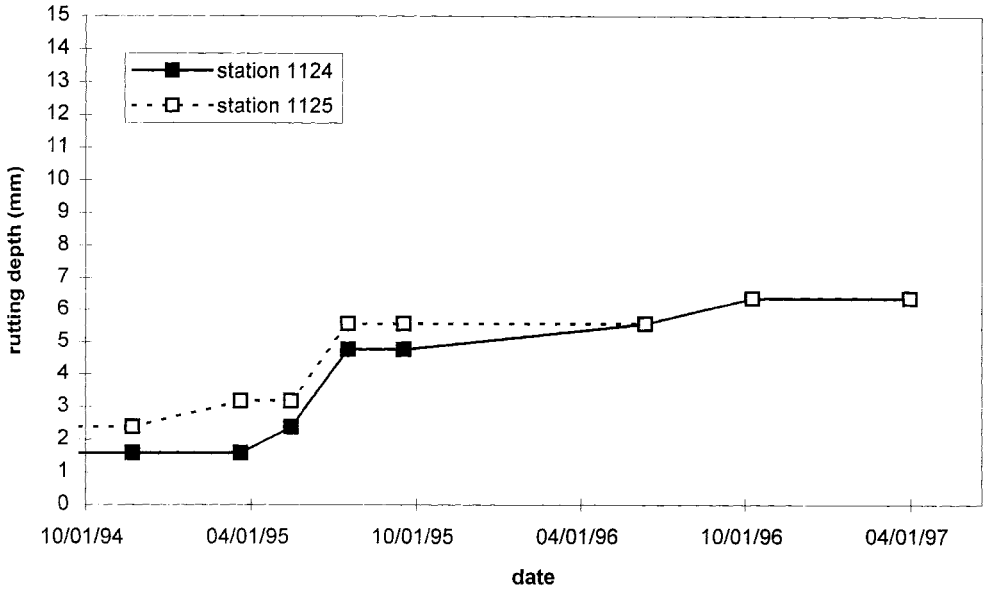

Figure 7.50 Rutting Depths, Section 4, Right Lane, Left Wheel Path

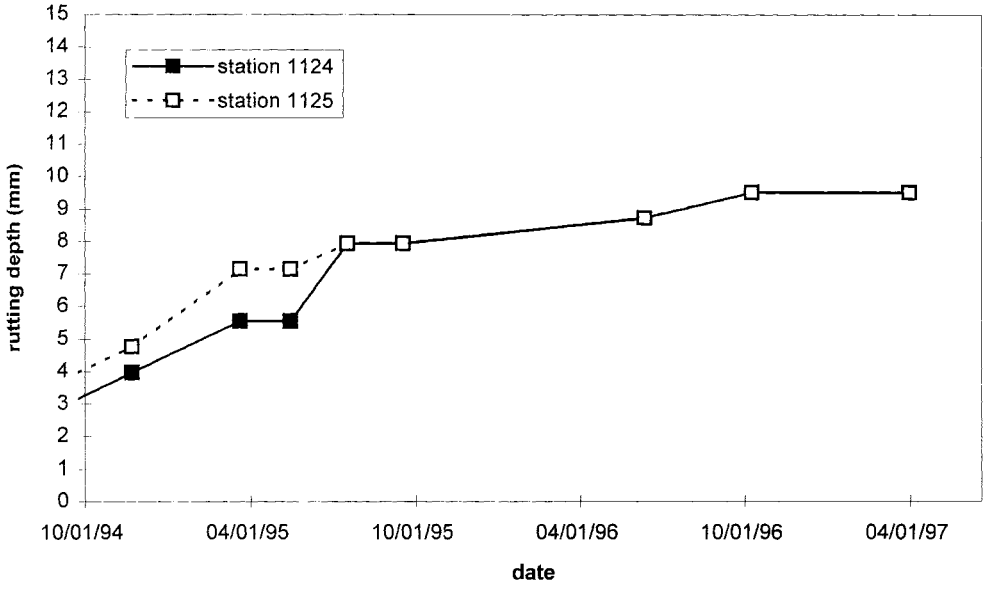

Figure 7.51 Rutting Depths, Section 4, Right Lane, Right Wheel Path

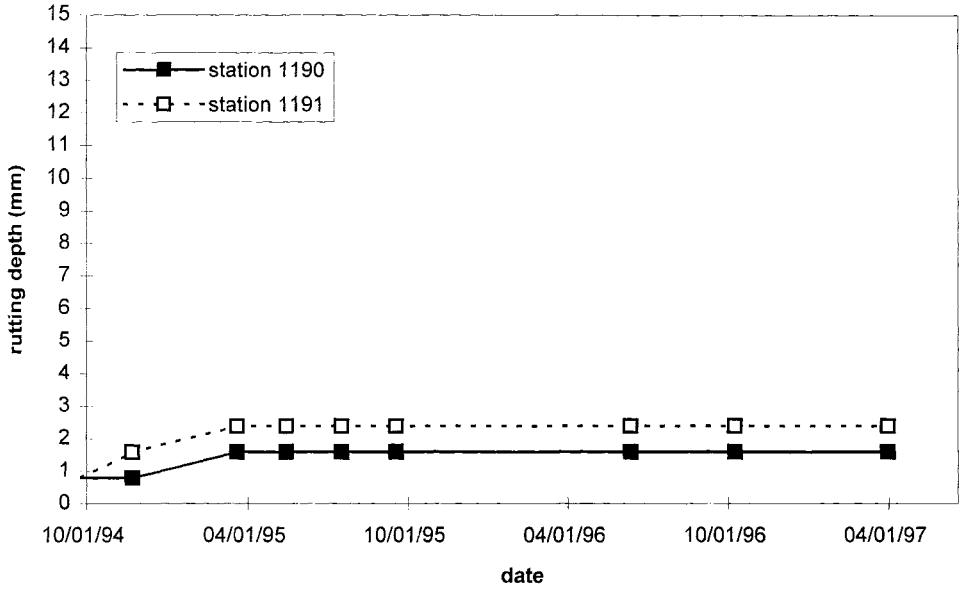

Figure 7.52 Rutting Depths, Section 14, Left Lane, Left Wheel Path

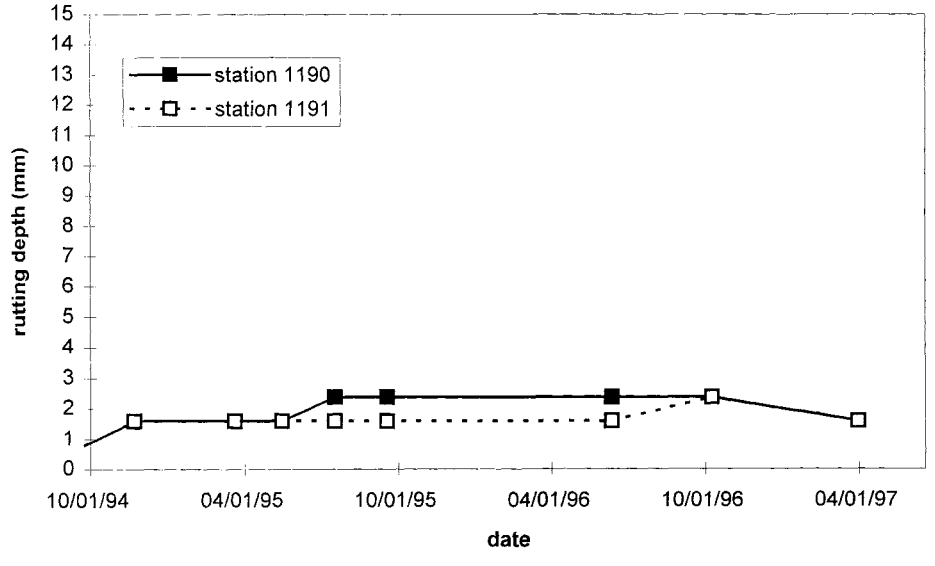

Figure 7.53 Rutting Depths, Section 14, Left Lane, Right Wheel Path

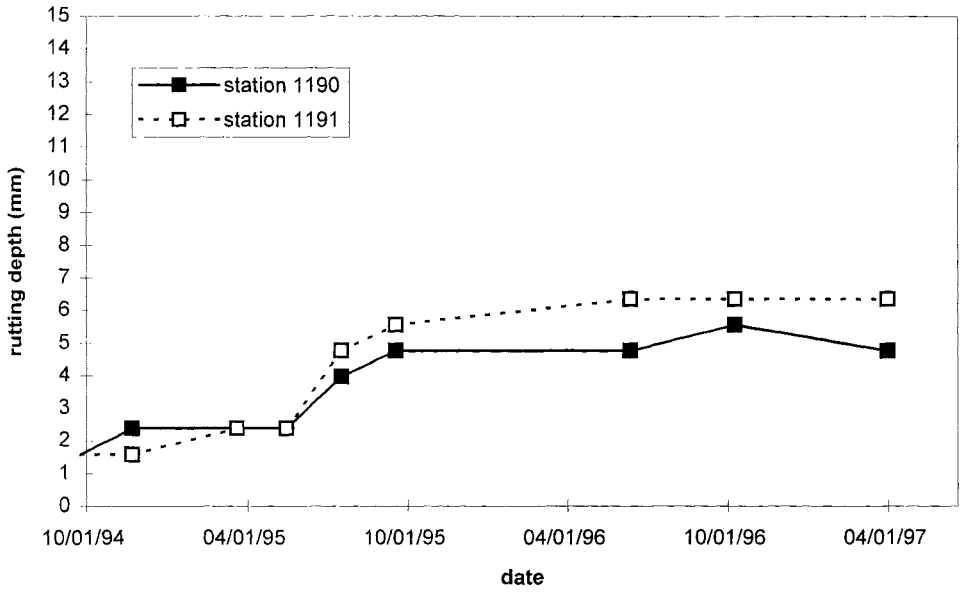

Figure 7.54 Rutting Depths, Section 14, Right Lane, Left Wheel Path

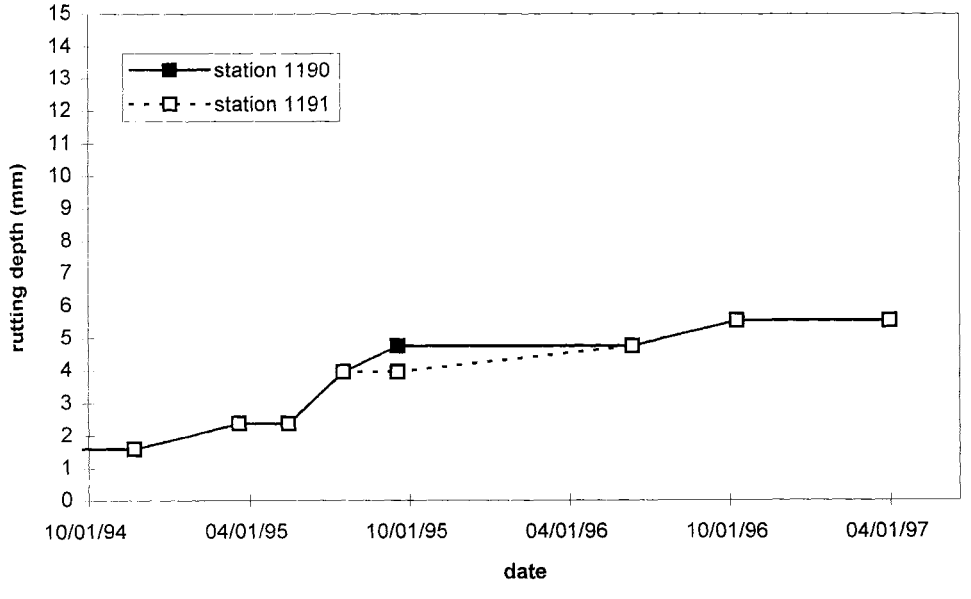

Figure 7.55 Rutting Depths, Section 14, Right Lane, Right Wheel Path

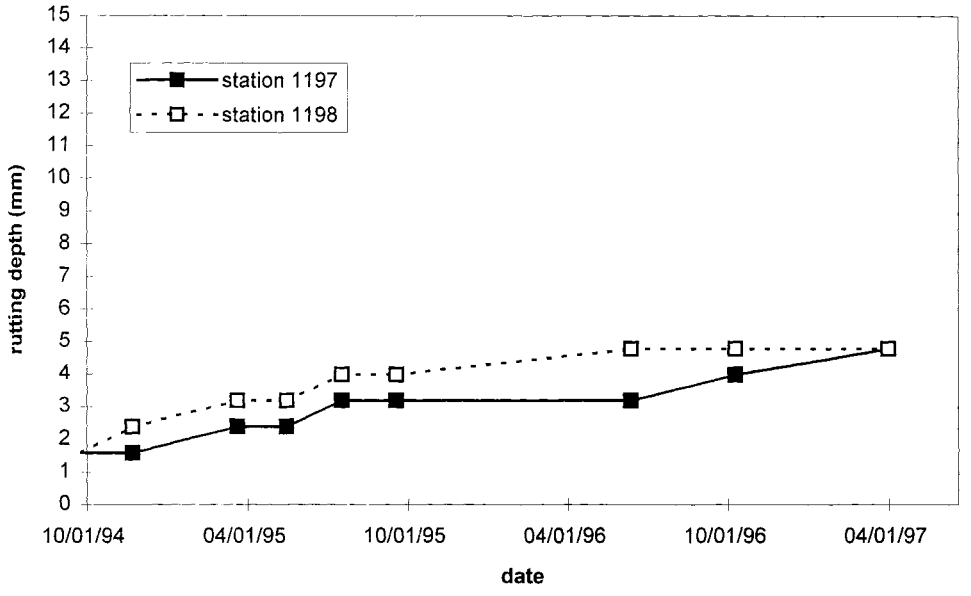

Figure 7.56 Rutting Depths, Section 15, Left Lane, Left Wheel Path

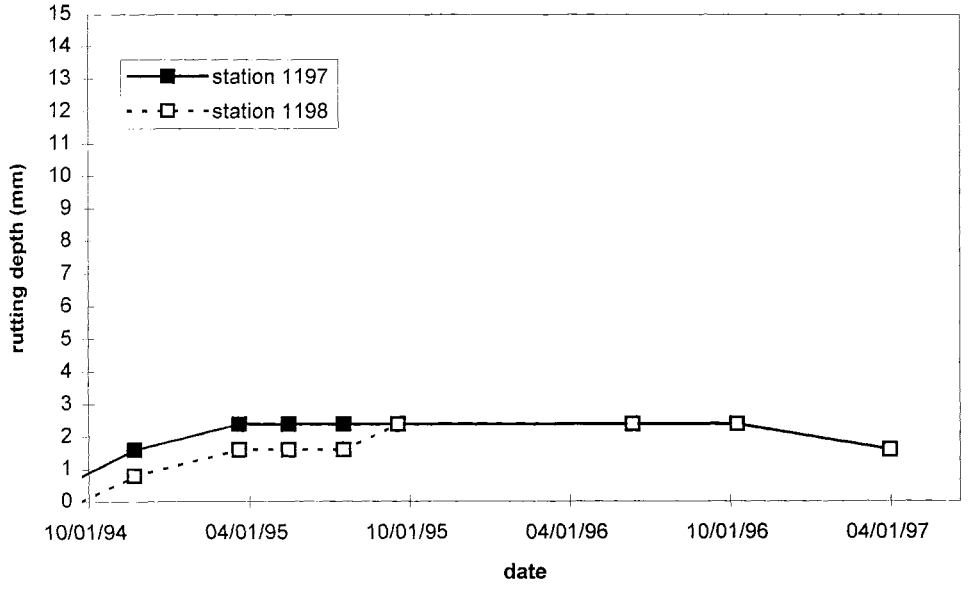

Figure 7.57 Rutting Depths, Section 15, Left Lane, Right Wheel Path

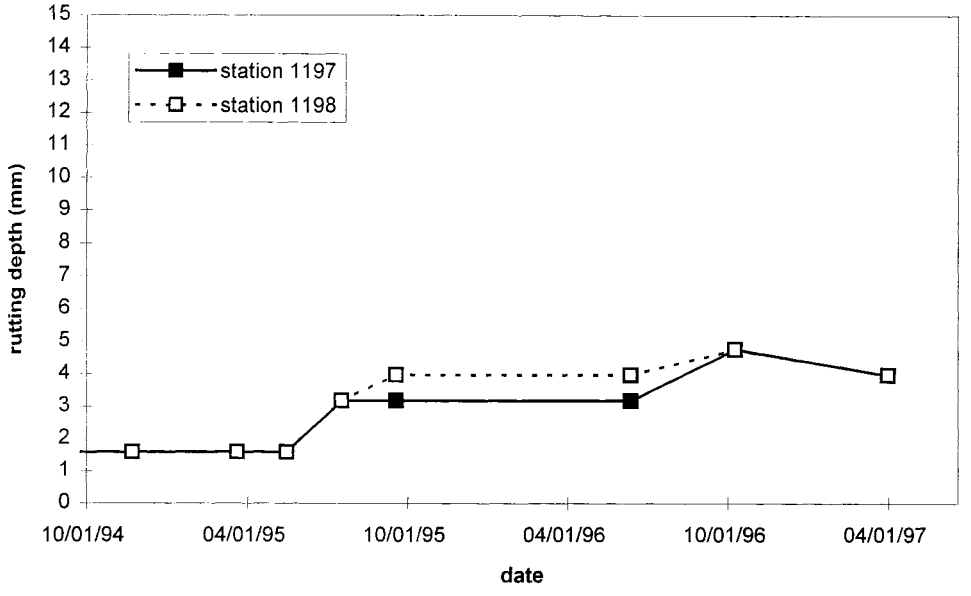

Figure 7.58 Rutting Depths, Section 15, Right Lane, Left Wheel Path

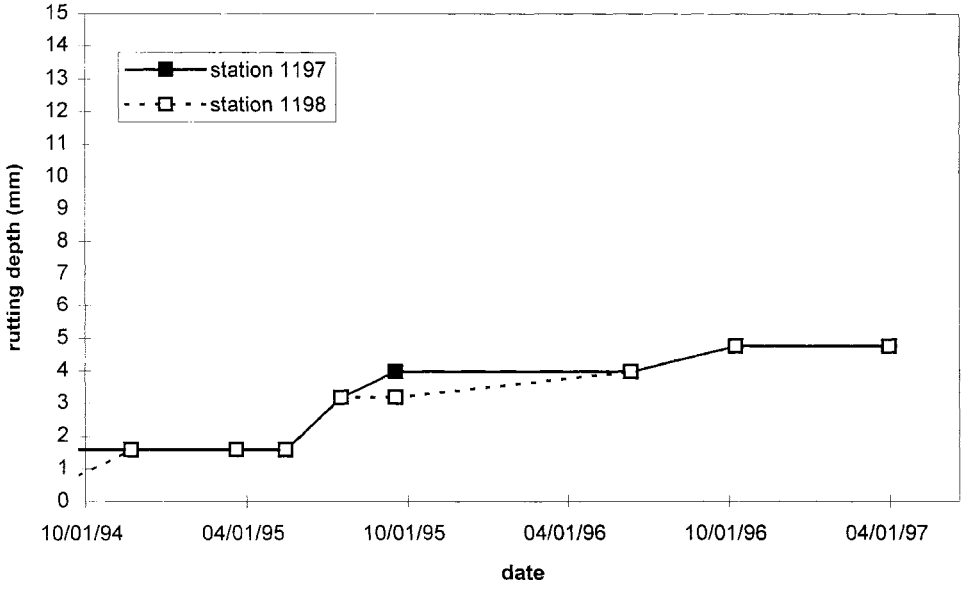

Figure 7.59 Rutting Depths, Section 15, Right Lane, Right Wheel Path

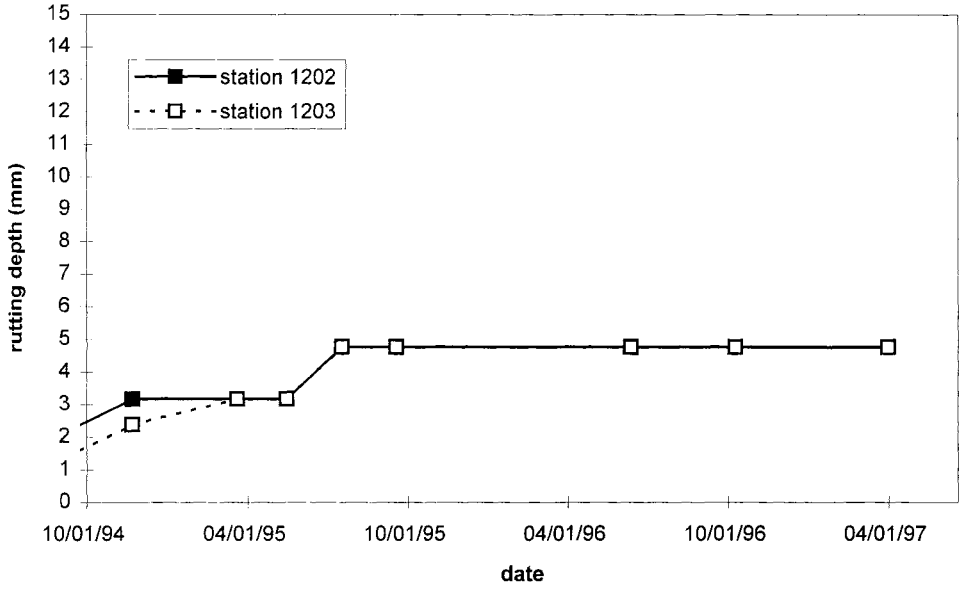

Figure 7.60 Rutting Depths, Section 16, Left Lane, Left Wheel Path

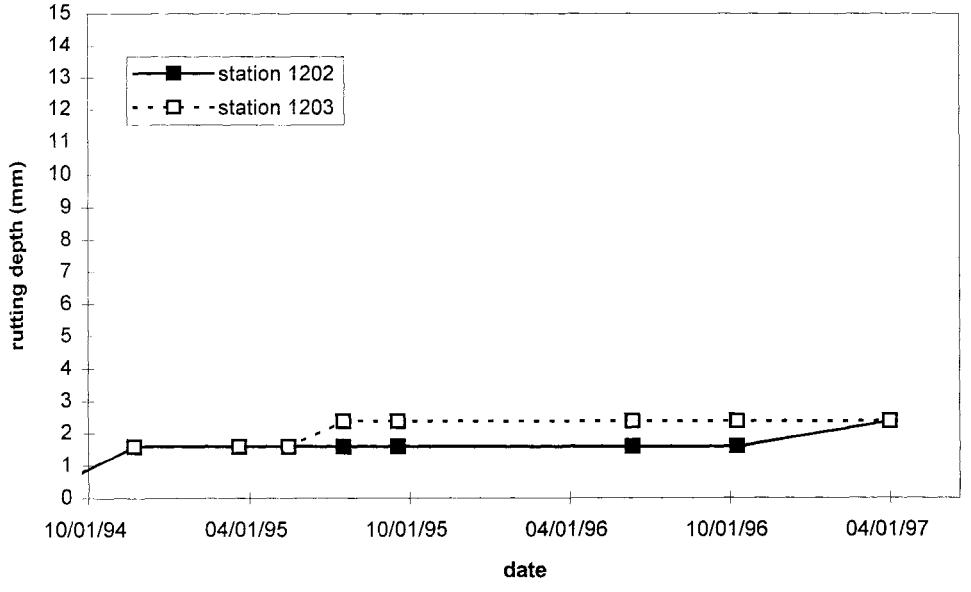

Figure 7.61 Rutting Depths, Section 16, Left Lane, Right Wheel Path

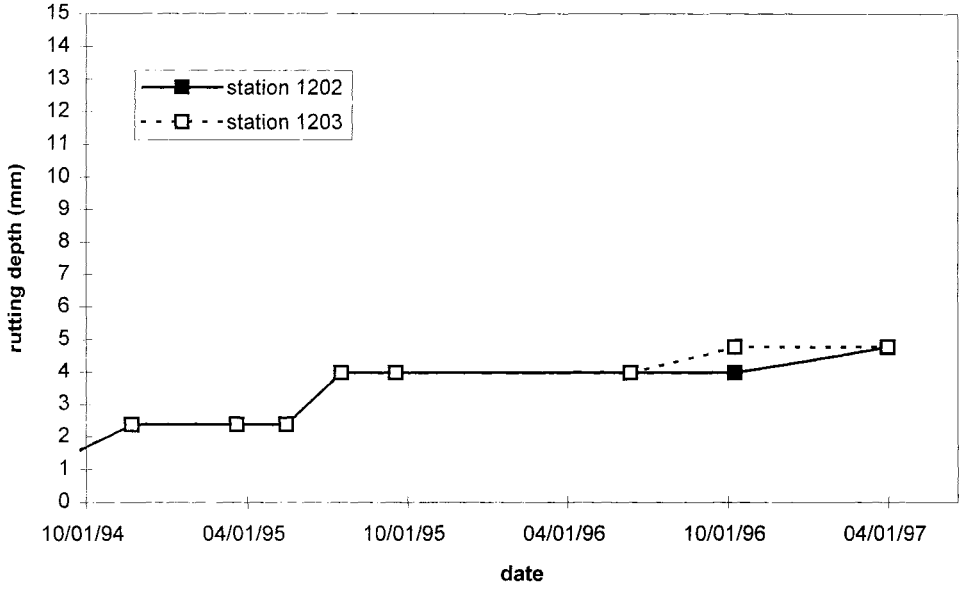

Figure 7.62 Rutting Depths, Section 16, Right Lane, Left Wheel Path

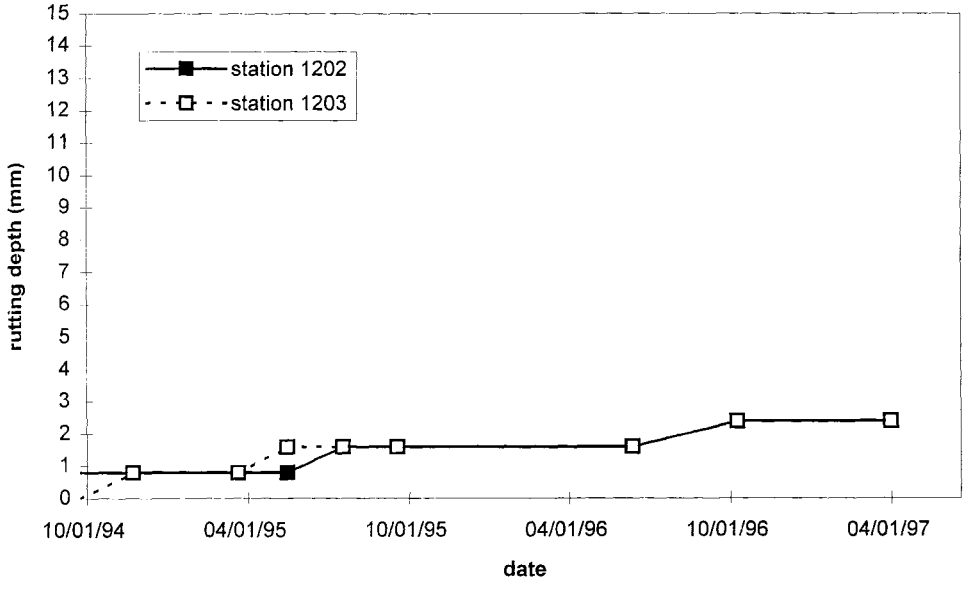

Figure 7.63 Rutting Depths, Section 16, Right Lane, Right Wheel Path

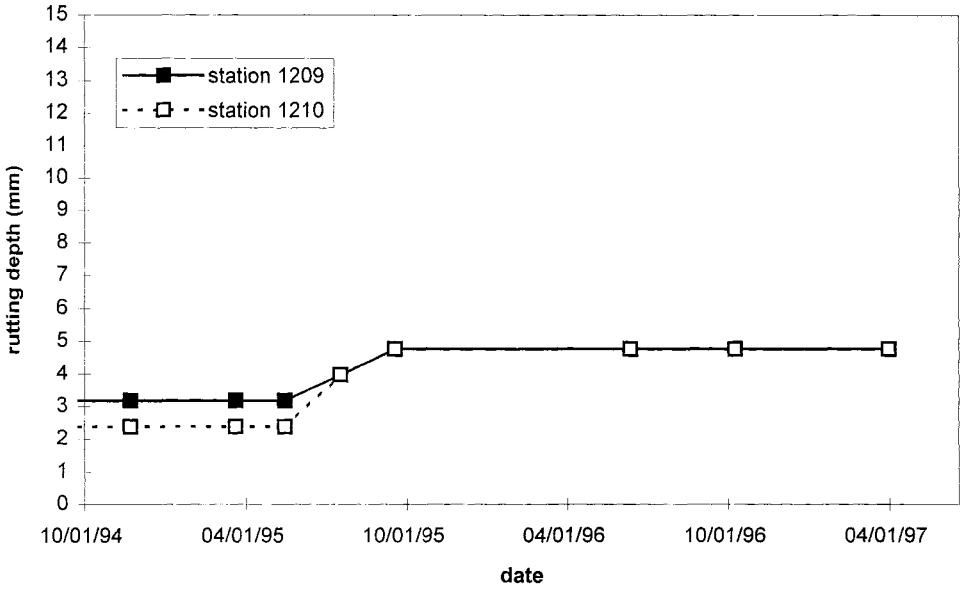

Figure 7.64 Rutting Depths, Section 17, Left Lane, Left Wheel Path

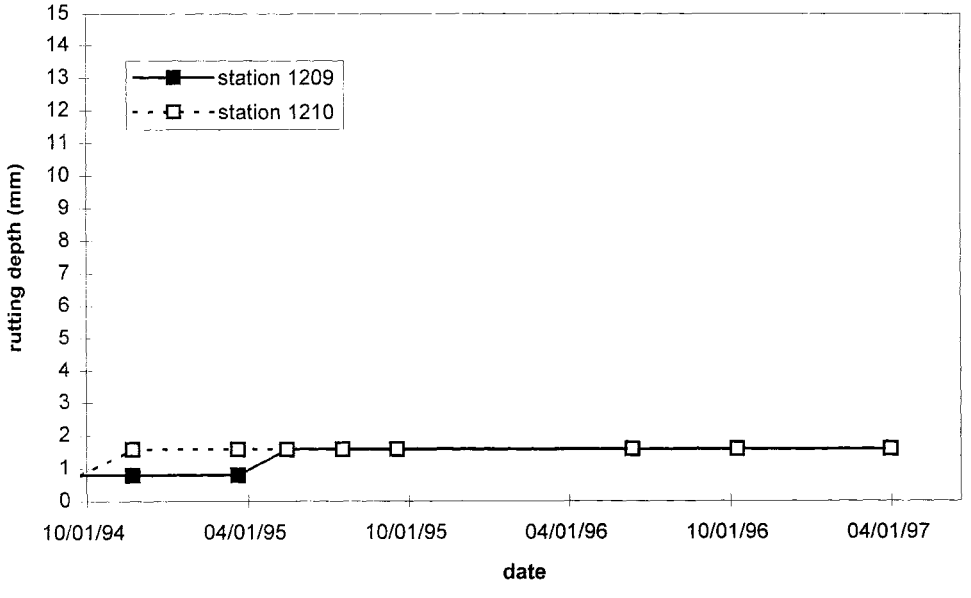

Figure 7.65 Rutting Depths, Section 17, Left Lane, Right Wheel Path

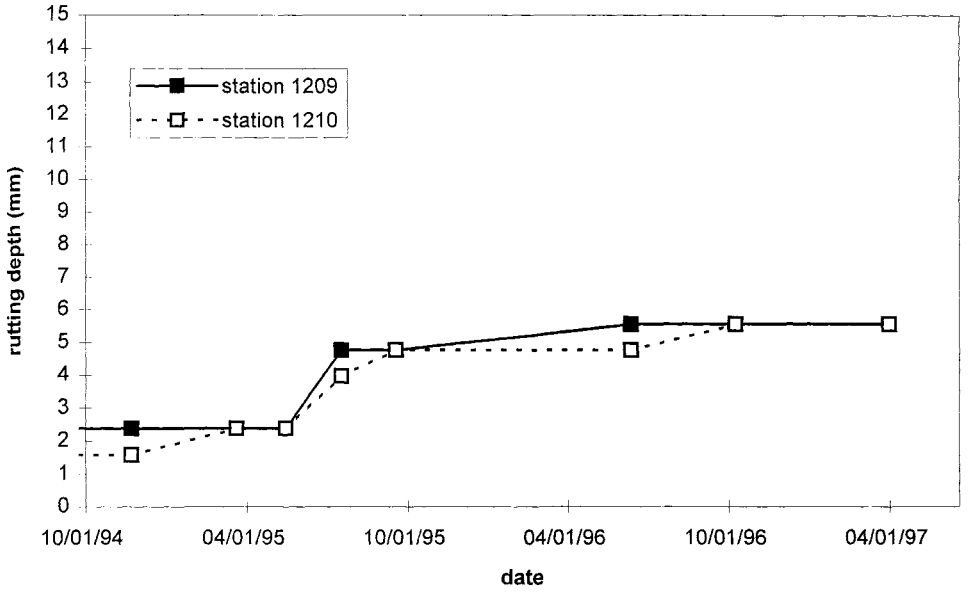

Figure 7.66 Rutting Depths, Section 17, Right Lane, Left Wheel Path

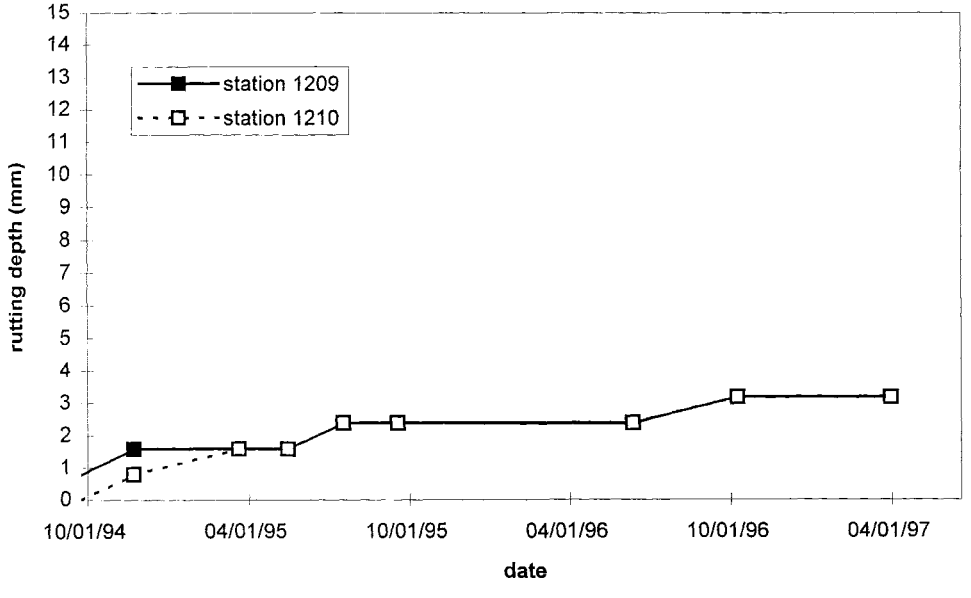

Figure 7.67 Rutting Depths, Section 17, Right Lane, Right Wheel Path

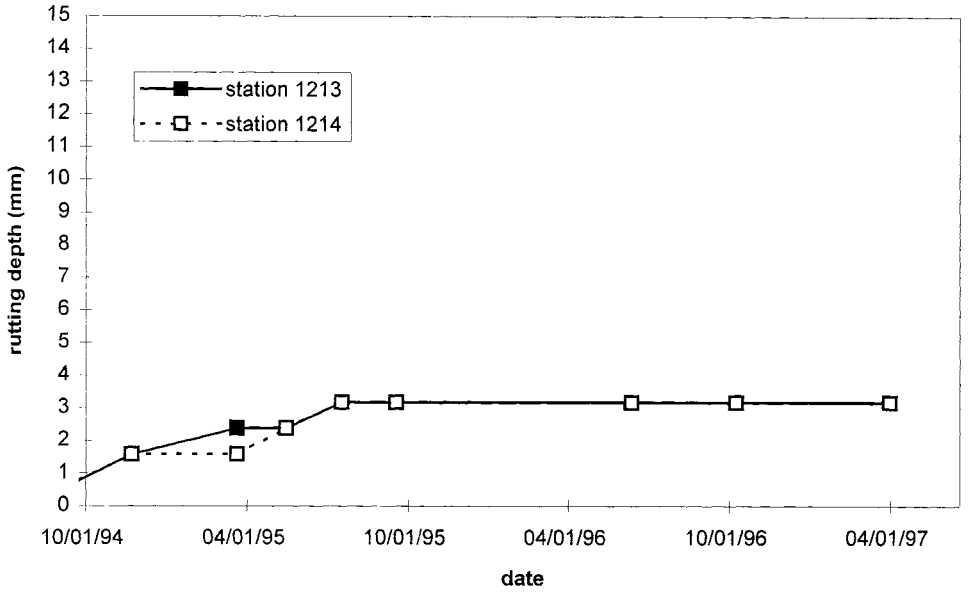

Figure 7.68 Rutting Depths, Section 18, Left Lane, Left Wheel Path

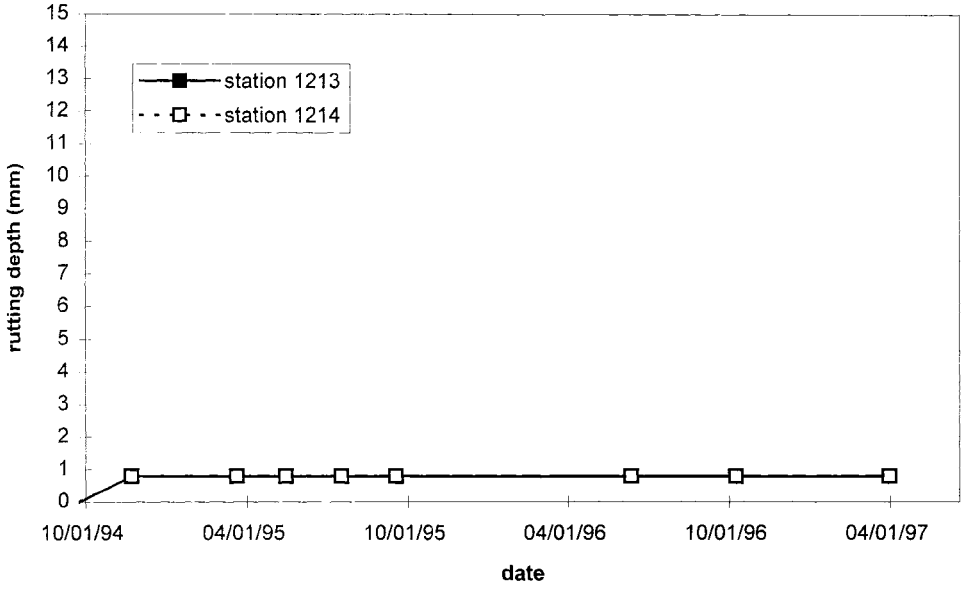

Figure 7.69 Rutting Depths, Section 18, Left Lane, Right Wheel Path

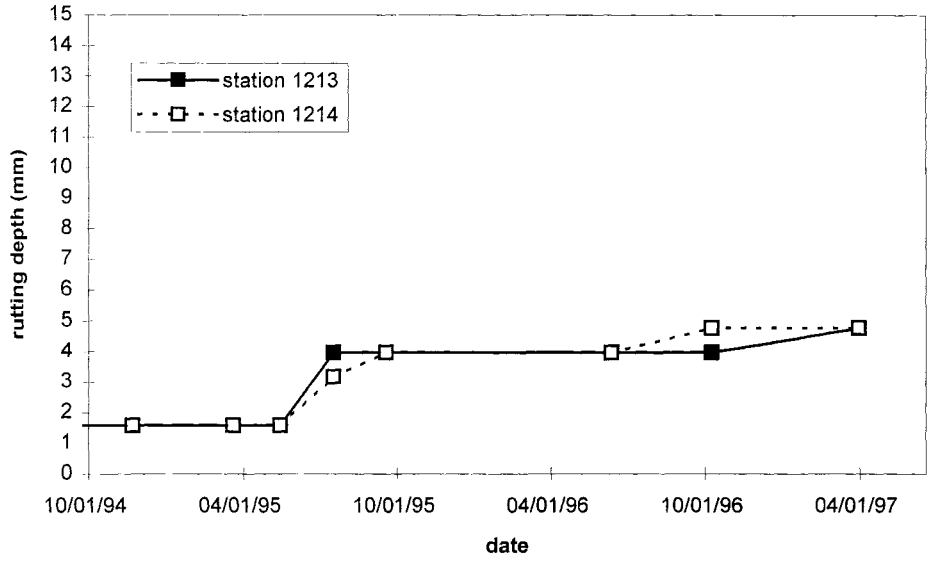

Figure 7.70 Rutting Depths, Section 18, Right Lane, Left Wheel Path

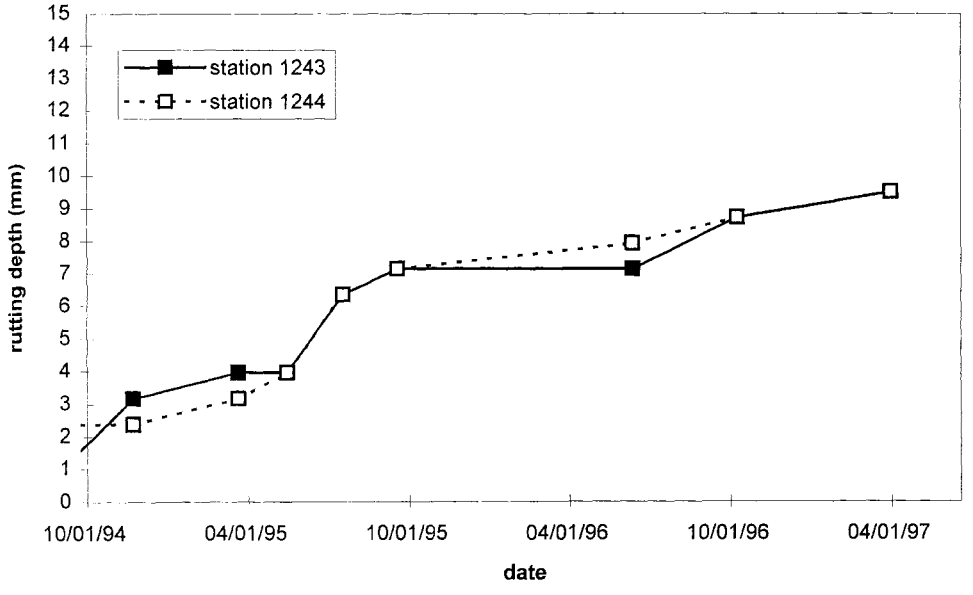

Figure 7.71 Rutting Depths, Section 18, Right Lane, Right Wheel Path

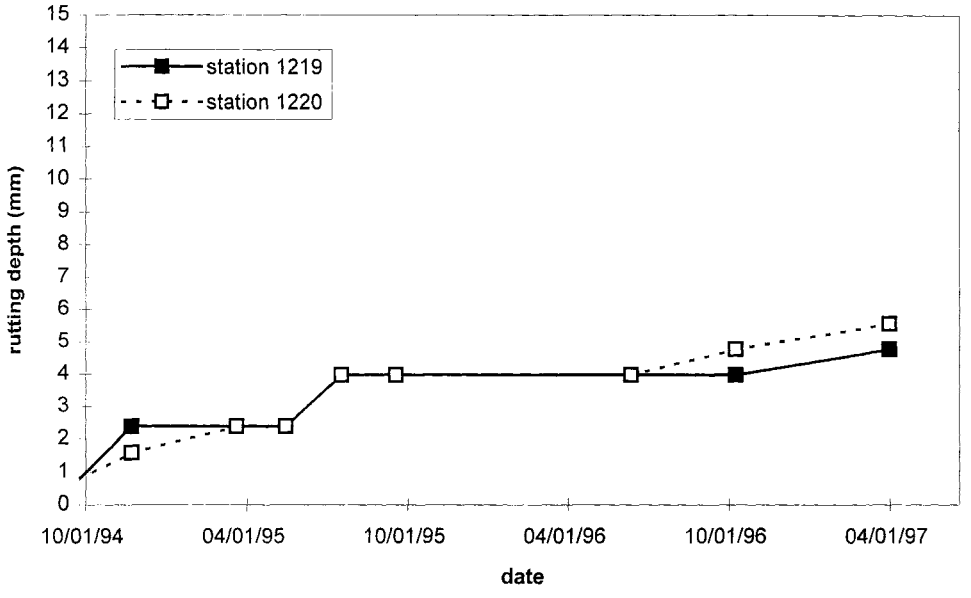

Figure 7.72 Rutting Depths, Section 19, Left Lane, Left Wheel Path

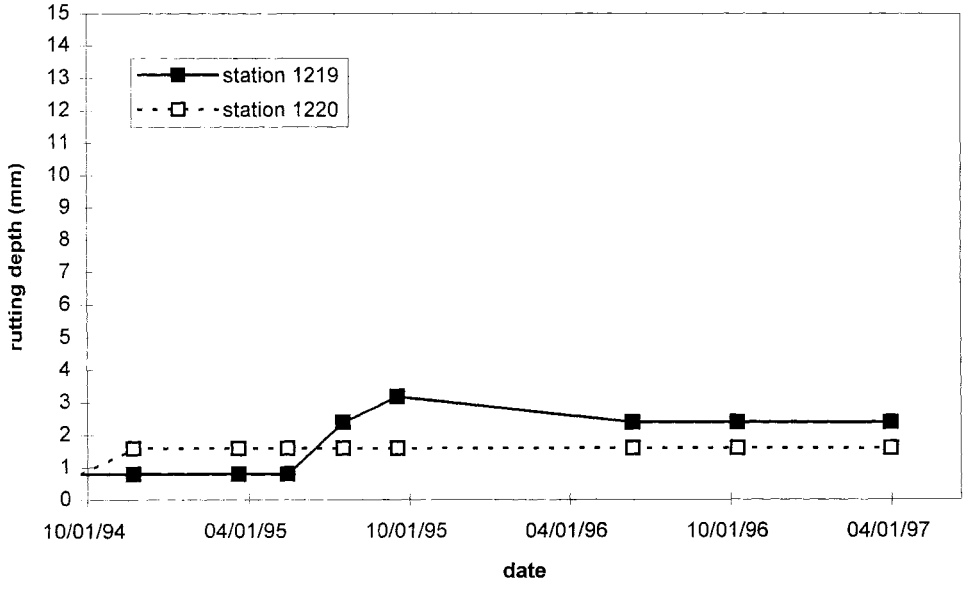

Figure 7.73 Rutting Depths, Section 19, Left Lane, Right Wheel Path

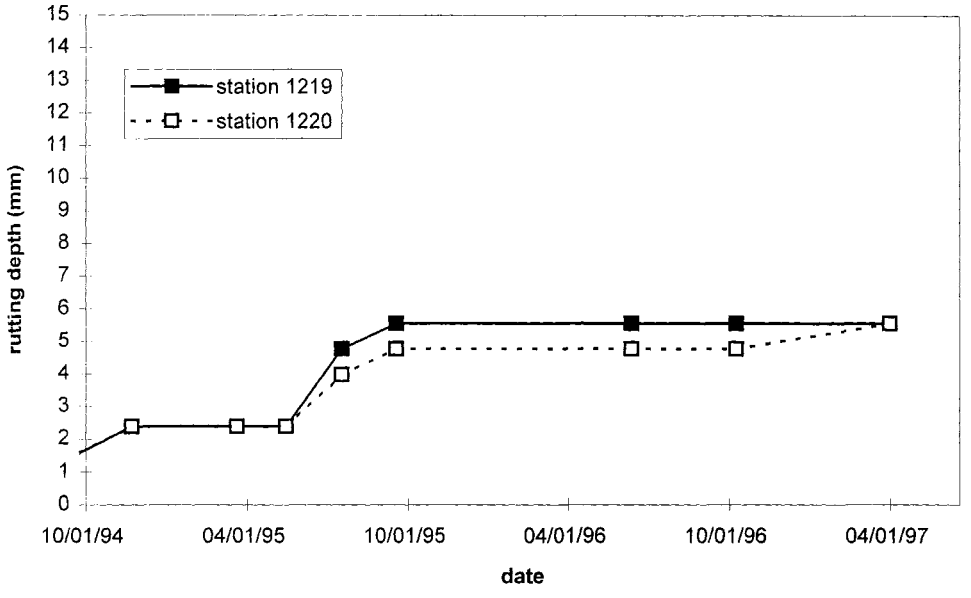

Figure 7.74 Rutting Depths, Section 19, Right Lane, Left Wheel Path

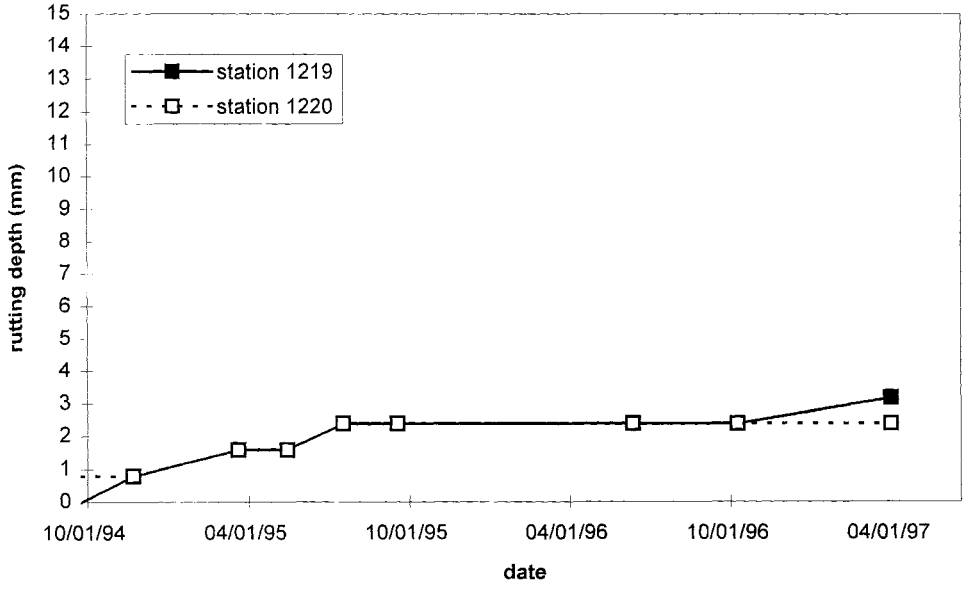

Figure 7.75 Rutting Depths, Section 19, Right Lane, Right Wheel Path

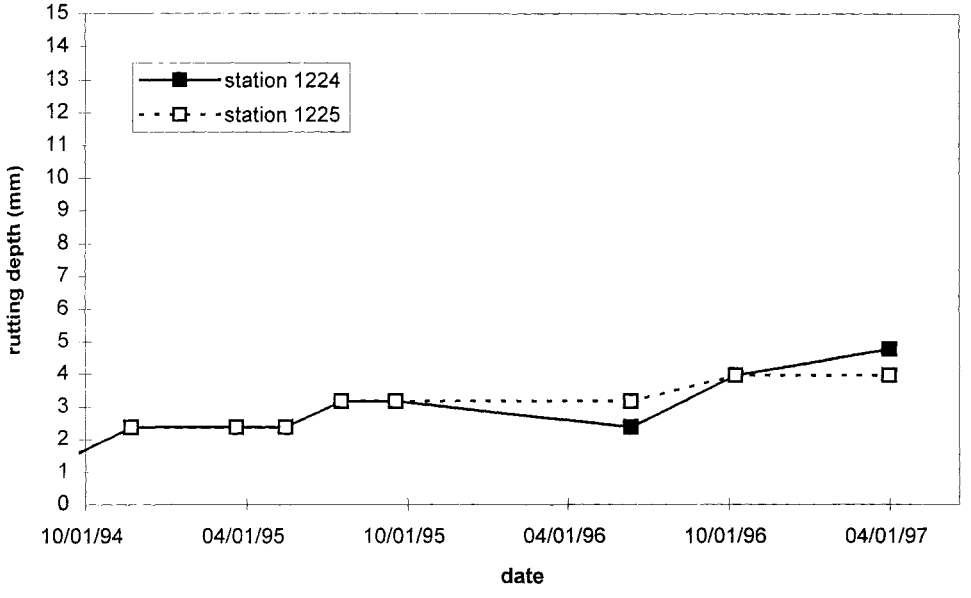

Figure 7.76 Rutting Depths, Section 20, Left Lane, Left Wheel Path

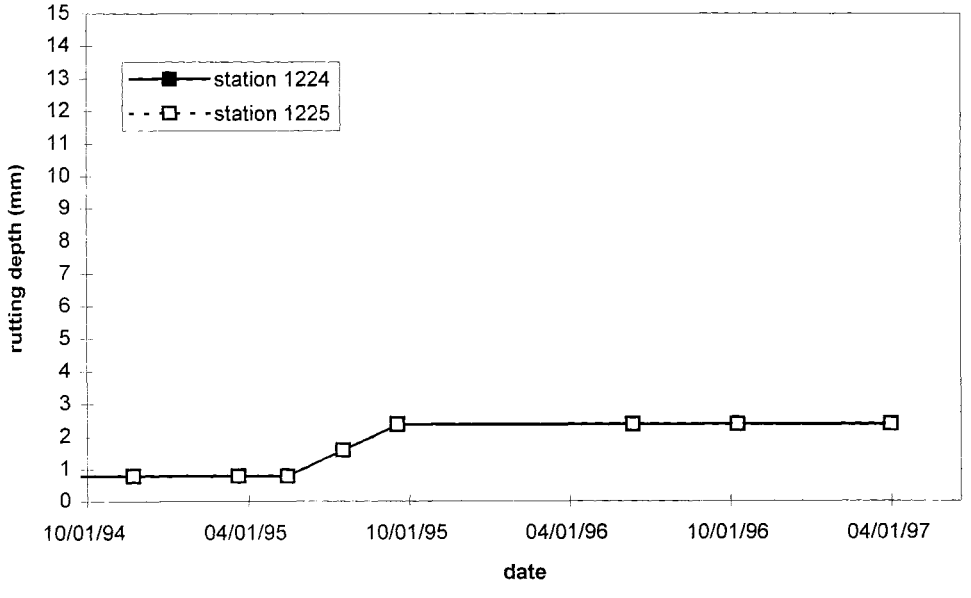

Figure 7.77 Rutting Depths, Section 20, Left Lane, Right Wheel Path

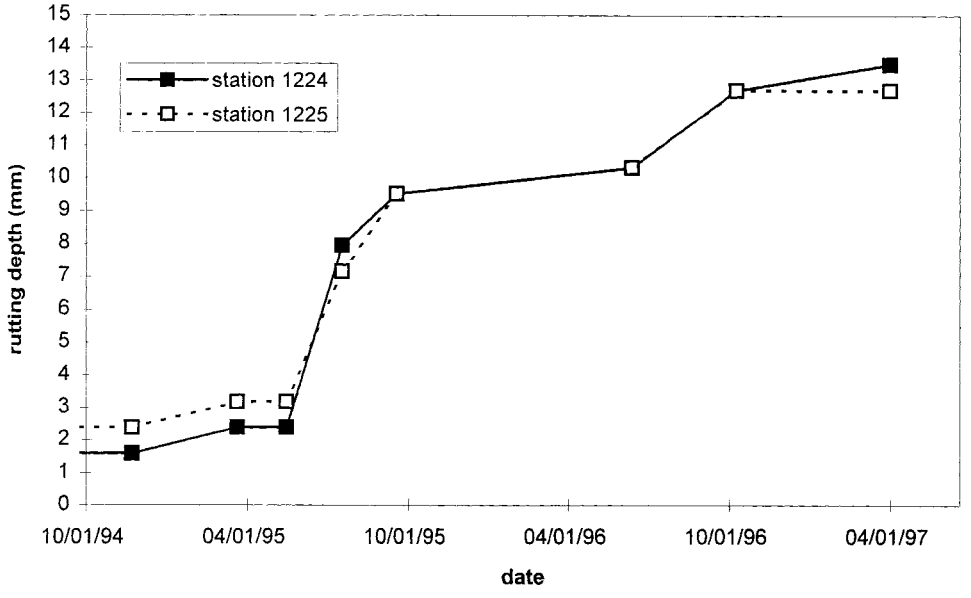

Figure 7.78 Rutting Depths, Section 20, Right Lane, Left Wheel Path

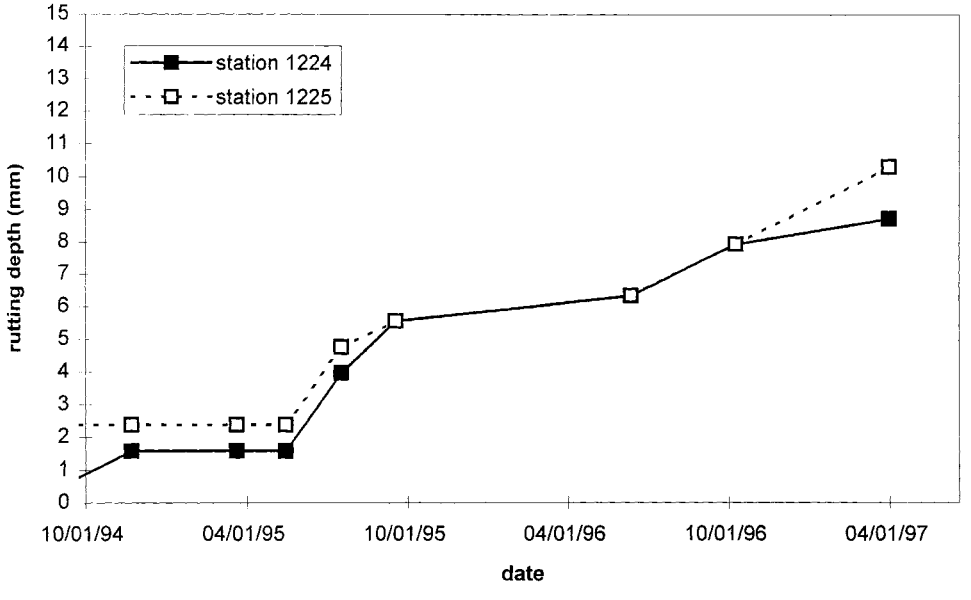

Figure 7.79 Rutting Depths, Section 20, Right Lane, Right Wheel Path

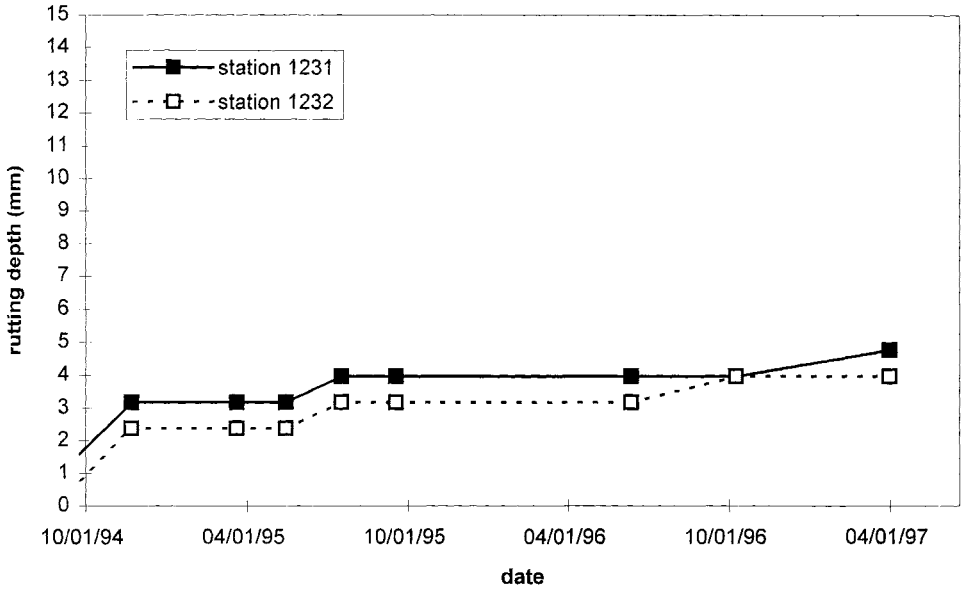

Figure 7.80 Rutting Depths, Section 21, Left Lane, Left Wheel Path

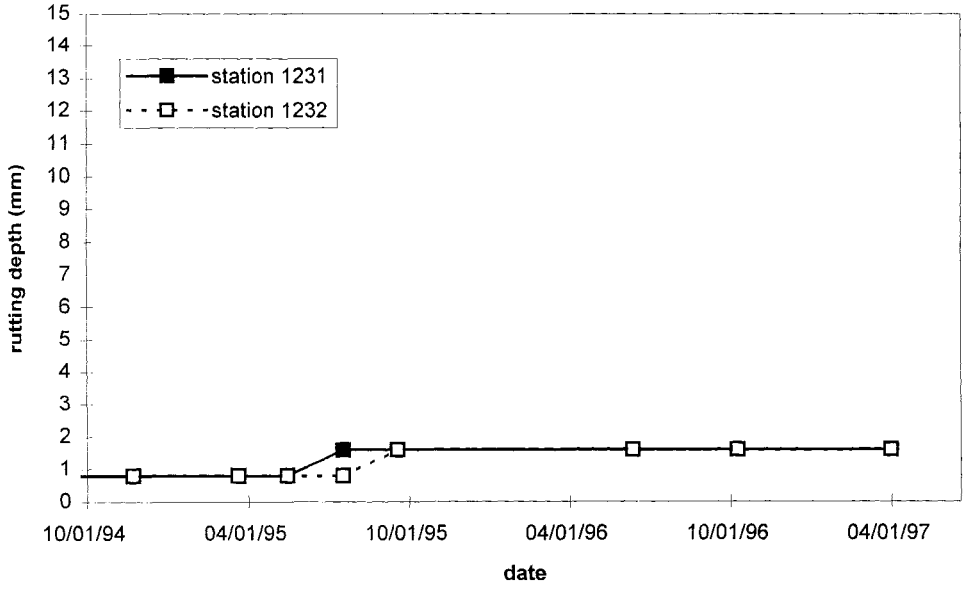

Figure 7.81 Rutting Depths, Section 21, Left Lane, Right Wheel Path

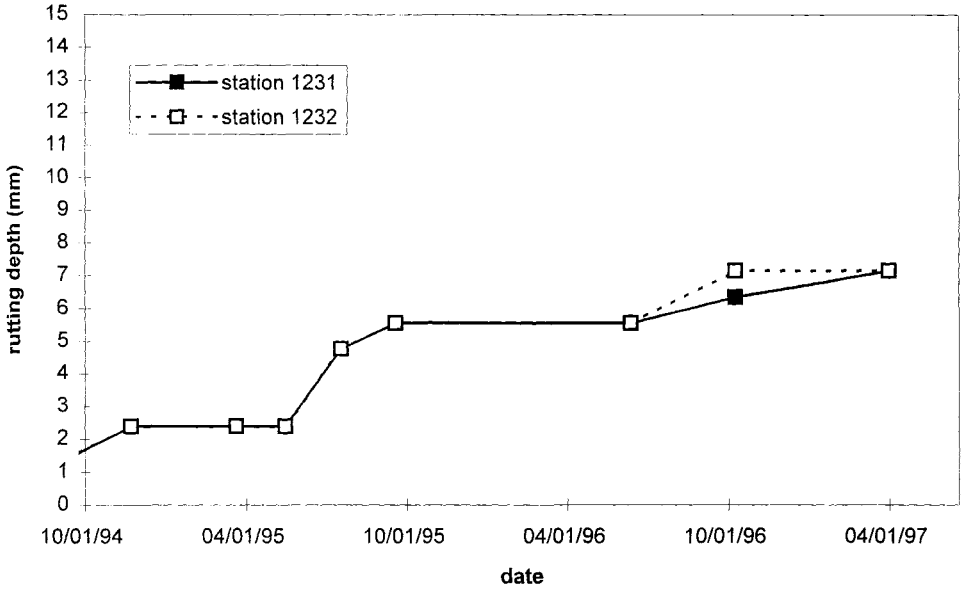

Figure 7.82 Rutting Depths, Section 21, Right Lane, Left Wheel Path

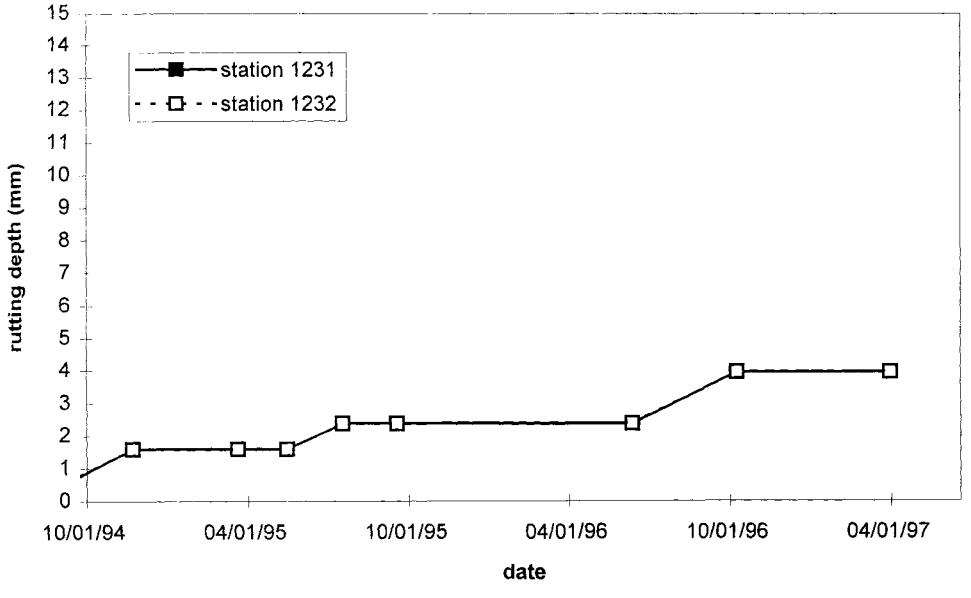

Figure 7.83 Rutting Depths, Section 21, Right Lane, Right Wheel Path

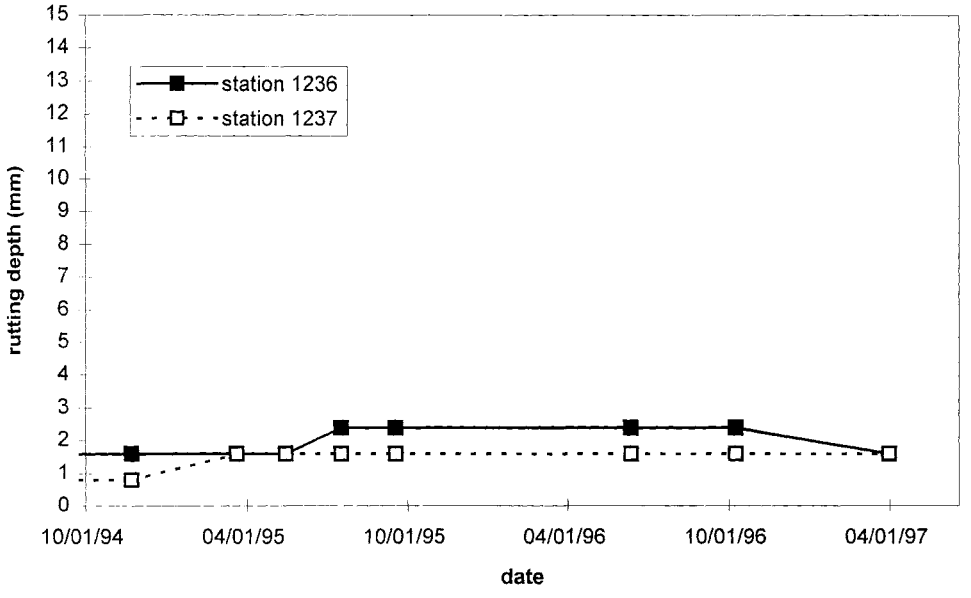

Figure 7.84 Rutting Depths, Section 22, Left Lane, Left Wheel Path

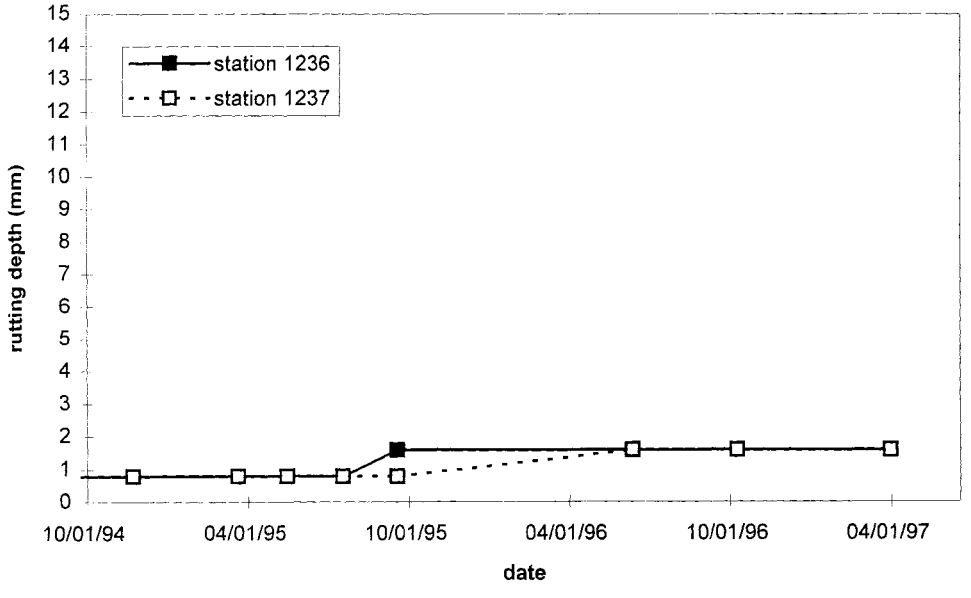

Figure 7.85 Rutting Depths, Section 22, Left Lane, Right Wheel Path

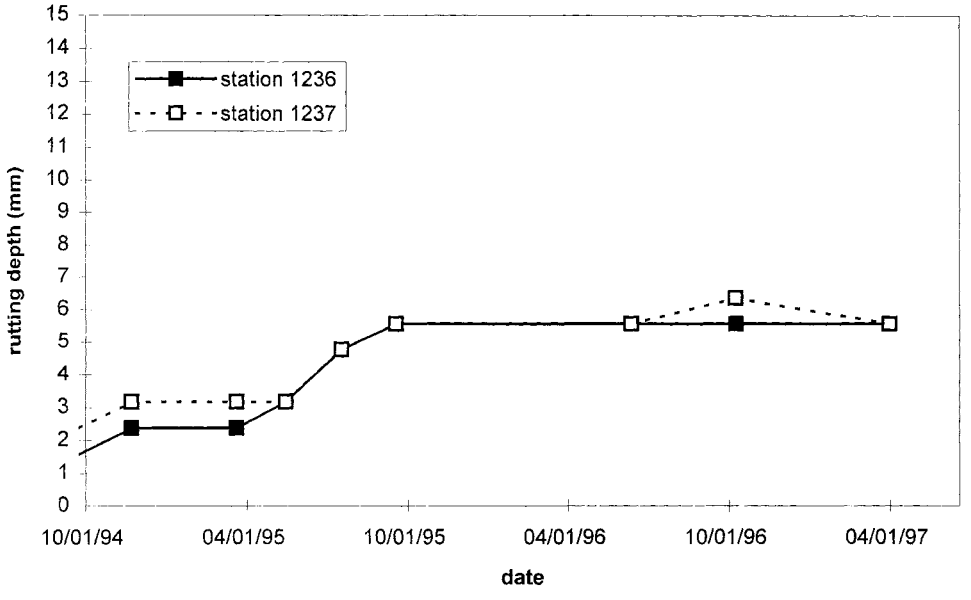

Figure 7.86 Rutting Depths, Section 22, Right Lane, Left Wheel Path

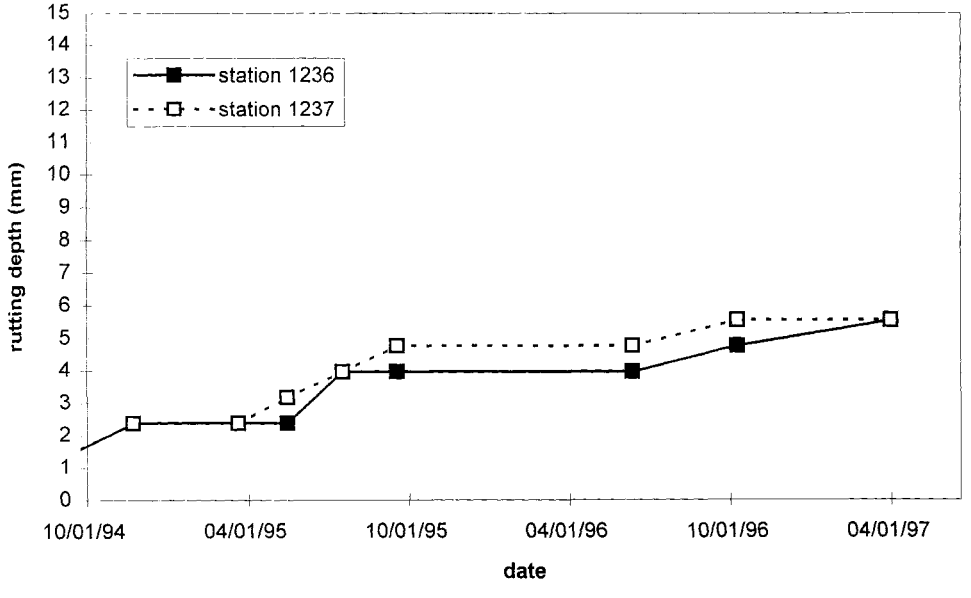

Figure 7.87 Rutting Depths, Section 22, Right Lane, Right Wheel Path

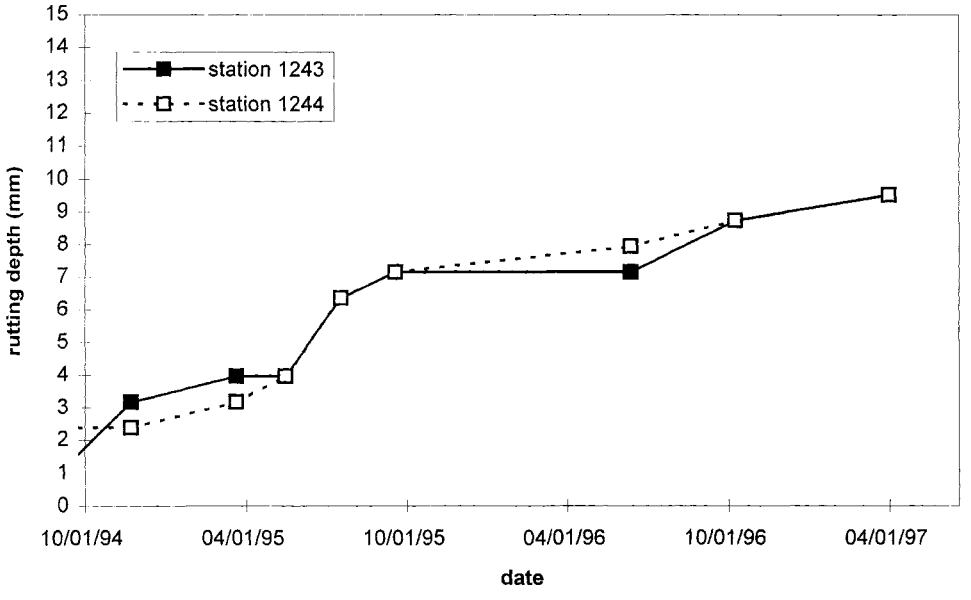

Figure 7.88 Rutting Depths, Section 23, Left Lane, Left Wheel Path

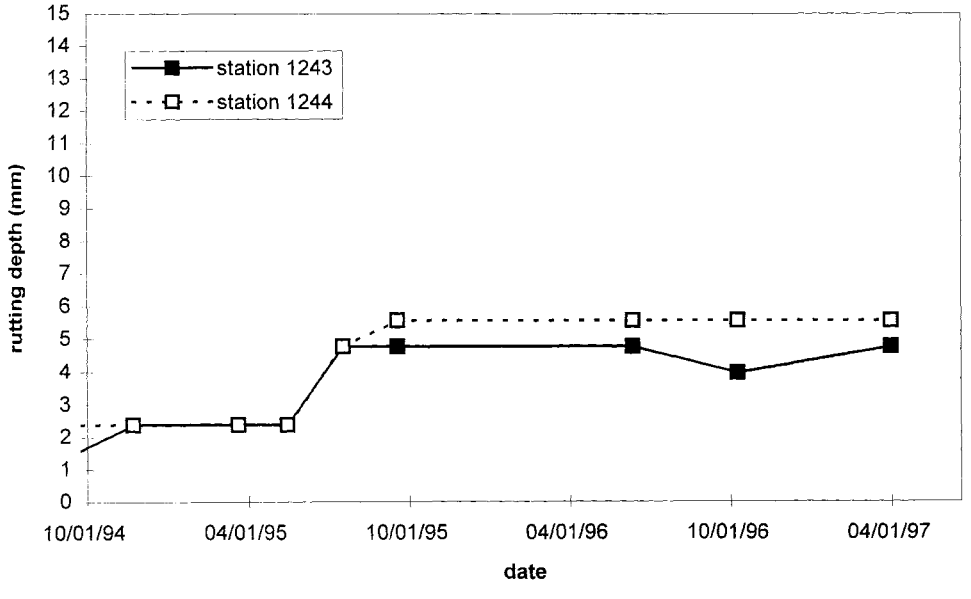

Figure 7.89 Rutting Depths, Section 23, Left Lane, Right Wheel Path

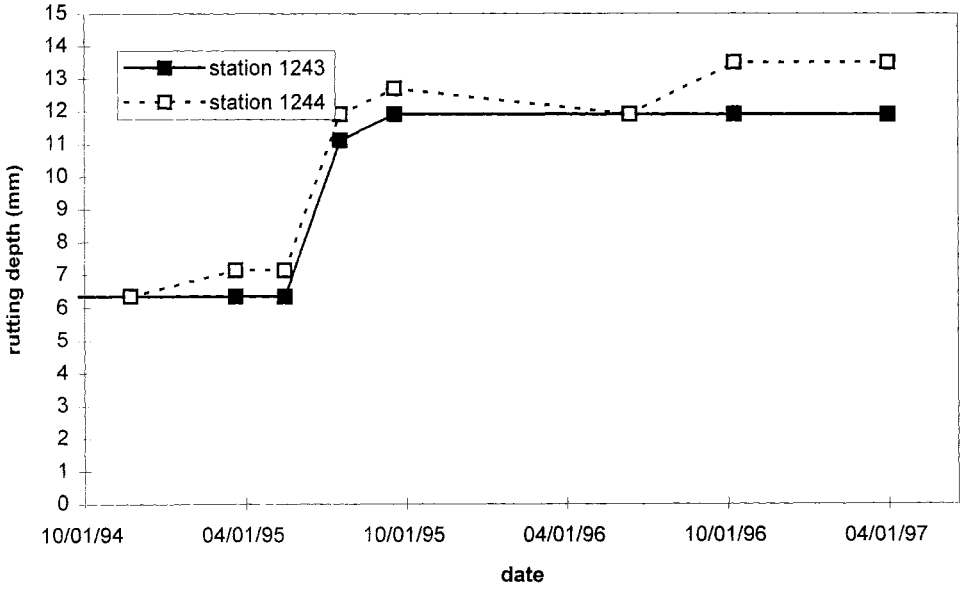

Figure 7.90 Rutting Depths, Section 23, Right Lane, Left Wheel Path

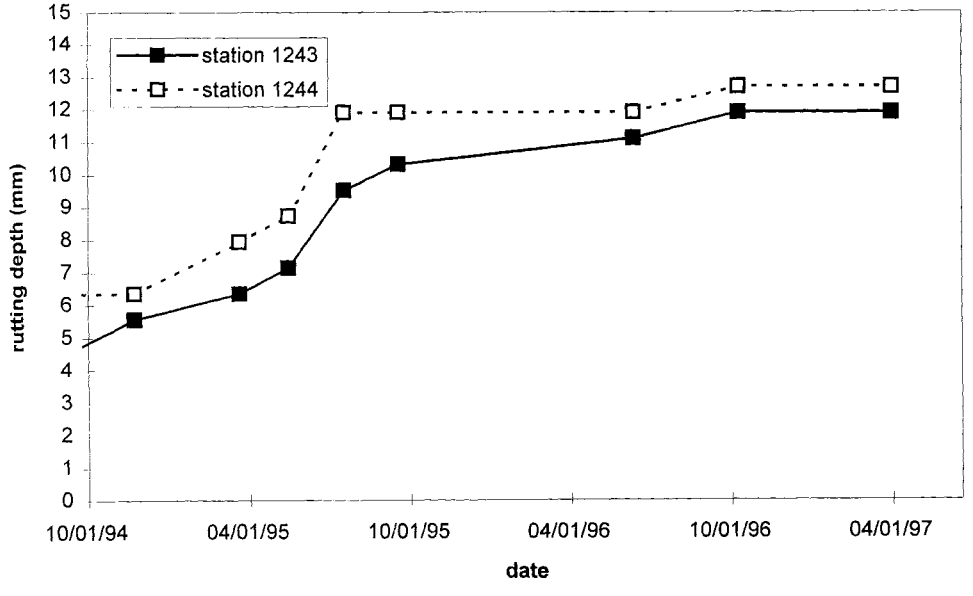

Figure 7.91 Rutting Depths, Section 23, Right Lane, Right Wheel Path

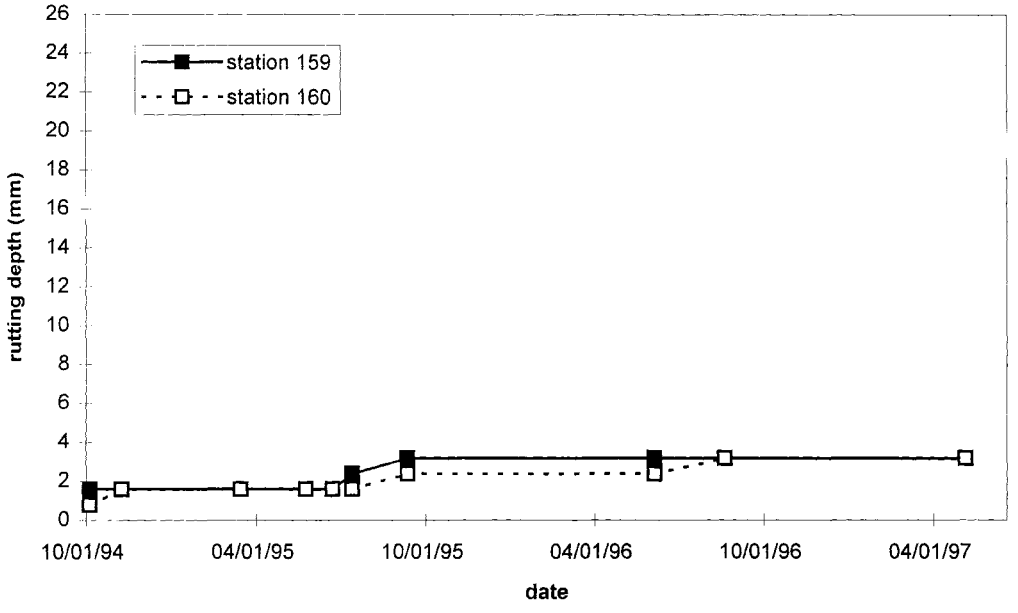

Figure 7.92 Rutting Depths, Section 24, 102500 Lane, Left Wheel Path

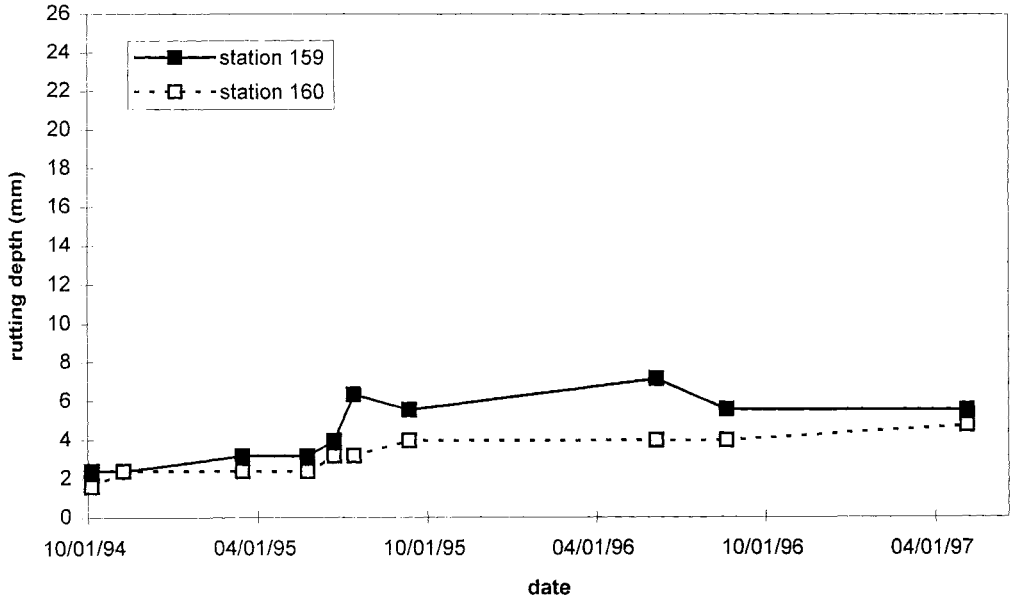

Figure 7.93 Rutting Depths, Section 24, 102500 Lane, Right Wheel Path

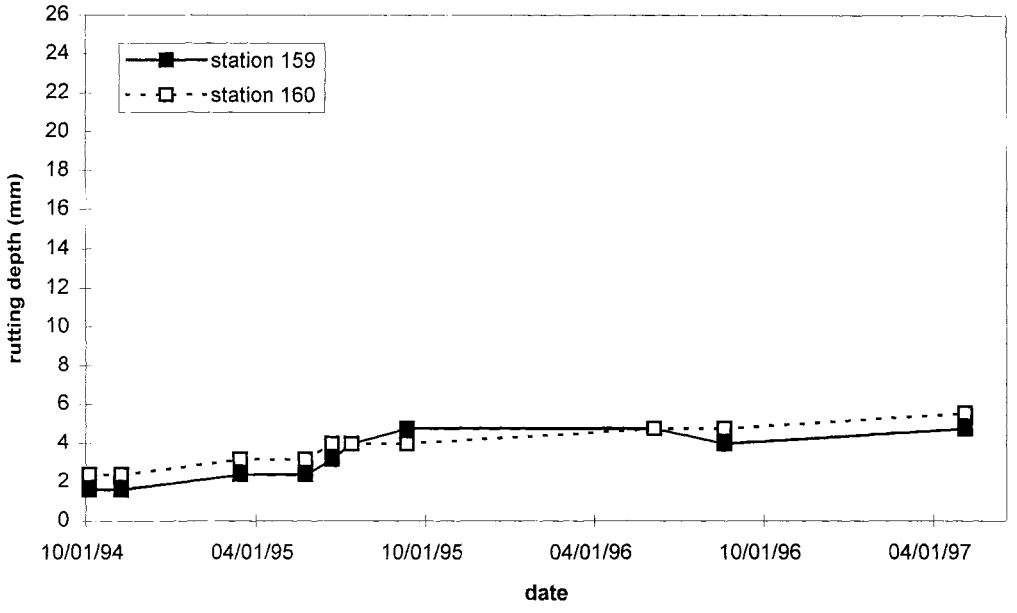

Figure 7.94 Rutting Depths, Section 24, 80000 Lane, Left Wheel Path

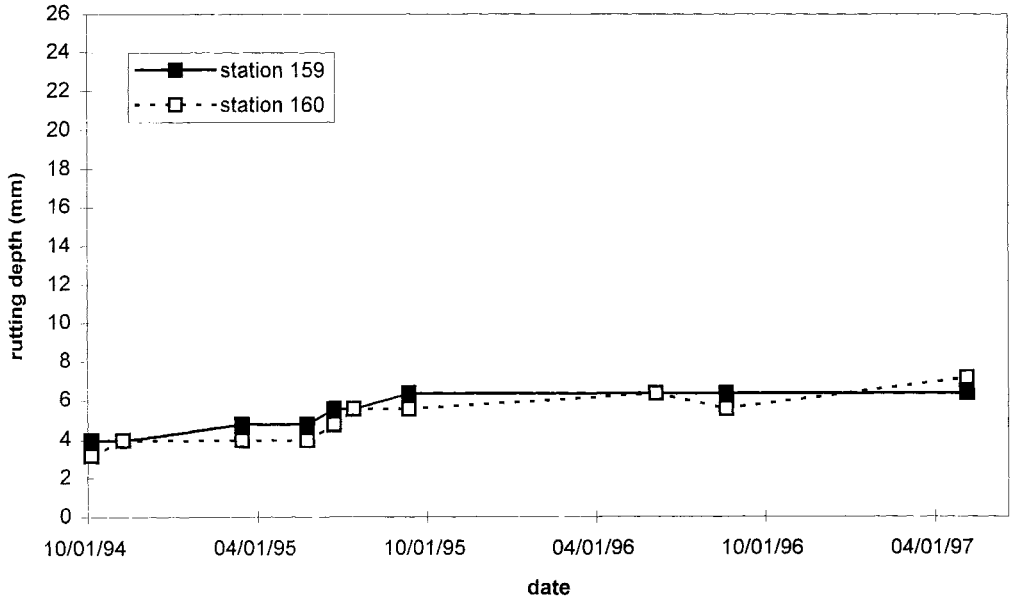

Figure 7.95 Rutting Depths, Section 24, 80000 Lane, Right Wheel Path

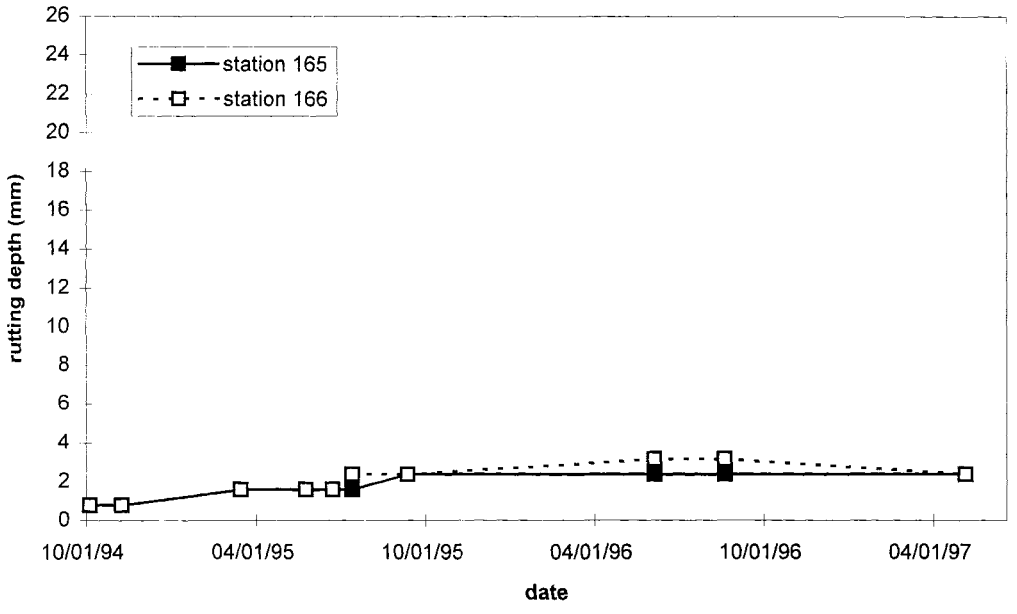

Figure 7.96 Rutting Depths, Section 25, 102500 Lane, Left Wheel Path

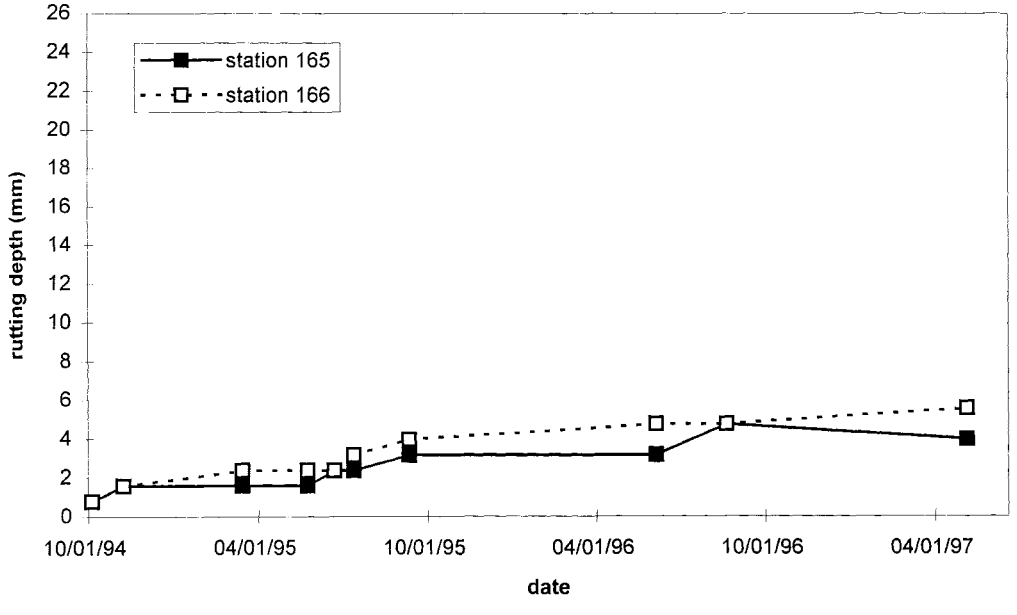

Figure 7.97 Rutting Depths, Section 25, 102500 Lane, Right Wheel Path

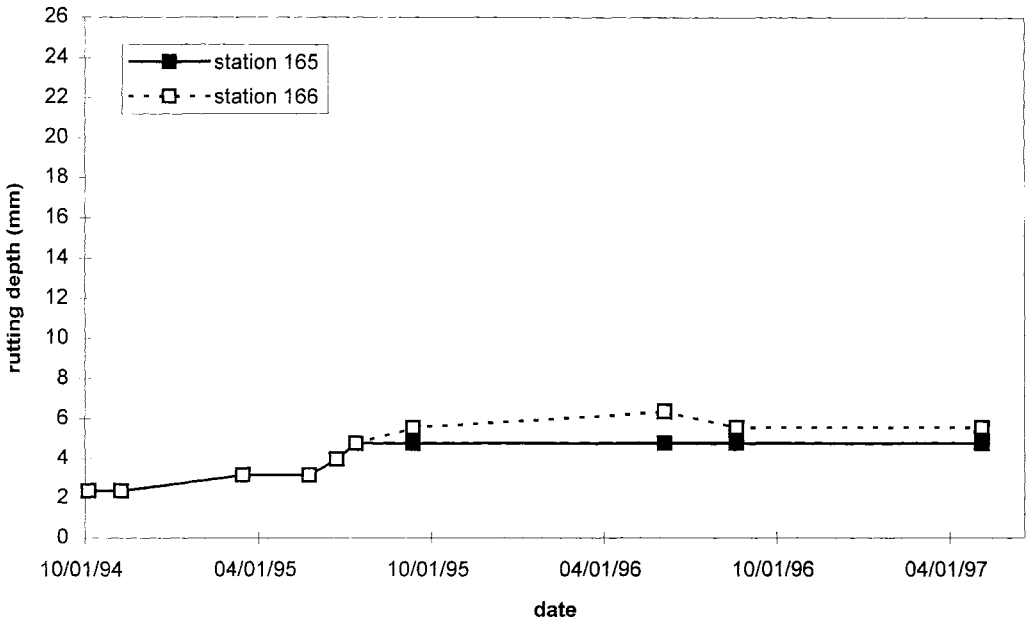

Figure 7.98 Rutting Depths, Section 25, 80000 Lane, Left Wheel Path

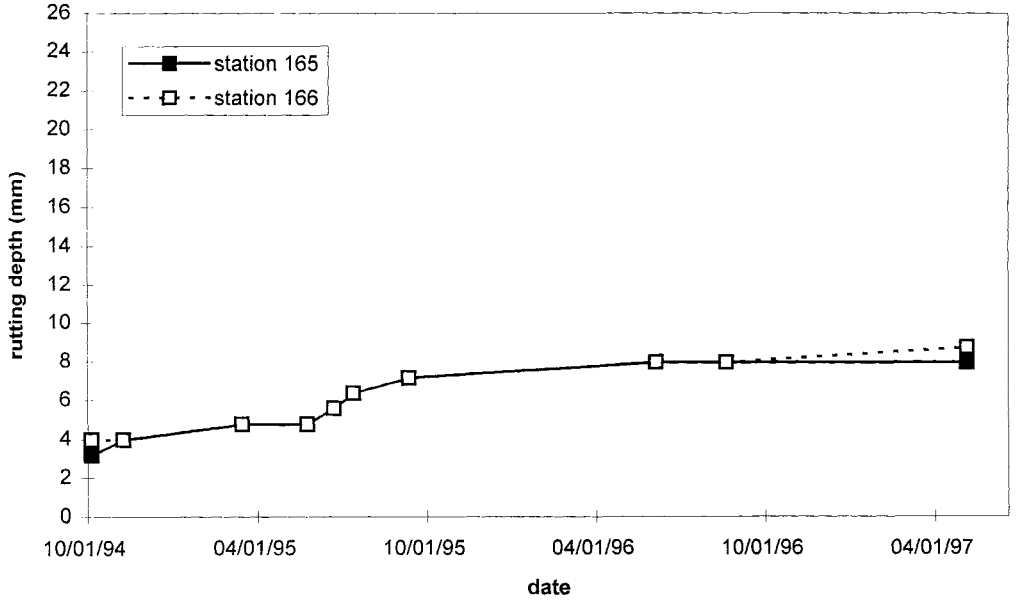

Figure 7.99 Rutting Depths, Section 25, 80000 Lane, Right Wheel Path

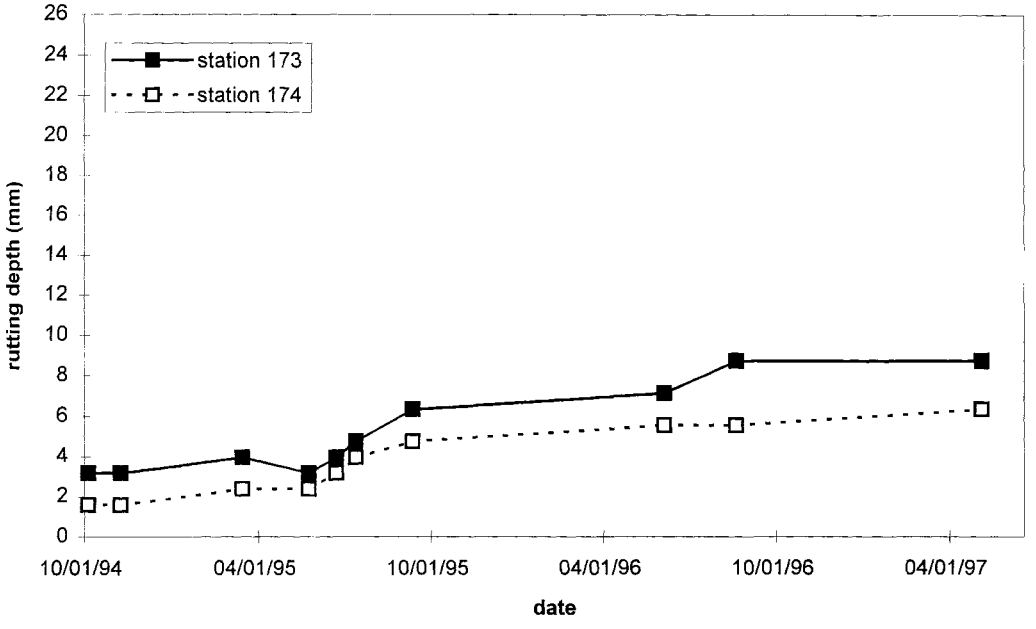

Figure 7.100 Rutting Depths, Section 26, 102500 Lane, Left Wheel Path

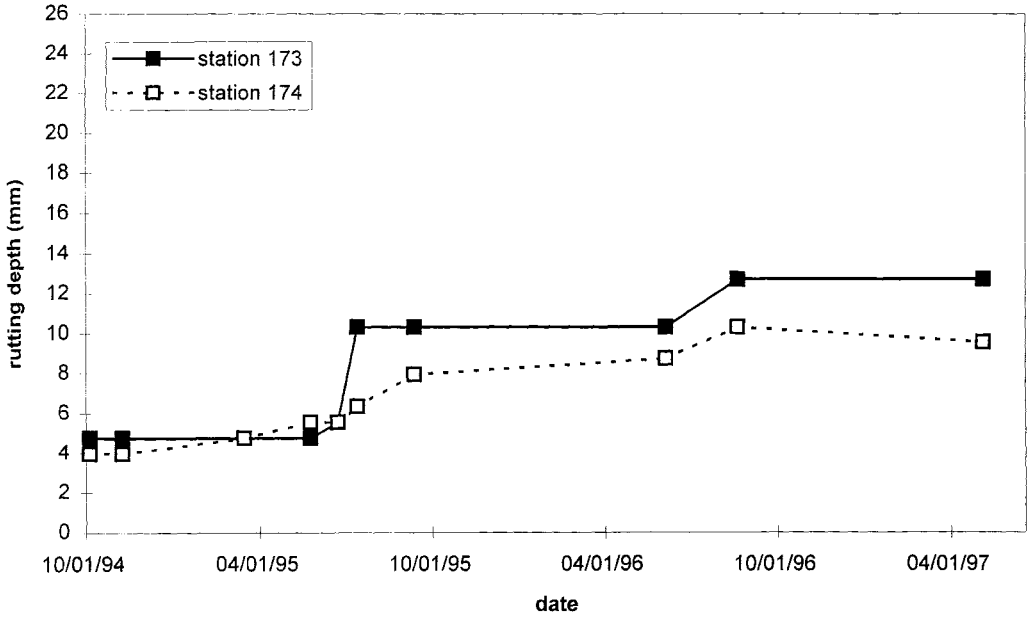

Figure 7.101 Rutting Depths, Section 26, 102500 Lane, Right Wheel Path

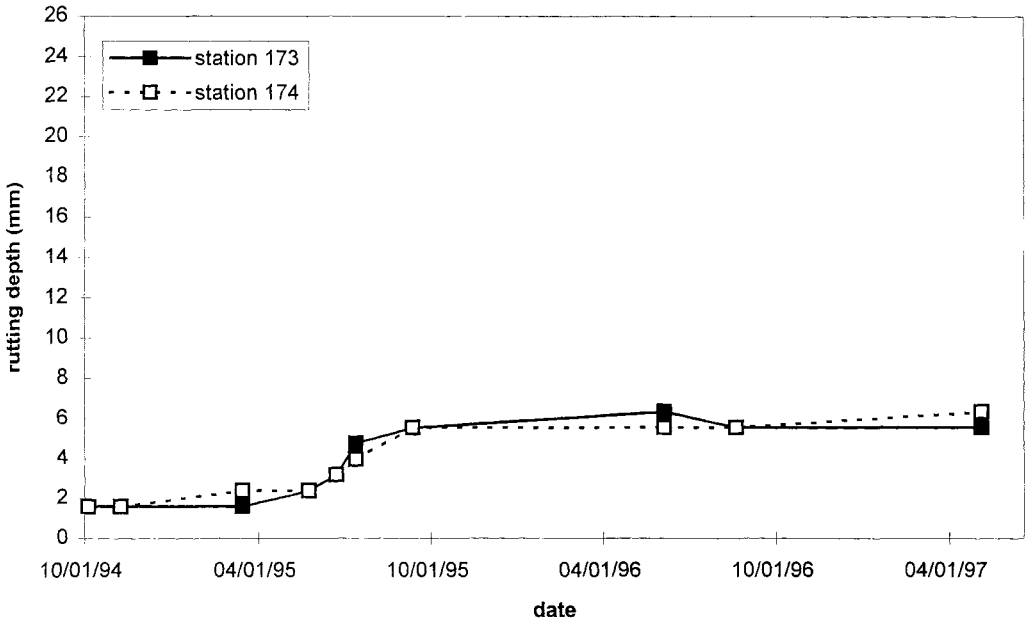

Figure 7.102 Rutting Depths, Section 26, 80000 Lane, Left Wheel Path

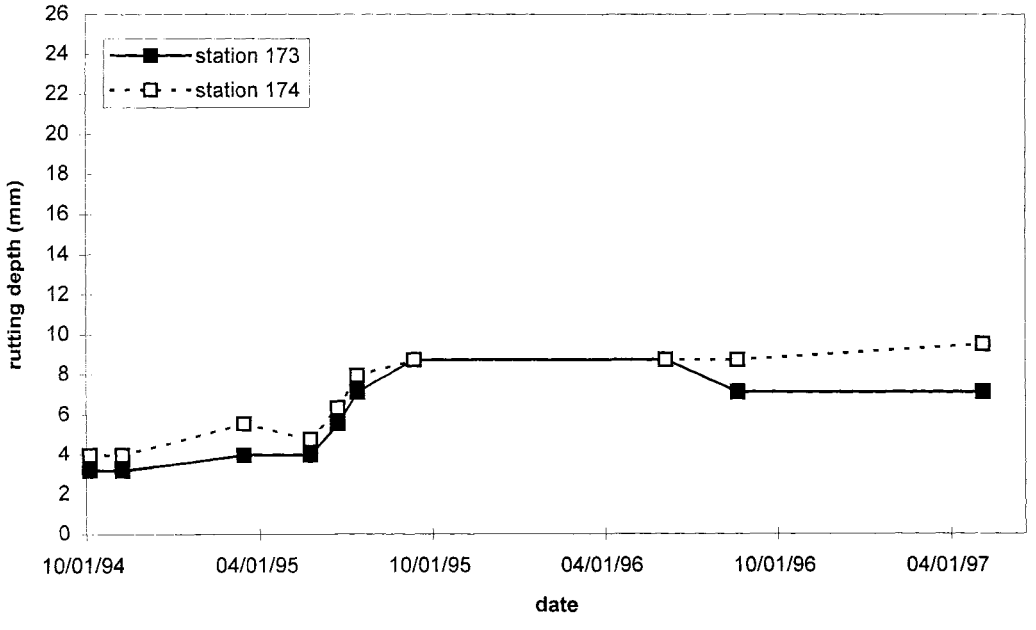

Figure 7.103 Rutting Depths, Section 26, 80000 Lane, Right Wheel Path

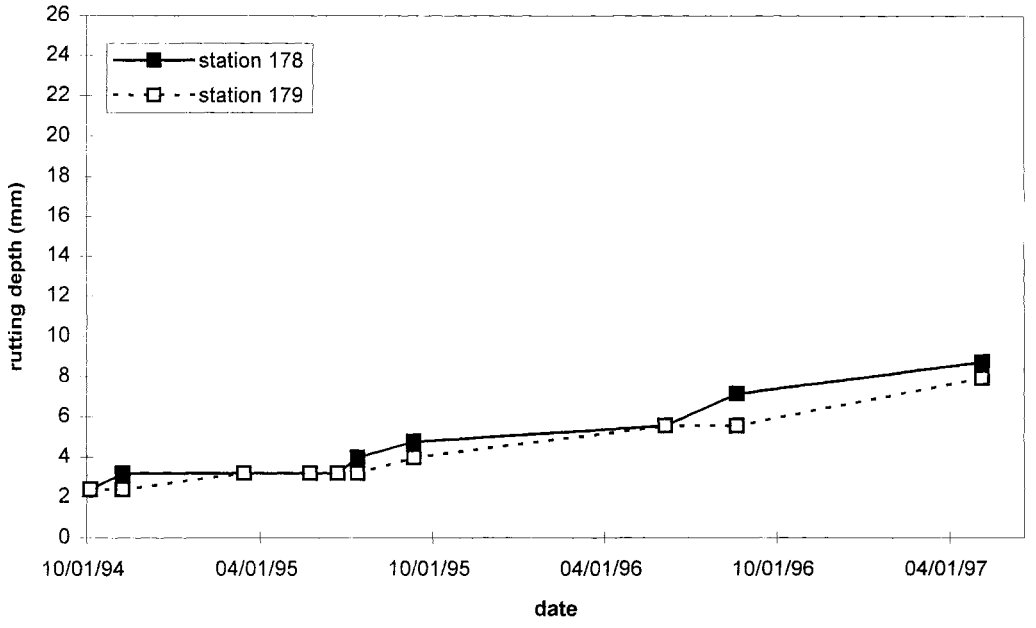

Figure 7.104 Rutting Depths, Section 27, 102500 Lane, Left Wheel Path

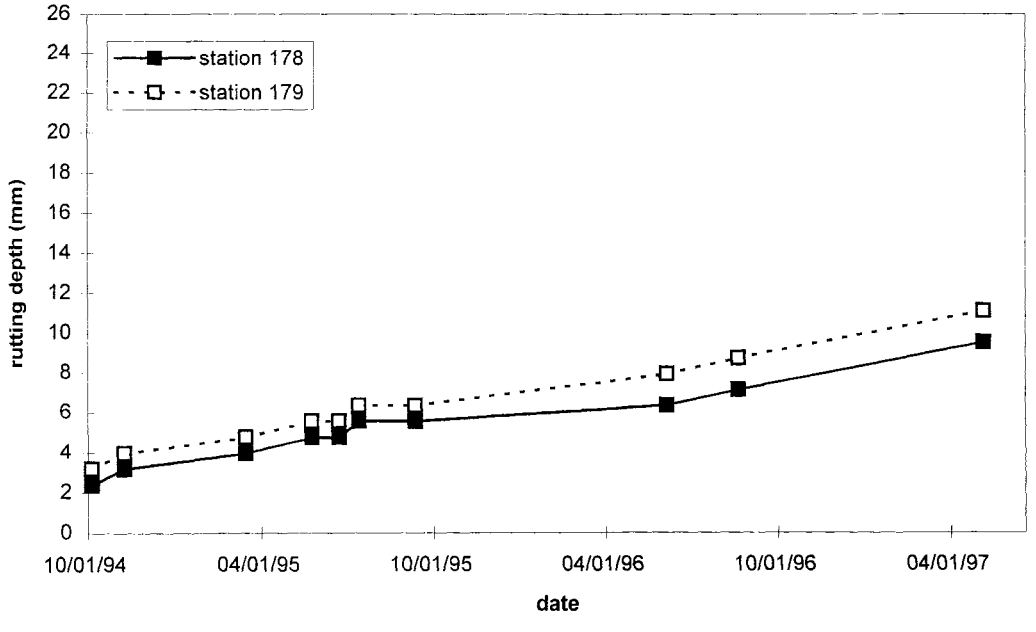

Figure 7.105 Rutting Depths, Section 27, 102500 Lane, Right Wheel Path

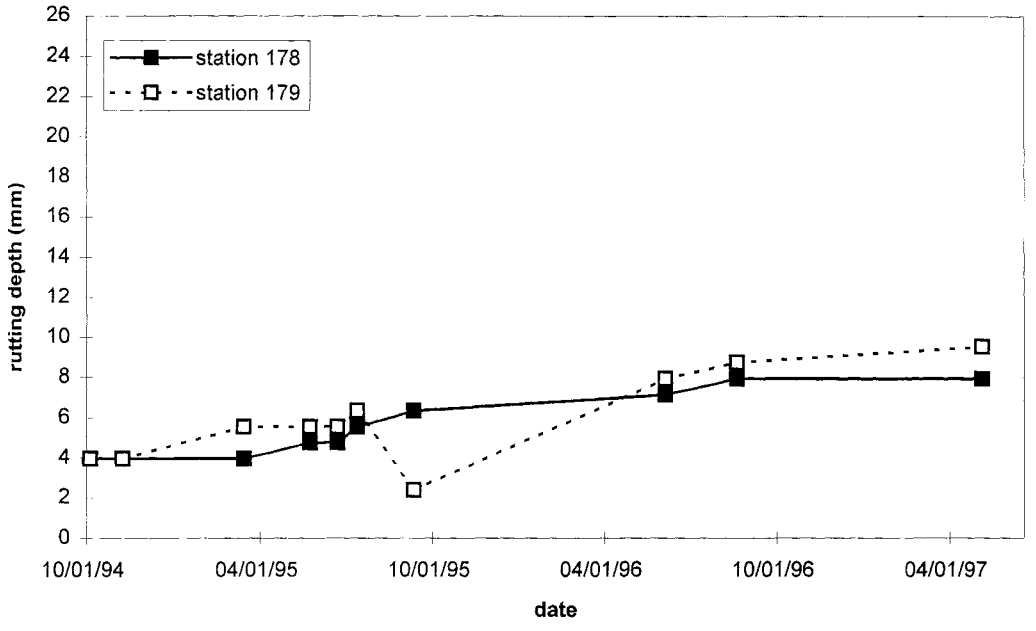

Figure 7.106 Rutting Depths, Section 27, 80000 Lane, Left Wheel Path

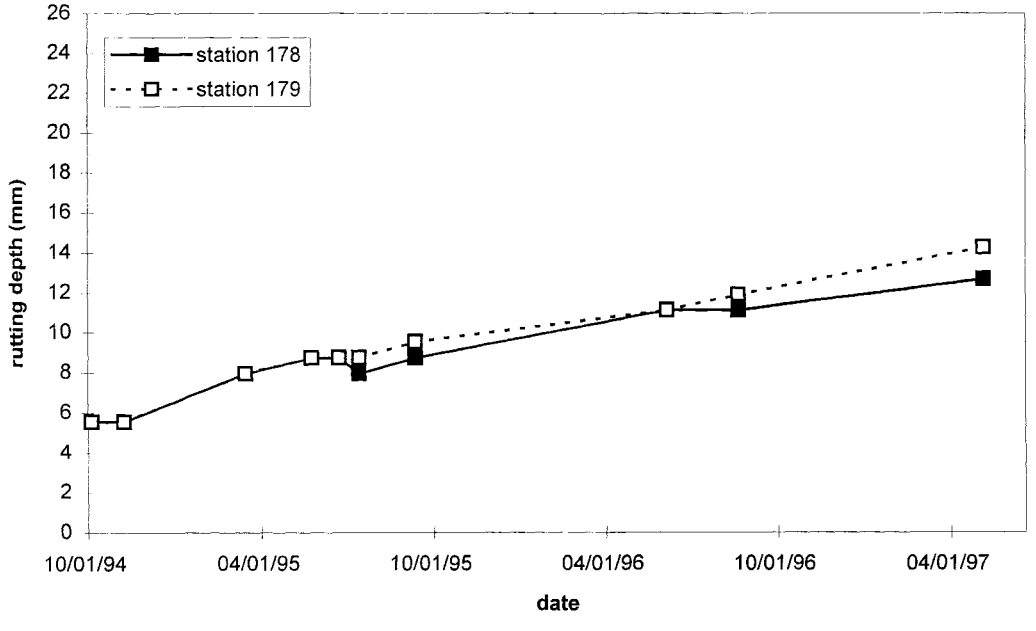

Figure 7.107 Rutting Depths, Section 27, 80000 Lane, Right Wheel Path

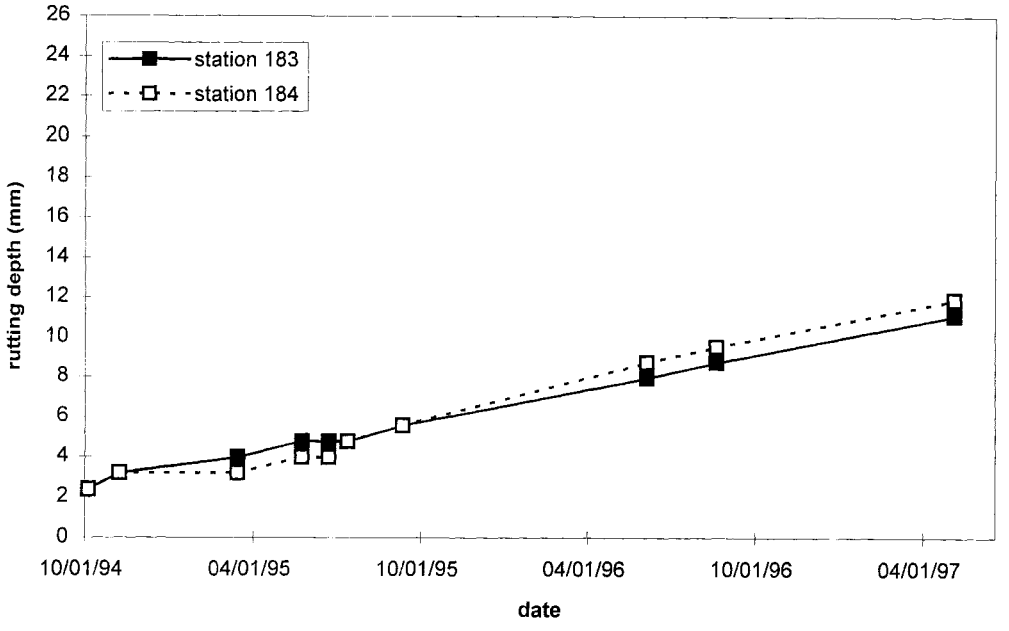

Figure 7.108 Rutting Depths, Section 28, 102500 Lane, Left Wheel Path

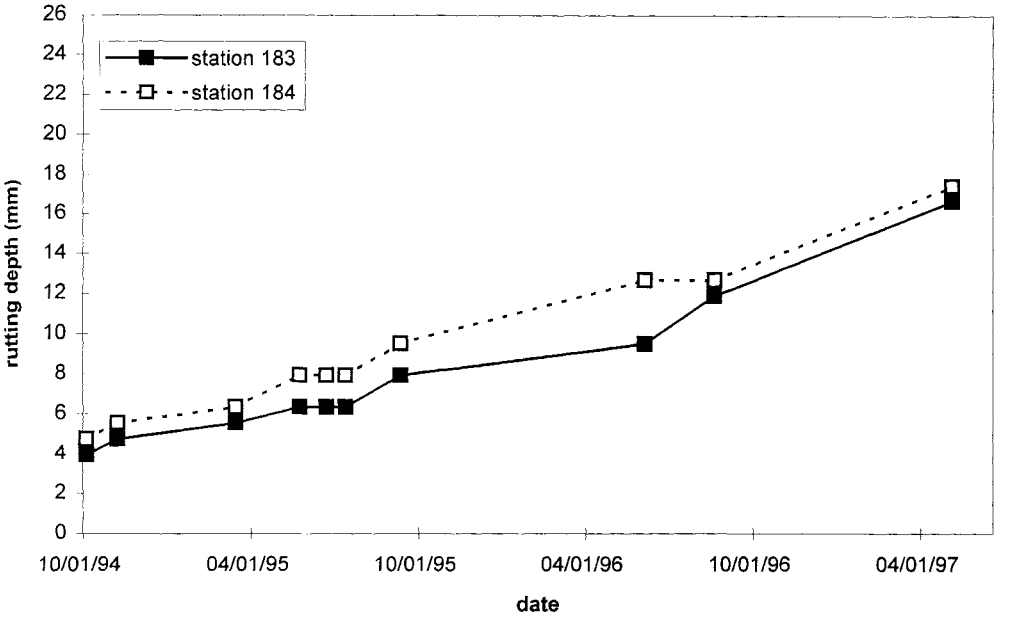

Figure 7.109 Rutting Depths, Section 28, 102500 Lane, Right Wheel Path

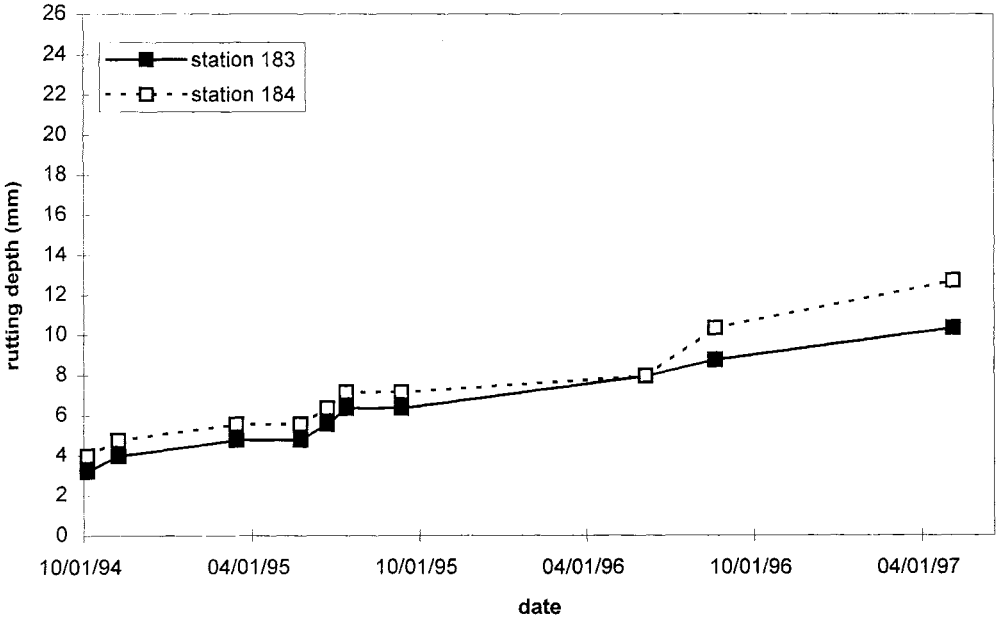

Figure 7.110 Rutting Depths, Section 28, 80000 Lane, Left Wheel Path

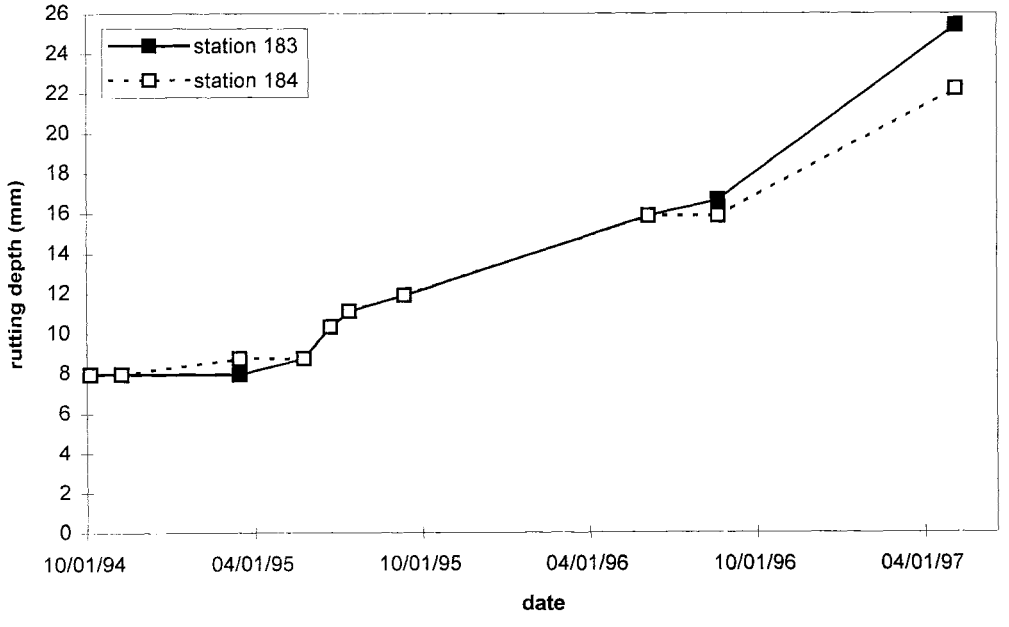

Figure 7.111 Rutting Depths, Section 28, 80000 Lane, Right Wheel Path

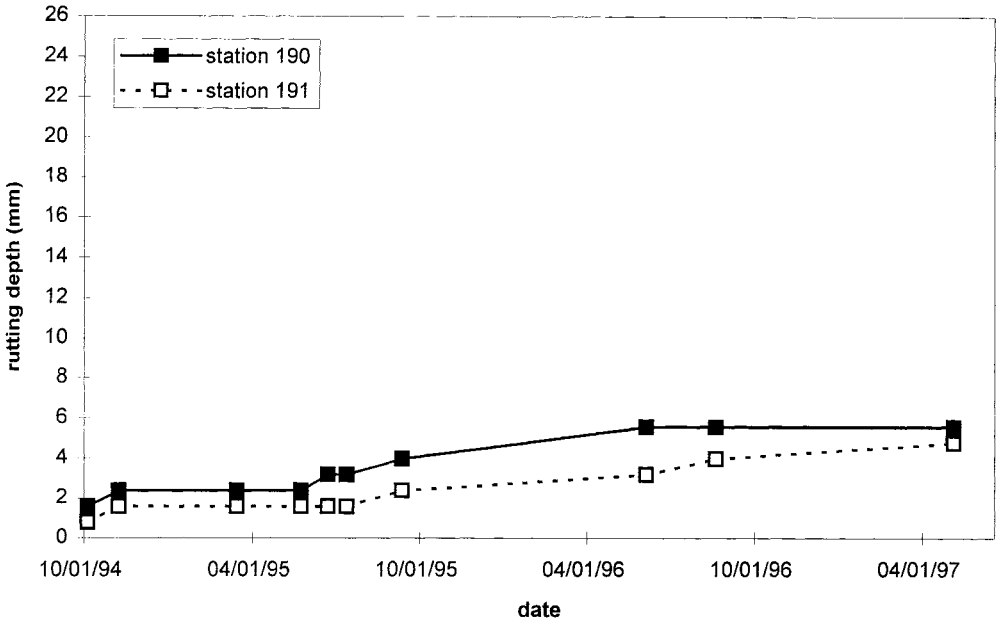

Figure 7.112 Rutting Depths, Section 29, 102500 Lane, Left Wheel Path

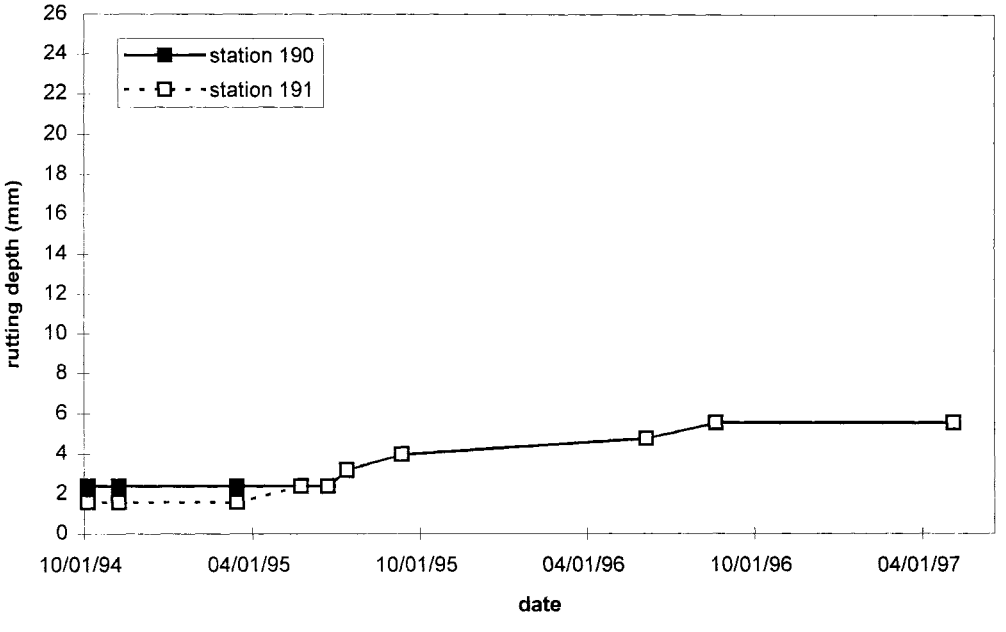

Figure 7.113 Rutting Depths, Section 29, 102500 Lane, Right Wheel Path

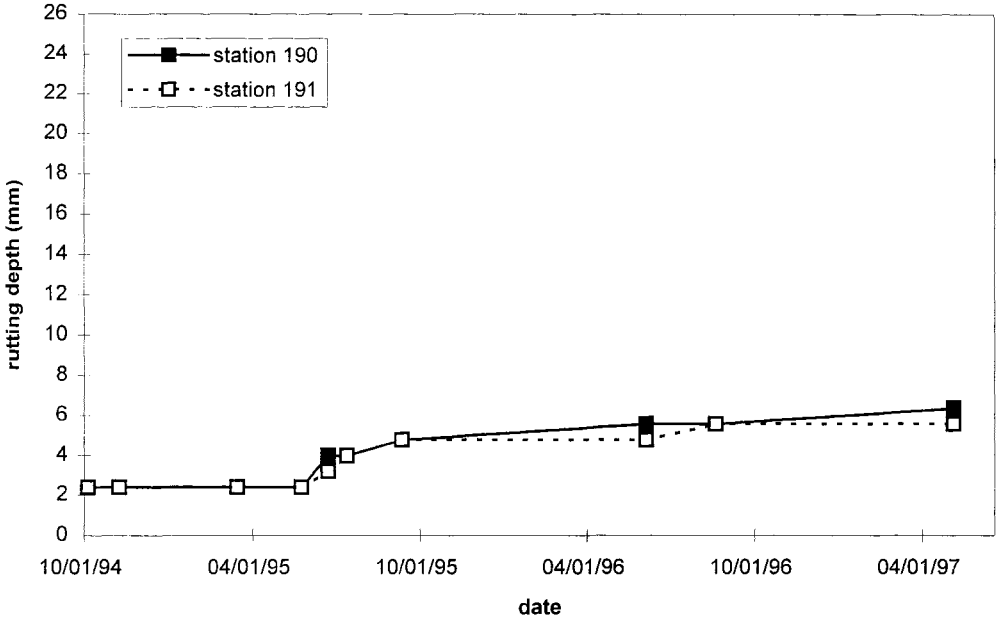

Figure 7.114 Rutting Depths, Section 29, 80000 Lane, Left Wheel Path

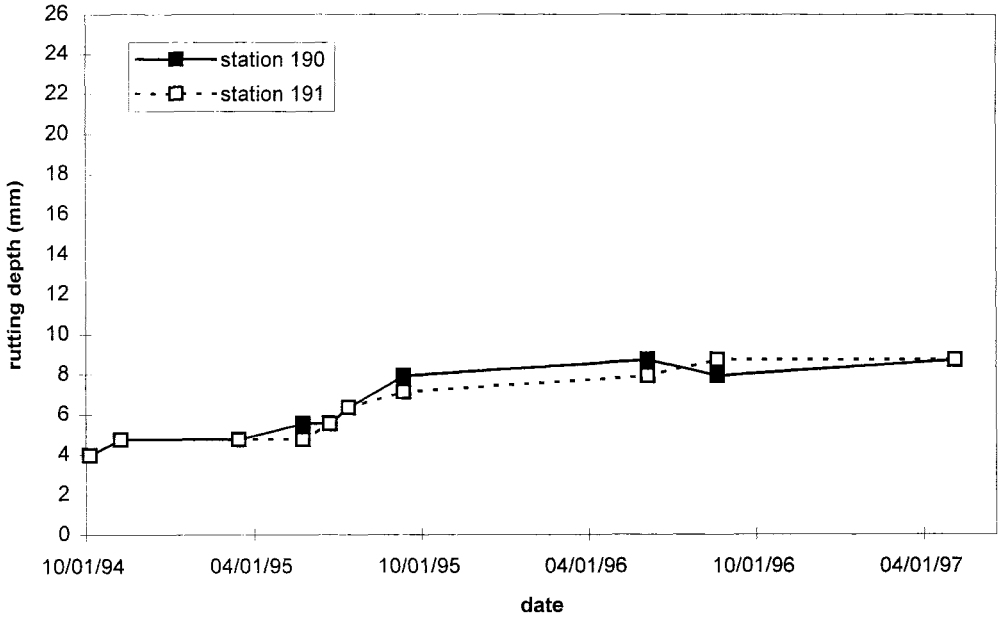

Figure 7.115 Rutting Depths, Section 29, 80000 Lane, Right Wheel Path

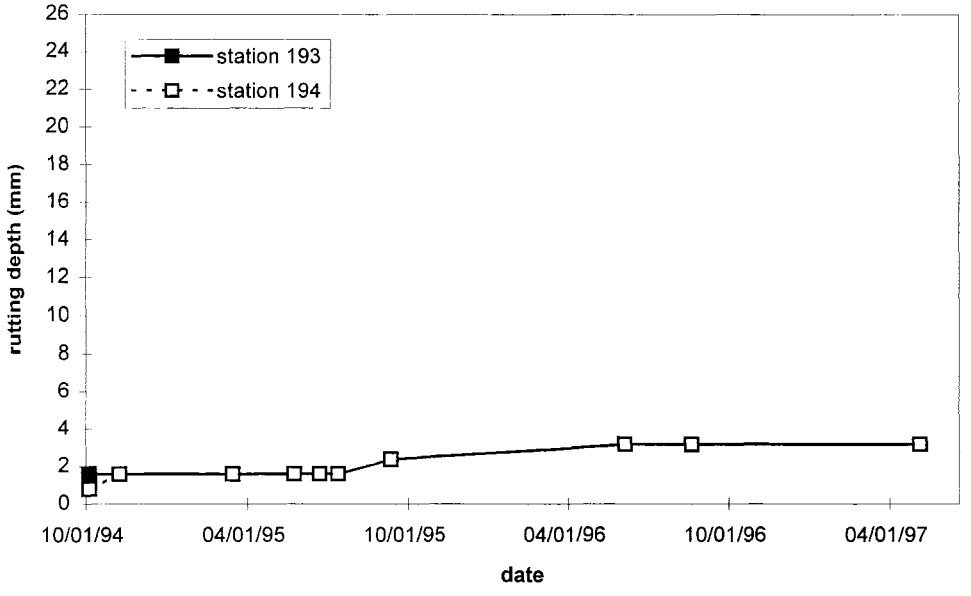

Figure 7.116 Rutting Depths, Section 30, 102500 Lane, Left Wheel Path

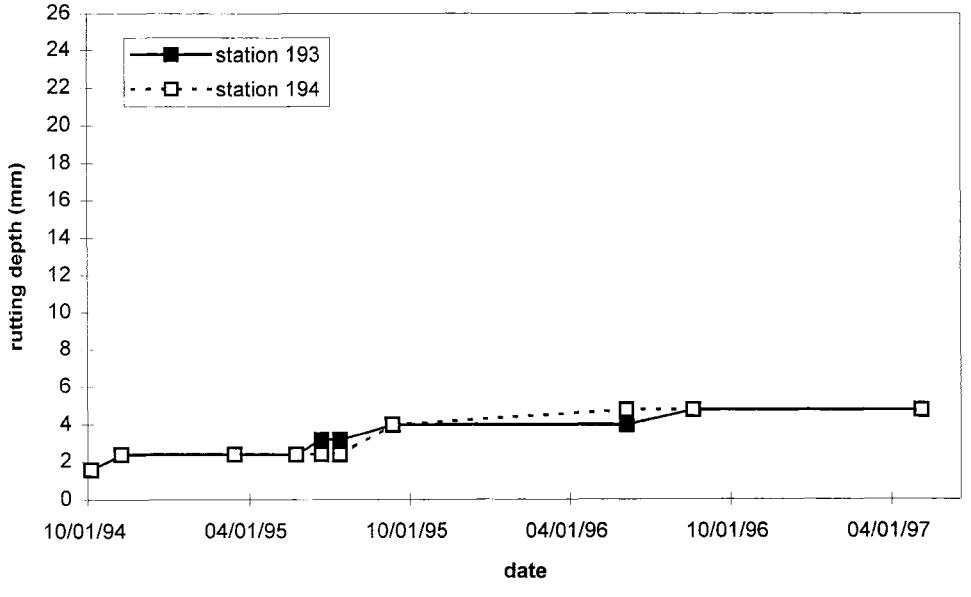

Figure 7.117 Rutting Depths, Section 30, 102500 Lane, Right Wheel Path

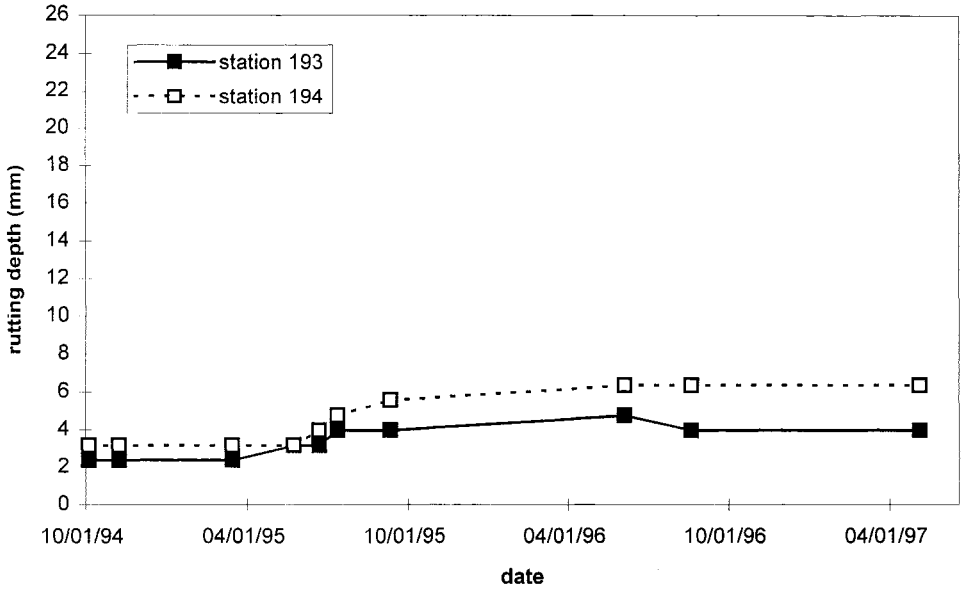

Figure 7.118 Rutting Depths, Section 30, 80000 Lane, Left Wheel Path

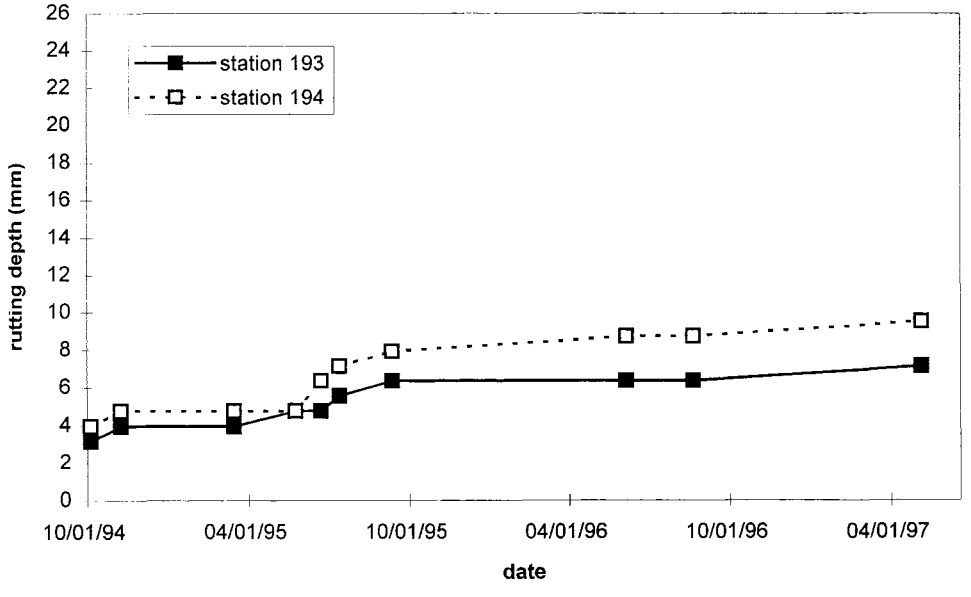

Figure 7.119 Rutting Depths, Section 30, 80000 Lane, Right Wheel Path

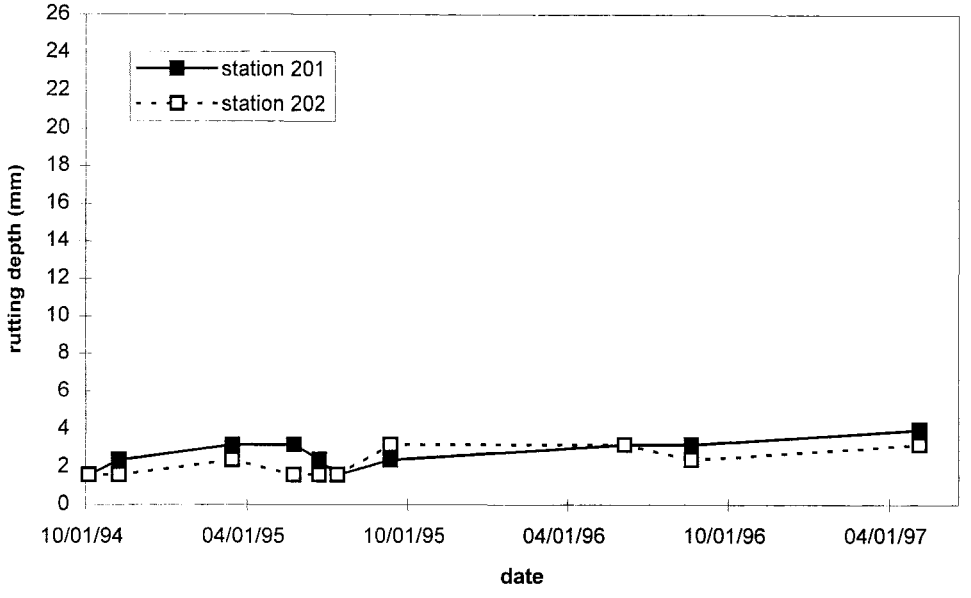

Figure 7.120 Rutting Depths, Section 31, 102500 Lane, Left Wheel Path

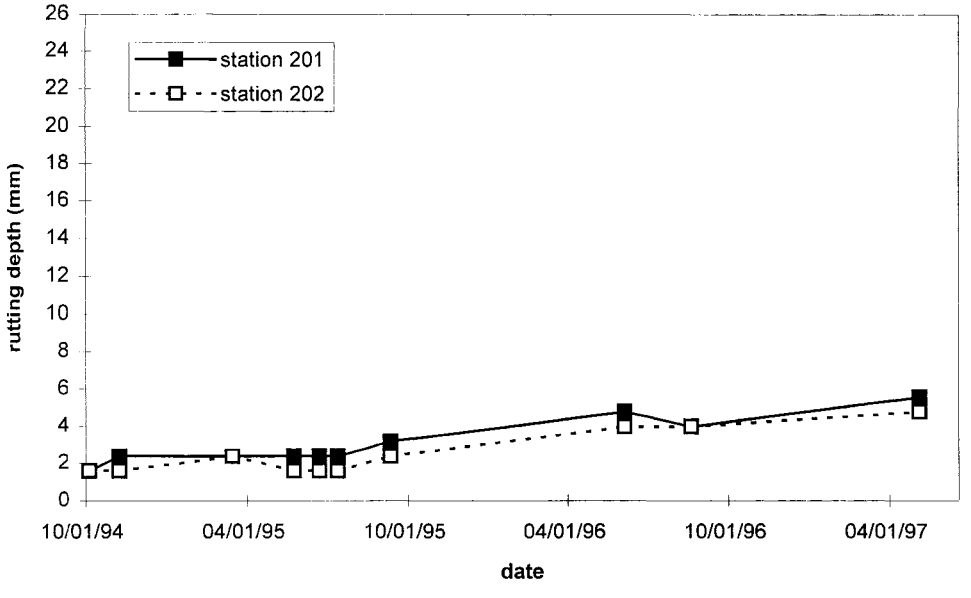

Figure 7.121 Rutting Depths, Section 31, 102500 Lane, Right Wheel Path

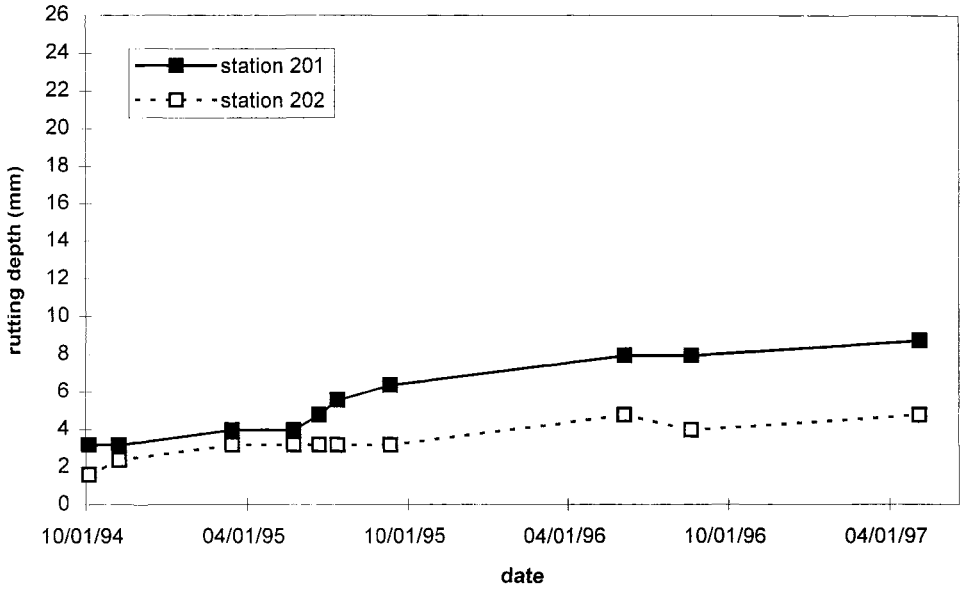

Figure 7.122 Rutting Depths, Section 31, 80000 Lane, Left Wheel Path

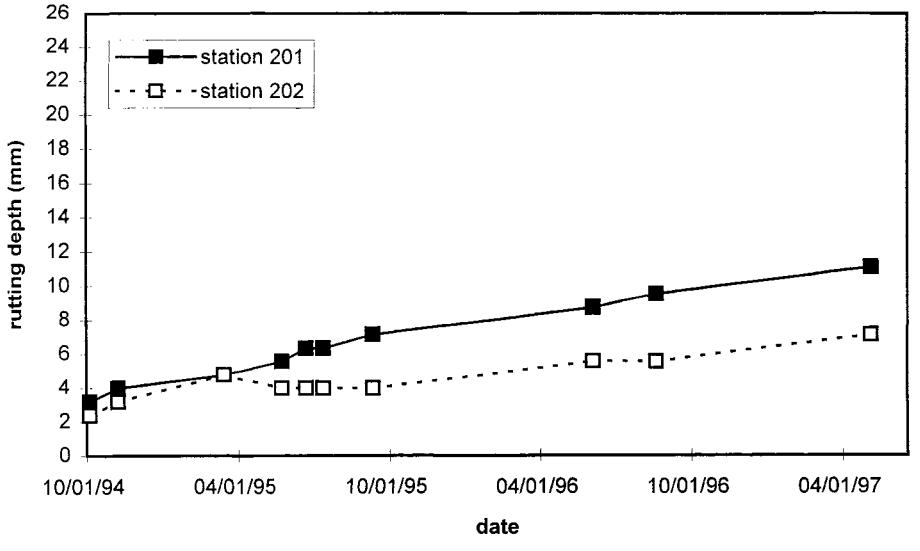

Figure 7.123 Rutting Depths, Section 31, 80000 Lane, Right Wheel Path

CRACK COUNT

This section presents the crack-data for asphalt Mn/ROAD sections. The measures that are used to quantify the crack data are the total number of cracks, total length of cracks, length of low-severity and medium-severity cracks, and the number of full transverse cracks for every section. The presented data cover the period through 4/18/96. There are no new cracks since 4/18/96

In terms of the length of the medium severity cracks, Sections 16,17,18 and 19 are the worst sections. These sections also have high values of the total number of cracks. It is interesting to note IRI linear models of these sections all have high slope measures relative to other sections: the ride quality at these sections seems to degrade quicker than for the other sections.

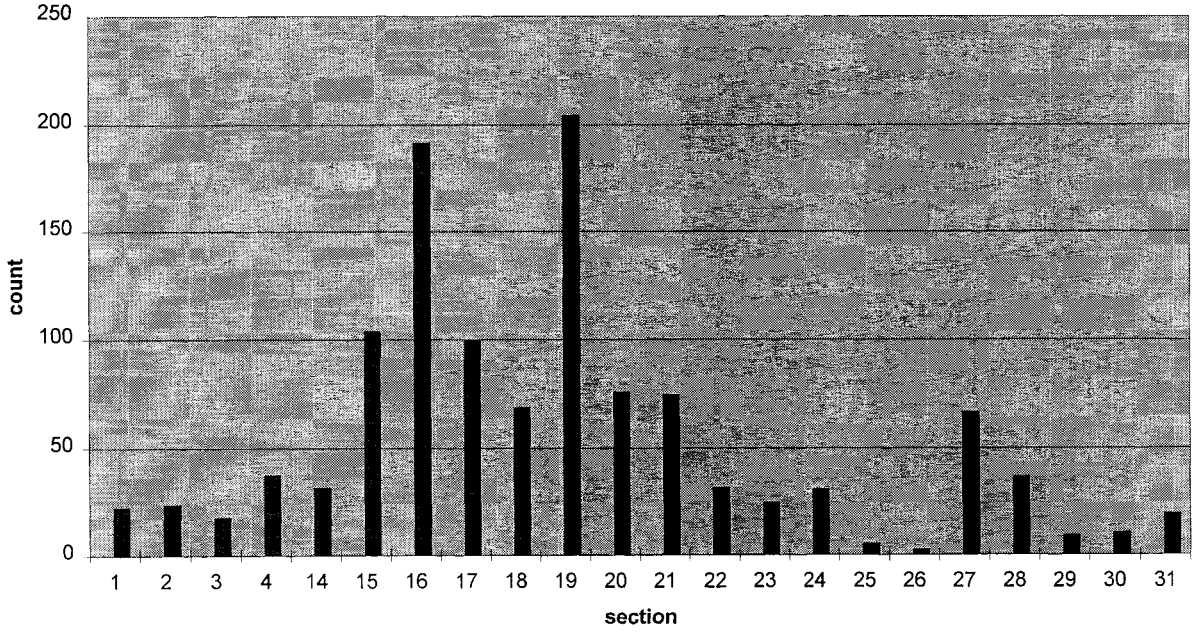

Figure 7.124 Total Number of Cracks

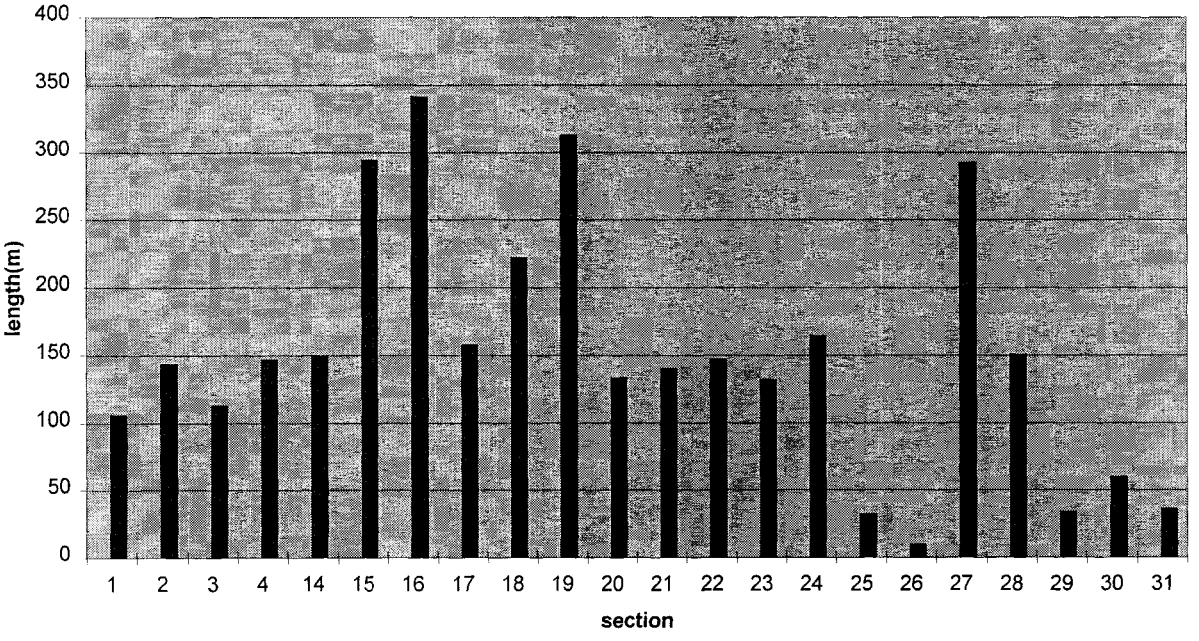

Figure 7.125 Total Length of Cracks

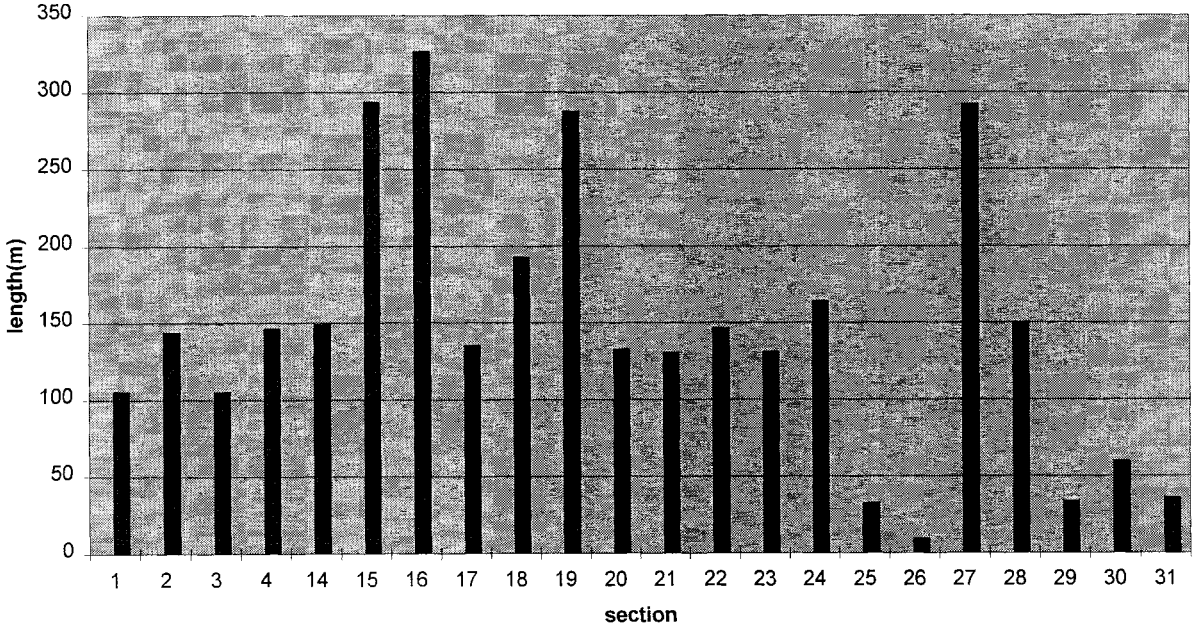

Figure 7.126 Total Length of Low Severity Cracks

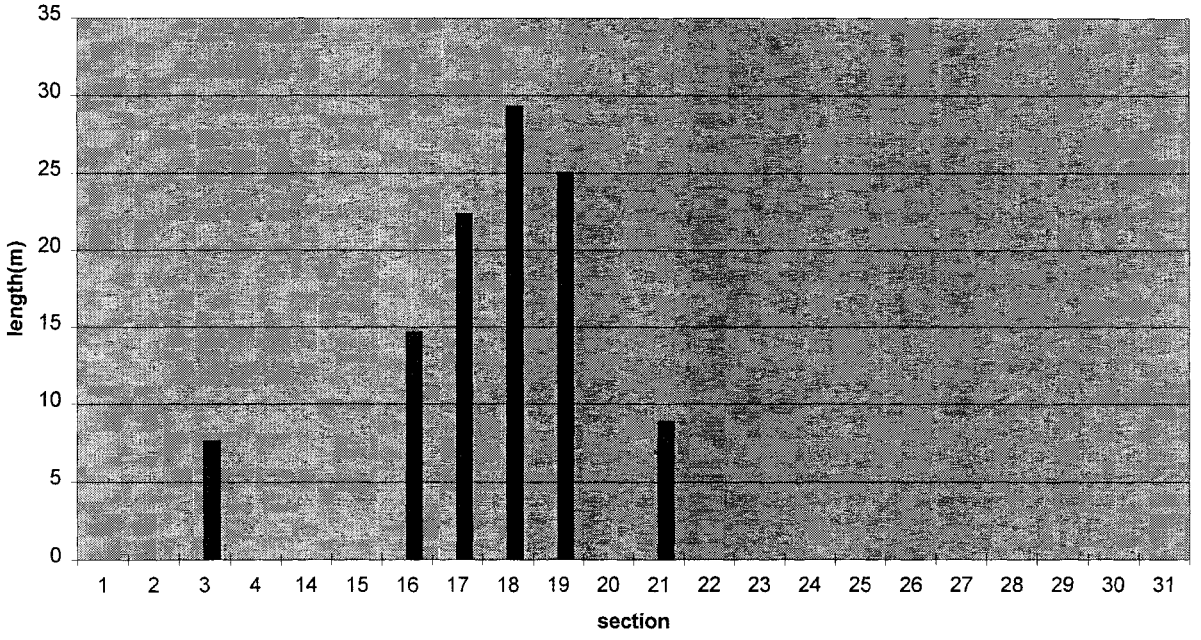

Figure 7.127 Total Length of Medium Severity Cracks

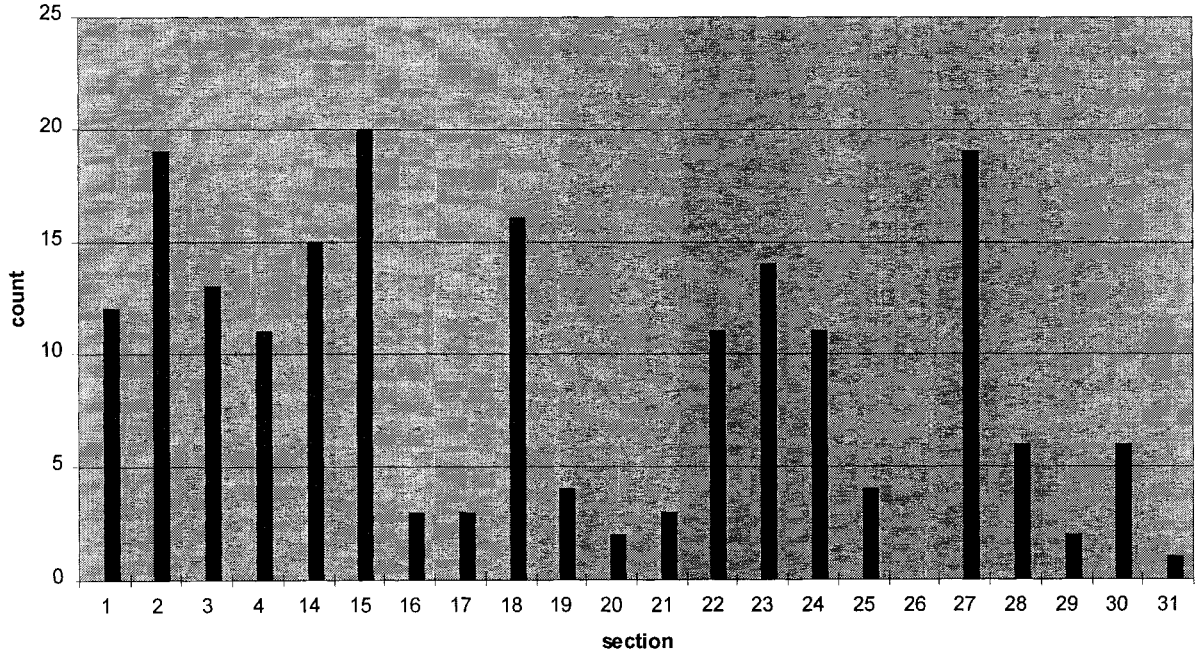

Figure 7.128 Number of Full Transverse Cracks

CHAPTER 8

CONCLUSIONS AND RECOMMENDATIONS

PAVEMENT THICKNESS

On the average the actual thickness is slightly thicker than the design called for. The average difference between the actual pavement thickness and the design pavement thickness is 5.08 mm (0.2 inches), and the standard deviation of the difference is 11.18 mm (0.44 inches).

The distribution of the deviations between the design and constructed thickness is well-modeled by a common bell-shaped curve (i.e. a Normal distribution). As such, there is a significant chance that the as-built pavement thickness can be in error by more than 2.5 cm (1 inch).

For thicker design sections such an error is relatively small, for thinner design sections such an error is relatively large. In all cases, under-construction by more than an inch can cause a significant weakening of the pavement structure. This is particularly problematic when the under-construction occurs over a significant area (on the order of 2's to 30's of square meters) and does not merely occur in small isolated patches (on the order of square centimeters to a few square meters).

The variogram for the pavement thickness deviations consistently showed a range of about 7.5 meters and virtually no nugget effect. Thus, overly thin zones will occur in areas on the order of 10's of square meters, on the average. Furthermore, this indicates that thickness errors are not only due to random undulations in the subgrade, but a significant contribution comes from larger-scale systemic construction calibration or quality control errors. For example, a number of sections at Mn/ROAD were under-constructed over more that half of their total area (e.g. Sections 20 and 26).

This analysis is conducted on one particular site and the ability to generalize to other sites is uncertain. Furthermore, the Mn/ROAD site was created for research. It is then likely that it has been designed and built carefully, perhaps more carefully than usual. Therefore, the errors identified and quantified at this site may underestimate the magnitude of such errors in general. It would be interesting and very worthwhile to conduct the same analysis on other GPR thickness data from other roads in order to compare the results.

SPATIAL VARIABILITY OF SUBGRADE STRENGTHS

There is no apparent spatial correlation of the measured subgrade strengths at the Mn/ROAD site. This is due to the truncated length of the various test sections, the pre-construction geologic homogeneity of the Mn/ROAD site, and the careful construction practices applied at the Mn/ROAD site. Thus, the impact of spatial subgrade variability on the spatial variability of pavement performance can not be investigated using the Mn/ROAD data.

RELATIONSHIP BETWEEN PERFORMANCE AND FWD

Table 8.1 summarizes the relationships between two of the more discerning physical parameters (Structural Number and the Benkelman Beam at 80°) and the available measures of pavement performance. These relationships may be more easily visualized graphically (see Figures 8.1 through 8.10).

The rutting depths are the most consistent and reliable measure of performance of those considered in this project. The rutting depths correlate more closely to the Structural Number than do the IRI or crack data. Nonetheless, even the rutting depths do not appear to be correlated to the Structural Number when the Structural Number is greater than about 3. This indicates that at the time of this study the pavement structures have not degraded sufficiently to clearly correlate long term pavement performance with the FWD-based measures of stiffness. It is strongly suggested that a study of this sort be reconsidered as the various pavement sections approach their design life.

Section	Average Rutting Depth (mm)			Crack Length (m)	IRI (m)			SN	BB80 (mils)
	94	95	96		Right/ 102000	Left/ 80000	Avg.		
1	1.600	2.489	3.912	105.2	0.917	1.074	0.9955	6.75	21.2
2	2.261	2.464	3.734	143.0	0.967	1.040	1.004	6.84	20
3	1.448	1.575	2.210	112.2	1.181	1.184	1.183	7.75	19.7
4	1.778	3.886	4.572	146.0	1.336	1.406	1.371	2.74	19.2
14	1.549	1.448	2.794	148.4	0.911	1.093	1.002	3.51	14.9
15	1.118	1.270	2.489	293.5	0.875	1.127	1.001	3.71	14.7
16	1.245	1.524	2.337	340.5	0.861	0.984	0.923	7.52	16.5
17	1.651	2.057	3.150	157.0	1.001	1.049	1.025	7.37	16.7
18	1.016	1.067	1.956	221.3	0.917	1.111	1.014	6.28	16.8
19	1.143	1.372	2.819	312.1	0.934	1.036	0.985	7.46	16.4
20	1.727	1.651	4.394	132.3	0.818	1.047	0.933	6.96	18.3
21	1.422	1.880	2.692	139.3	0.821	1.014	0.918	6.43	16.6
22		1.600	2.438	146.0	0.863	1.051	0.957	5.58	17.6
23	4.547	5.156	7.391	130.8	1.109	1.259	1.184	4.21	17.1
24	2.413	3.658	4.039	163.4	1.122	0.827	0.975	1.63	24.8
25	2.007	3.353	4.623	31.7	0.995	0.854	0.924	1.79	22.8
26	3.327	5.131	7.163	9.1	1.442	1.536	1.489	1.71	32.3
27	4.089	5.258	8.153	291.7	1.333	1.233	1.283	2.22	38.1
28	4.013	6.045	8.915	149.7	1.032	0.925	0.978	2.46	38.8
29	2.489	3.404	5.029	33.2	1.007	0.975	0.991	2.69	32.5
30	2.464	3.556	5.309	59.1	1.117	1.010	1.064	3.08	28.9
31	2.769	3.073	4.597	35.7	1.555	1.126	1.341	2.94	34.2

Table 8.1 Section-By-Section Comparison of Physical Parameters with Performance

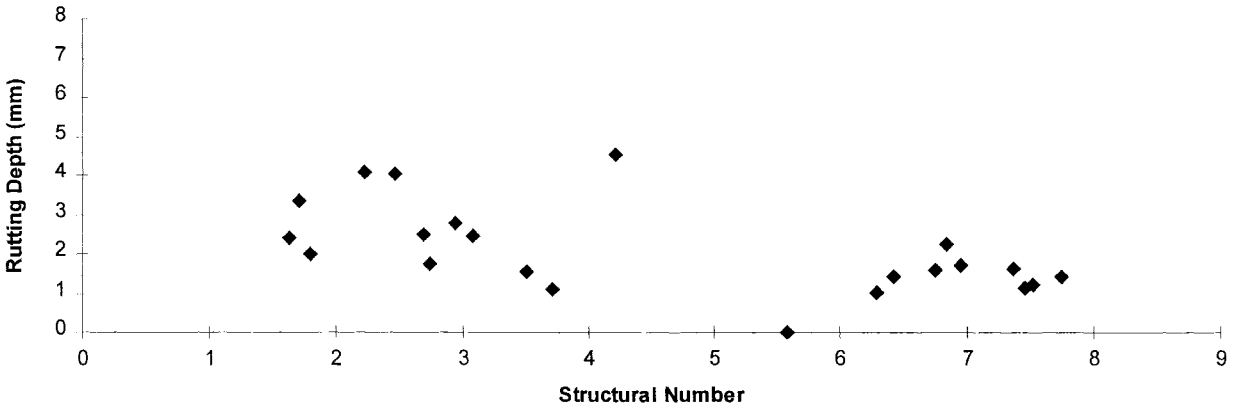

Figure 8.1 Structural Number Versus 1994 Rutting Depths

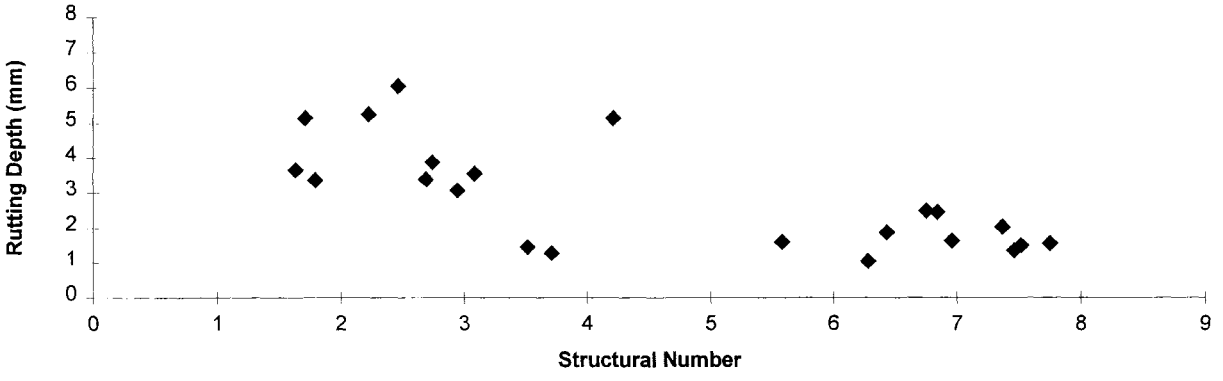

Figure 8.2 Structural Number Versus 1995 Rutting Depths

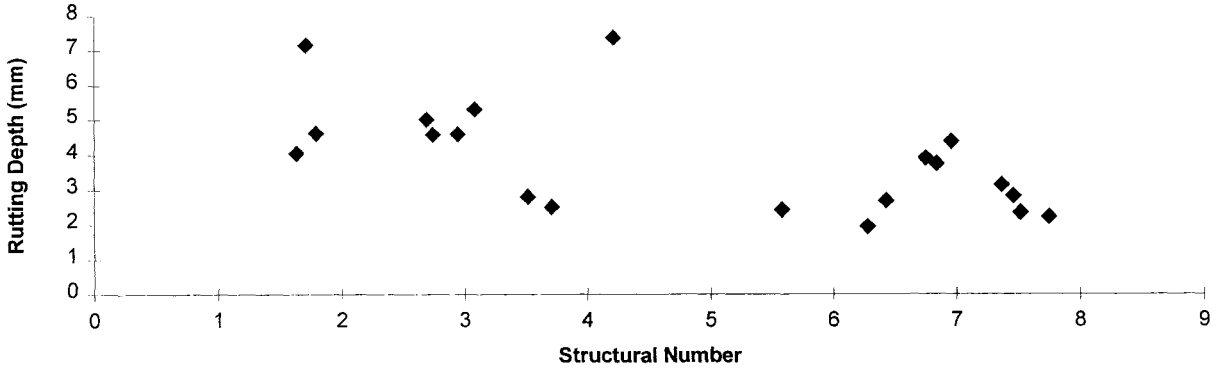

Figure 8.3 Structural Number Versus 1996 Rutting Depths

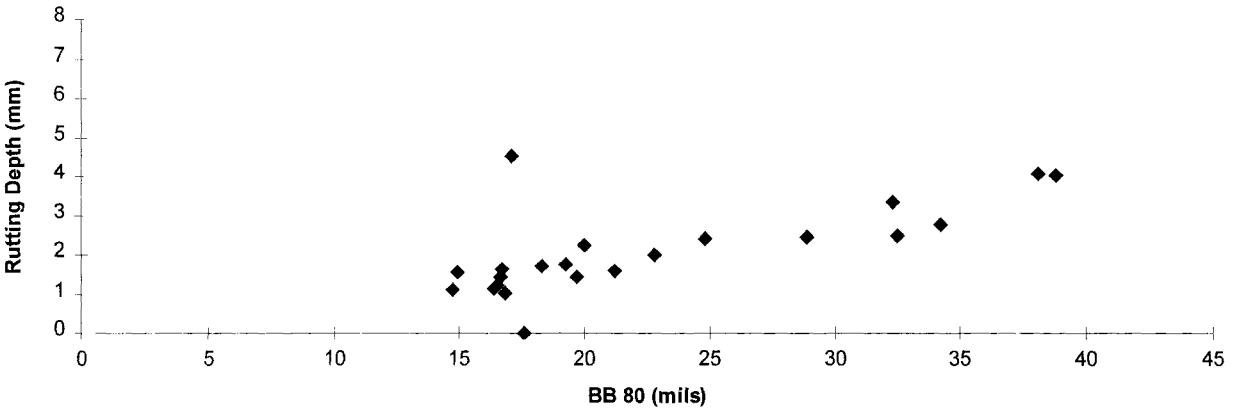

Figure 8.4 Benkelman Beam at 80° Versus 1994 Rutting Depths

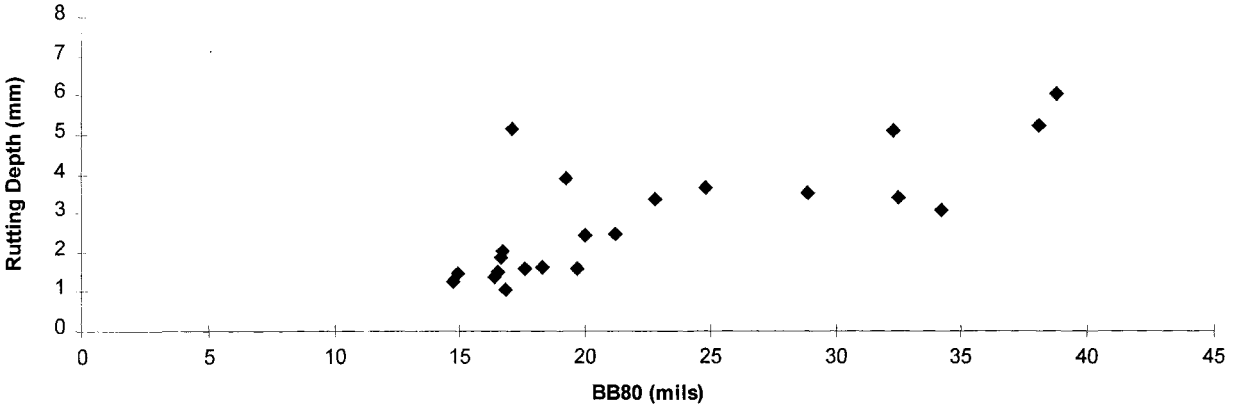

Figure 8.5 Benkelman Beam at 80° Versus 1995 Rutting Depths

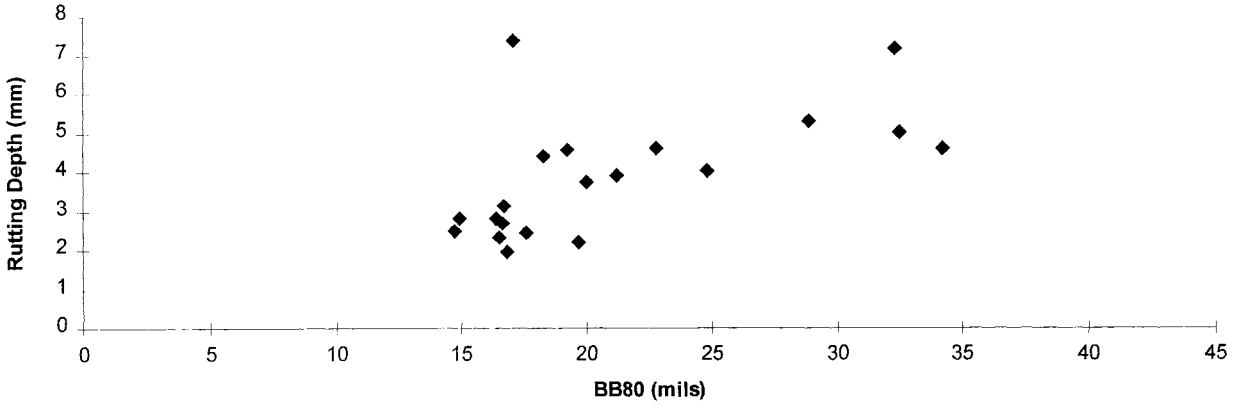

Figure 8.6 Benkelman Beam at 80° Versus 1996 Rutting Depths

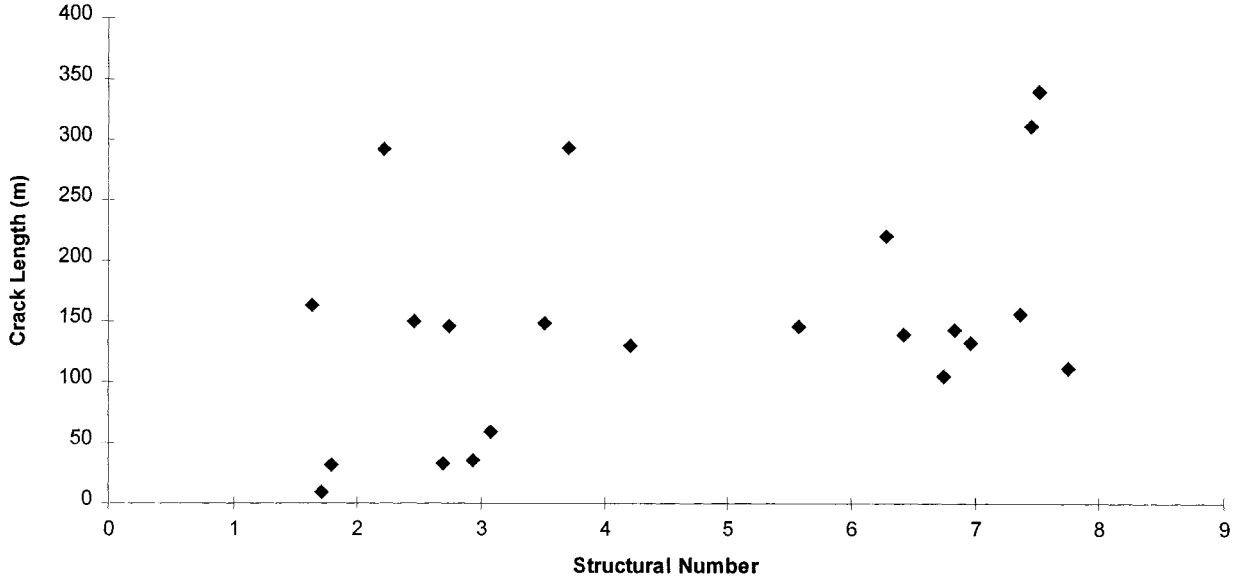

Figure 8.7 Structural Number Versus Total Crack Length

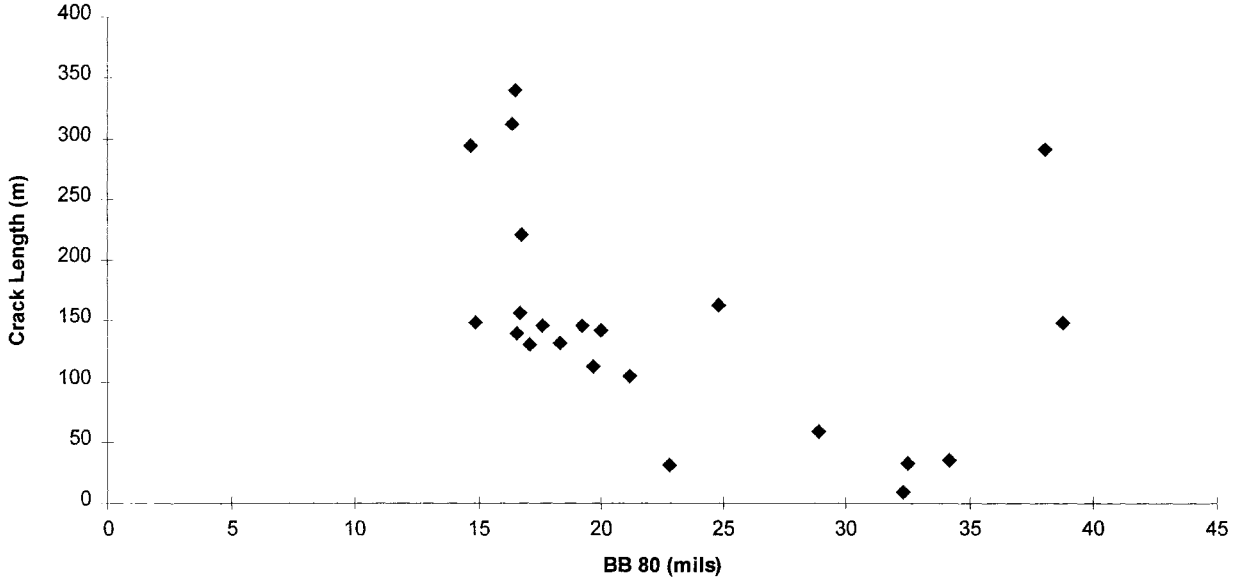

Figure 8.8 Benkelman Beam at 80° Versus Total Crack Length

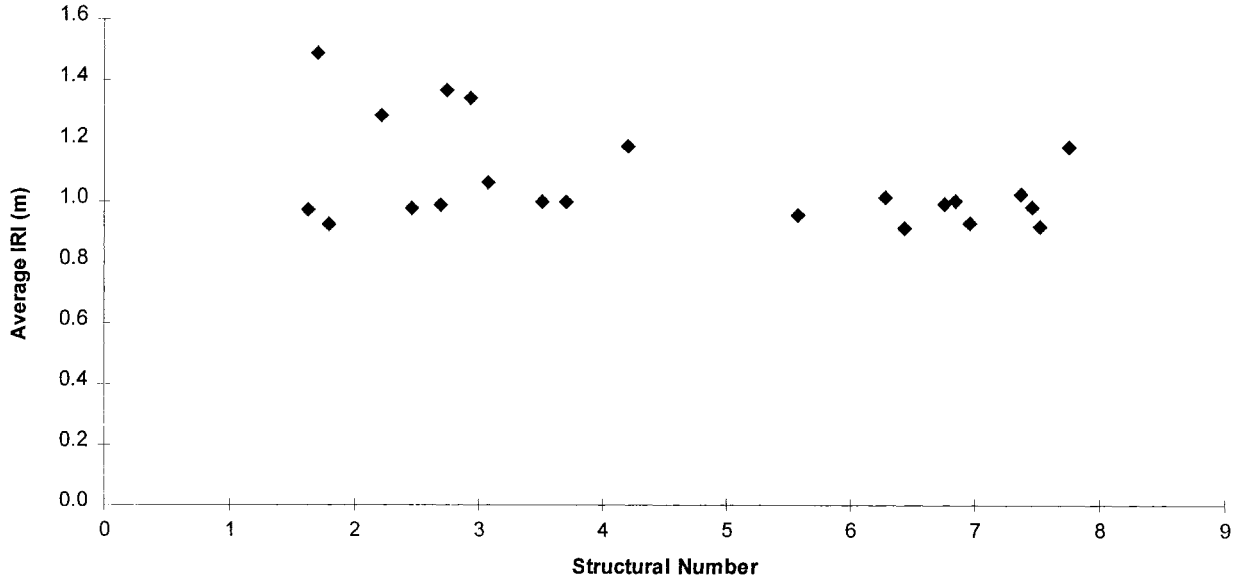

Figure 8.9 Structural Number Versus Average IRI

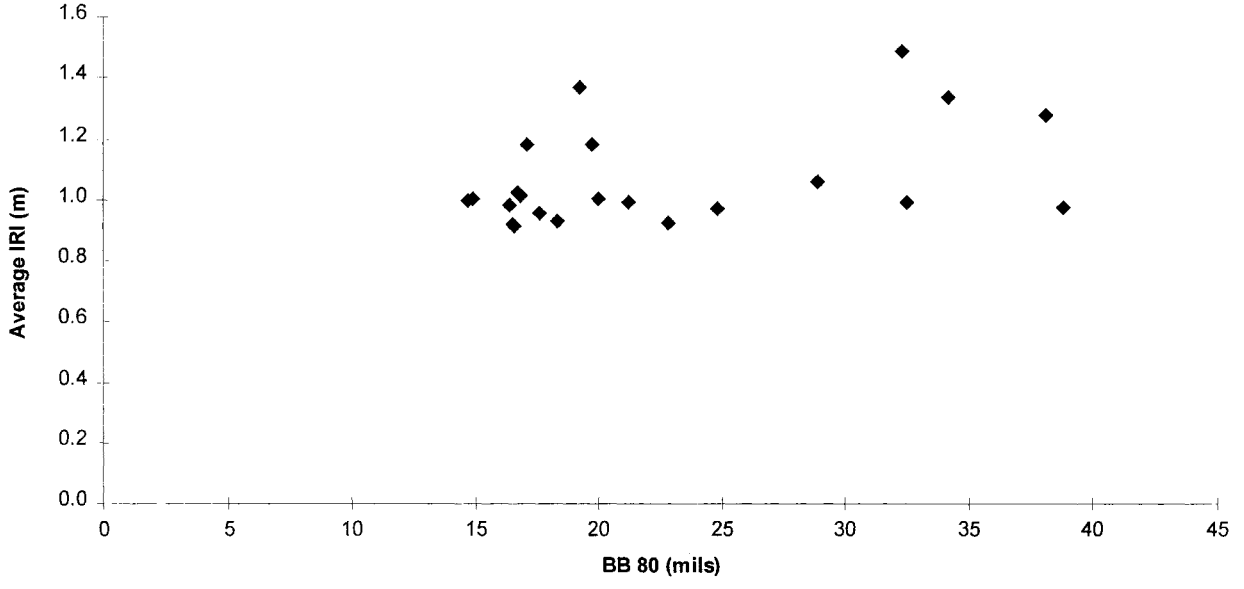

Figure 8.10 Benkelman Beam at 80° Versus Average IRI

SOIL MOISTURE AND GROUNDWATER EFFECTS

Soil moisture and groundwater is known to have severe adverse effects on the performance of pavement structures. Mechanism like freeze/thaw and subgrade pumping are related to the availability of soil water. Due the apparent environmental homogeneity of the site, and difficulties with the available data at the Mn/ROAD site, a quantitative comparative study of these mechanism and their effect on the variability of pavement performance was not possible.

REFERENCES

1. Cressie, N., Statistics for Spatial Data, John Wiley and Sons, New York, 1991, 900 pp.

2. Isaaks, E.H., and Srivastava, R.M., An Introduction to Applied Geostatistics, Oxford University Press, New York, 1989, 561 pp.

3. Kitanidis, P. K., Introduction to Geostatistics: Applications in Hydrogeology, Cambridge University Press, Cambridge, U.K., 1997, 249 pp.

4. AASHTO Guide for Design of Pavement Structures, 1993, Appendix MM.

5. Kruse, C. G., and E. L. Skok, Flexible Pavement Evaluation with the Benkelman Beam, Minnesota Department of Highways, Investigation No. 603, 1968.

6. Minnesota Department of Transportation, Geotechnical and Pavement Manual, 1994.